Master's thesis

NTNU
Norwegian University of Science and Technology
Faculty of Engineering
Department of Mechanical and Industrial Engineering

Torunn Bakken

Non-Destructive Inspection of Polymer Composite Pipelines

Master's thesis in Mechanical Engineering
Supervisor: Andreas Echetermeyer
July 2022

NTNU
Norwegian University of
Science and Technology

Torunn Bakken

Non-Destructive Inspection of Polymer Composite Pipelines

Master's thesis in Mechanical Engineering
Supervisor: Andreas Echetermeyer
July 2022

Norwegian University of Science and Technology
Faculty of Engineering
Department of Mechanical and Industrial Engineering

NTNU
Norwegian University of
Science and Technology

Abstract

Fibre-reinforced polymer (FRP) composite pipes have the potential to replace metal pipes in the offshore oil and gas industry due to their advantageous properties such as light weight, high strength and corrosion resistance. However, a main bottleneck for their implementation in safety-critical areas is the lack of integrity management systems, including reliable non-destructive test (NDT) methods. The following aims to evaluate NDT methods for detecting critical failure mechanisms in thick composite materials, focusing on digital image correlation (DIC) and ultrasonic testing (UT).

Two-dimensional digital image correlation (2D-DIC) in combination with low tensile load and ultrasonic pulse echo testing has been used to inspect 21.5 mm thick glass fibre reinforced epoxy laminate specimens containing flat bottom holes (FBH) and fabricated delaminations made of PTFE Teflon film. Three different frequency transducers, 5 MHz, 2.25 MHz and 0.5 MHz, were used for the ultrasonic inspection. The defects were introduced at different depths throughout the laminate ranging from 10.7 mm to 20.0 mm from the inspected surface. It was found that DIC could detect all FBH and delaminations up to 13.8 mm from the inspected surface by evaluating the tensile strain field at a strain level of 0.4% average tensile strain. Comparably, all defects could be detected with UT at all three frequencies, with 2.25 MHz enabling inspection at the lowest receiver gain.

Moreover, UT techniques for inspecting curved geometry pipe samples have been explored. Polyethylene (PE) and fibre-reinforced PE pipe samples with FBH have been inspected using contact testing with and without a contoured wedge and immersion technique. The methods enabled proper coupling between the transducer and the inspected specimens, enabling the detection of FBH within the pipe samples.

Keywords: Non-destructive testing (NDT), Digital Image Correlation (DIC), Ultrasonic Testing (UT), Composites, Pipeline Inspection

Sammendrag

Rør laget av fiberforsterket kompositttplast (FRP) har potensial til å erstatte metalliske i olje- og gassindustrien, grunnet deres fordelaktige egenskaper som lav vekt, høy styrke og motstand mot korrosjon. En stor hindringen for implementasjon i områder med høye krav til sikkerhet er mangelen på system for integritetsstyring av denne typen rør (PIMS), inkludert pålitelige ikke-destruktive inspeksjonsmetoder (NDT). Det videre arbeidet har til hensikt og evaluerer ikke-destruktive inspeksjonsmetoder (NDT) for å oppdage kritiske feilmekanismer i tykke kompositttmaterialer, med fokus på digital bildekorrelasjon (DIC) og ultralydinspeksjon (UT).

Todimensjonal bildekorrelasjon (2D-DIC) i kombinasjon med lav strekkbelastning og puls-ekko ultralydtesting har blitt benyttet for å inspisere 21.5 mm tykke prøver laget av glassfiberforsterket epoxylaminat med flate hull (FBH) og fabrikerte delamineringer laget av folie av PTFE Teflon. Trandusere med tre ulike frekvenser, 5 MHz, 2.25 MHz og 0.5 MHz, ble benyttet til ultralydprøvingen. Feilene ble introdusert på ulike dybder gjennom laminatet fra 10.7 mm til 20.0 mm fra den inspiserte overflaten. Det ble funnet at DIC kunne detektere alle flate hull og delamineringer posisjonert 13.8 mm fra den insipserte overlfaten ved evaluering av strekktøyningsfeltet på ved 0.4% strekktøyning. Ved sammenligning, kunne alle feilene bli oppdaget med UT ved alle de tre frekensene benyttet, der den laveste forsterkningen av mottakersignalet kunne benyttes ved 2.25 MHz .

Videre ble ulike UT teknikker for inspeksjon av runde geometrier utforsket. Rør laget av polyetylene- og fiberforsterket polytelyene, med flate hull i ulike størrelser, har blitt inspisert ved kontakttesting med og uten bruk av konturformet kile, og med testing av prøver nedsenket i vann. De benyttede metodene la til rette for god kontakt mellom transduser og prøvstykke slik at hull drillet i rørprøvene kunne bli oppdaget.

Nøkkelord: Ikke-destruktiv testing (NDT), Digital bildekorrelasjon (DIC), Ultralyd, Kompositt, Rør

Acknowledgements

I would like to thank my supervisor, Professor Andreas Echtermeyer at the Department of Mechanical and Industrial Engineering, NTNU, for valuable insight and guidance throughout this Masters project work. Moreover, I would like to thank PHD candidates on the C.PIMS project Mohd Fadzil Bin Mohd Tahir and Victor Maneval for their help with and training on the ultrasonic inspection device and digital image correlation equipment.

I would also like to express my gratitude to the rest of the composite group for interesting discussions and for creating a pleasant work environment in the lab.

Finaly, a special thanks goes to Erlend Austad Wesseltoft for moral support and encouragement throughout the work on this thesis.

Torunn Bakken

Trondheim, July 2022

Table of Contents

List of Figures

List of Tables

List of Abbreviations

BWE back wall echo

CFRP carbon fibre reinforced polymer

DIC digital image correlation

FBH flat bottom holes

FE finite element

FRP fibre reinforced polymer

FWE front wall echo

GFRP glass fibre reinforced polymer

MB blank main bang blank

PE polyethylene

PIMS Pipeline Integrity Management System

PuE pulse-echo

ROI region-of-interest

TDG time-dependant gain

TT through-transmission

UT ultrasonic testing

VART vacuum assisted resin transfer

1 Introduction

1.1 Background and Motivation

Thermoplastic pipes and fibre-reinforced thermoplastic pipes have the potential to replace metallic pipes in the oil and gas industry. Thermoplastic and fibre-reinforced thermoplastic pipes can potentially replace metallic pipes in the oil and gas industry. Such pipes can be used for the transportation of water, oil, gas, and eventually hydrogen, both on- and offshore. They have a high weight-to-strength ratio and are easy to install, enabling them to be used at reserves typically classified as hard-to-reach, such as in arctic conditions or ultra-deep waters, where metal pipes are reaching the limits of their capabilities [1]. Further, they are cost-efficient and roughly corrosion-free, with good thermal insulation and excellent damping and fatigue performance [2], [3].

The use of composite pipelines is rapidly increasing, but so far, only in lower-risk applications, like pipes containing water at low pressure. A major bottleneck for implementation in areas with high safety requirements is the lack of a Pipeline Integrity Management System (PIMS) [2], [3].

This project is a part of a larger industry project called C.PIMS – Composite Pipelines Integrity Management System, led by DNV. The industry project aims to develop PIMS for composites of the same quality as those existing for steel pipes today, allowing large-scale implementation of composite pipes and use in safety-critical applications.

PIMS is a combination of threat identification, risk assessment, planning, inspection, monitoring, testing, integrity assessment, mitigation, intervention, and repair. It is essential for safe and reliable pipeline operation over an entire life cycle and must provide methods for detecting and classifying damages and determining the need for maintenance or repair [4], [5]. Such systems are widely used for quality control, maintenance evaluation, and inspection of metal pipes. However, the same systems cannot be used for composite pipelines as their failure mechanisms, and fatigue behaviour are more complex and less predictable than for metals [1]. Unlike metals, whose fatigue degradation sets in after a certain number of load cycles, composites experience complex progressive damage over the whole lifetime of the component[6].

1.2 Problem Description

This thesis will investigate the capabilities of selected non-destructive inspection methods for polymer composite. Detection of common failure mechanisms within composite laminates will be investigated, and the results will be discussed concerning the structural integrity evaluation of composites.

Two inspection methods will be reviewed experimentally: digital image correlation (DIC) and ultrasonic testing (UT). These will be used to inspect thick composite laminate samples to determine the methods' limitations regarding the size and location of defects. Inspection of curved geometries will be explored using ultrasonic testing to further assess the method for composite pipeline applications.

1.3 Objectives

The main objectives of this thesis include:

- Investigate the capabilities of digital image correlation and ultrasonic testing as non-destructive inspection methods for composites.
- Assess what type of damage can be detected and the limitations set by damage size and laminate thickness.
- Explore techniques for inspection of curved components.
- Discuss how inspection results can be used for evaluating the integrity of polymer and polymer composite pipelines.

1.4 Scope of Work

This thesis focuses on the failure mechanism delamination. Other common failure mechanisms, including debonding, matrix cracking, fibre failure, and voids, are also discussed, but merely on a theoretical level and are not included in the experimental part of the thesis. The main inspection methods evaluated are digital image correlation (DIC) and ultrasonic testing (UT). Other relevant inspection methods are presented but not investigated in detail.

The work related to DIC presented in this project concerns 2D-DIC, while for UT, pulse-echo testing is used. This thesis does not go into detail about more advanced DIC techniques such as stereo-DIC or other UT inspection techniques. The main focus is on the application of the two methods. It does, therefore, not go into aspects such as geometrical

optics, acoustic wave physics, or algorithm optimization. Applications of the two methods beyond non-destructive inspection of polymers and polymer composites are not covered.

Moreover, it is assumed that the reader is familiar with the mechanics of composite materials, such as stress and strain relation and laminate theory. For more information on the topic, [7] can be consulted.

1.5 Report Structure

Chapter 1 - *Introduction*: This chapter provides background information, objectives, scope and structure of the thesis.

Chapter 2 - *Theoretical Background*: An overview of common failure mechanisms and non-destructive inspection techniques for polymer composites are given in this chapter. Further, essential concepts of digital image correlation (DIC) and ultrasonic testing (UT) are presented.

Chapter 3 - *State of the Art*: This chapter discusses the potential of DIC and UT to detect defects in composite materials and presents a literature review of relevant findings from previous research.

Chapter 4 - *Experimental method*: An overview of the materials and the geometry of the test specimens, as well as equipment and test setup, is given in this chapter. Three different experimental methods have been used, 2D-DIC on flat glass fibre specimens, ultrasonic inspection of flat glass fibre specimens, and ultrasonic inspection of pipe samples.

Chapter 5 - *Results*: The main findings from the experimental tests are presented in this chapter.

Chapter 6 - *Discussion*: In this chapter, the quality of the obtained results is discussed, along with possible sources of error. The two methods evaluated and compared and their significance for evaluating composite pipelines' structural integrity are discussed.

Chapter 7 - *Conclusions*: A summary of the findings is presented in this chapter.

Chapter 8 - *Further Work*: In the final chapter, suggestions for further work are listed.

1.6 Disclaimer

The work presented in this thesis is the continuation of the author's specialization project from the fall of 2021. With the aim of making this thesis a complete and independent report in and of itself, parts of Sections 2.1-2.2, 2.4, and 3.2-3.3 replicated from the specialization project work [8], with minor changes only

2 | Theoretical Background

The use of carbon- and glass fibre reinforced polymer (FRP) composites is increasing in various applications requiring high strength and stiffness, such as aerospace, automobile, sporting equipment, as well as the offshore oil and gas industry. The increasing use is due to their advantageous properties compared to metals, such as high strength-to-weight ratio and corrosion resistance [9].

This chapter will discuss the failure mechanisms commonly found in FRP composite materials, hereby referred to as composite materials, and their relevance in composite pipelines. Further, a brief overview of existing non-destructive test (NDT) methods used for composites will be presented before a more detailed description of the most common method, ultrasonic testing, and a less explored inspection method, Digital Image Correlation, will be given.

2.1 Failure Mechanisms

Composite pipes may experience several types of defects, both during production and during their operational lifetime. Composite laminates have three main failure mechanisms: matrix cracking, delamination, and fibre failure [10]. Debonding may also occur for laminates attached to a liner, which is the case for thermoplastic FRP pipes. The most significant concern of production-related defects is voids or air bubbles within the laminate [11]. This chapter will give an overview of the most common failure mechanisms that may occur in polymer composite materials.

2.1.1 Matrix Cracking

Matrix cracking is typically the first failure to occur under increased load or cycling loading of a polymer composite material [12]. Fibre-reinforced composite materials offer high strength and stiffness in the fibre direction of the material; in the transverse direction, on the other hand, the properties are much lower, and so cracks can occur in the matrix-fibre interface or within the matrix itself [12]. Matrix cracks are generally not critical for struc-

tural integrity, as loads will be mainly carried out by the fibres. However, they can result in stress concentrations and induce more severe forms of damage, such as delamination and fibre failure [13]. Further, cracks in the matrix may cause leakage and give pathways for the entry of fluids. For pipelines, a liner is typically applied, so that leakage in the laminate will usually not cause any significant problems.

2.1.2 Delamination

Delamination refers to the separation of two adjoining plies within a laminate, which can be caused by through-thickness normal and shear stress [13]. The plane between the plies is often weak due to inhomogeneities. The load transfer between layers may lead to local stress concentrations causing delamination [14].

Growth of delamination cracks under external load leads to rapid deterioration of the mechanical properties, such as reduction in shear-and especially compressive strength, causing extensive micro buckling. This deterioration could develop into catastrophic failure of the composite [15].

Delaminations can also be caused by low-velocity impact loading, such as blunt impacts [11]. These may occur below the surface of the structure, while the surface appears undamaged by visual inspection and is called barely visible impact damage [16], [17]. Although the delamination may not be evident at the time of impact, it can cause severe internal damage and, equally as to under external fatigue or increasing loads, develop into rapid failure of the component [18].

Delamination is an excellent example of why NDT is necessary for composite structures. It is a critical damage mechanism that may be very difficult to inspect visually, especially for thick laminates, carbon fibre composites, or composite structures coated with a non-translucent paint or liner. Due to both the severity of the damage and the promising results using ultrasonic inspection as an NDT method for locating it, delamination has been the main focus of this project. Some results from previously conducted research are presented in Section 3.3, while experimental work conducted for this project is presented in Chapters 4 and 5.

2.1.3 Fibre Failure

Fibre failure refers to the breakage of one or more fibres in a laminate. Rupture of an individual or few fibres is not critical, as the matrix transfers stress around such defects. This is, however, only the case for very local loading, which is rarely the case, especially for pipelines. In most cases, fibre failure will start with the failure of individual fibres before the stress redistributing causes more fibres to break, which reduces the strength of the laminate drastically, eventually leading to the ultimate failure of the composite [13].

2.1.4 Voids

Voids, or air bubbles, are manufacturing induced defects and do not develop during service. It is one of the primary defects found in virtually all types of composite material, as it is nearly impossible to make laminates without voids [19]. Some air will nearly always get entrapped between the plies when laying up the layers. Thick laminates are particularly difficult to produce with a low void content, making this an especially relevant issue for composite pipelines [14]. Some amount of voids will have to be expected and will not affect the properties of the composite to a large degree. However, excessive void content may decrease the strength of the laminate [20].

2.1.5 Debonding

Debonding has similar characteristics as delamination, except that instead of the failure occurring between individual layers within the laminate, it occurs in the interface between a substrate and an adhesive material [10]. This failure is relevant for thermoplastic pipes, where a thick polymer liner is used on the inside of the composite.

2.1.6 Other Defects

Another in-service defect that may occur is matrix degradation. This is also an important aspect of polymer composite pipelines that need better understanding. It is, however, outside the scope of this project.

Other production related defects that may occur in composite laminates are using incorrect fibre or matrix material, kinked or wavy fibre tows, over-aged matrix material, matrix contamination, under-curing, incorrect stacking sequence of laminate plies, matrix misalignment, or omitting a layer [14]. These will not be covered in this thesis.

2.1.7 Evolution of Damage in Composite Laminates

While damage in metallic structures is relatively well understood, damage in composites is substantially more complicated [21]. Composite materials fail differently under tension than in compression, and they are prone to hidden damage from low-velocity impact [6]. Further, damage in composites is a progressive phenomenon; sub-critical for a while before ultimate failure occurs, making it more challenging to predict [6].

Figure 2.1 shows a conceptual description of fatigue damage evolution in polymer composite materials, beginning with matrix cracking, leading to delamination, and finally, fibre failure occurs; after this, ultimate failure takes place quickly. [13].

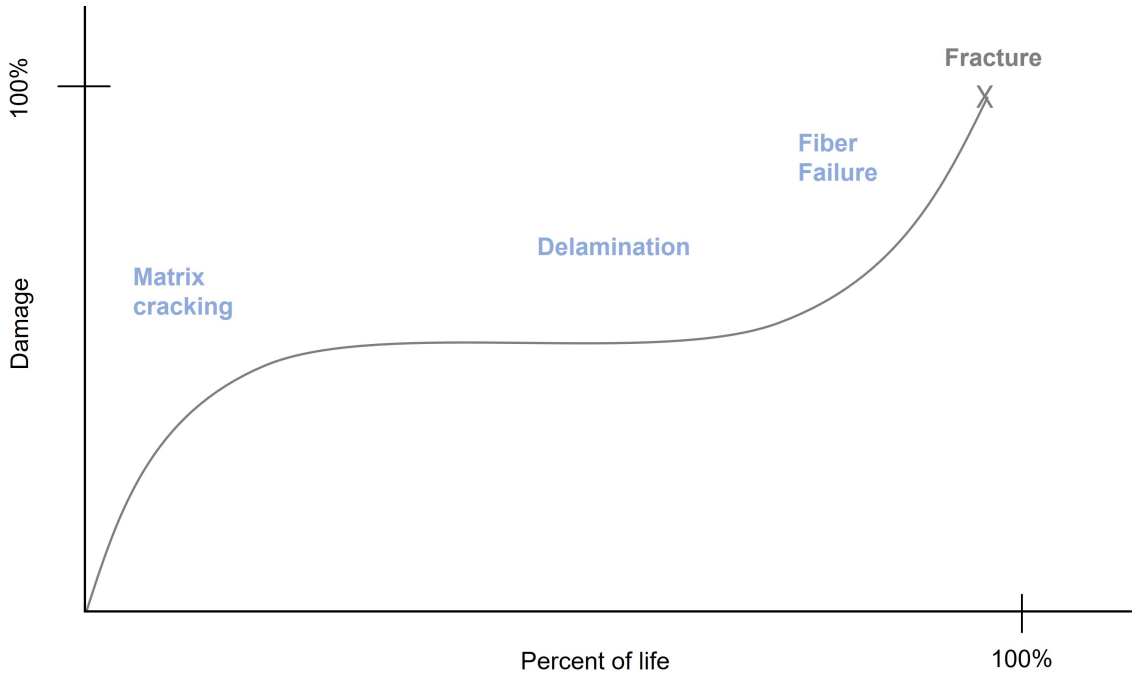

Figure 2.1: Fatigue damage evolution in polymer composites

2.2 Non-Destructive Testing (NDT) Overview

Non-destructive testing (NDT) refers to inspection techniques that enable the collection of data about a material without damaging or physically altering it [22]. NDT may also be called:

- NDE (non-destructive examination or evaluation)
- NDI (non-destructive inspection)

The techniques are utilised to detect, characterise, or measure the presence of damage mechanisms within a part or a structure. NDT can also be used to assess the material state condition and the parts remaining life. Many NDT techniques are capable of locating defects and determining features of the defects, such as size, shape, and orientation [22]. NDT can be used both for quality control after manufacturing and as in-service [23].

The purpose of NDT is to inspect a component in a safe, reliable, and cost-effective manner without shutting down operations or causing damage to the equipment. In contrast, in destructive testing, the part being tested is damaged or destroyed during the inspection process [23].

There are many NDT techniques for aluminium and steel, but far fewer options for glass fibre reinforced polymer (GFRP) and carbon fibre reinforced polymer (CFRP) [24]. Although composite materials have been used for a long time, including in critical structural applications, the effects of defects, damage mechanisms, fatigue and failure mechanisms are not as mature and well understood as for metals [1].

In the experimental part of this thesis, two NDT methods are considered, **DIC** and **UT**. These are further outlined in section 2.3 and section 2.4 respectively. Other NDT methods used for composite laminates are briefly described in the following sections.

2.2.1 Visual Inspection

Visually inspecting a laminate can reveal a fair amount about its condition. In translucent laminates, such as non-coated GFRP, both delamination and matrix cracks can be seen close to the surface. Visual inspection can be enhanced by additional tools such as microscopes and camera recording [6].

2.2.2 Coin Tap Method

Coin tap testing involves tapping on the surface of an object with a small hammer or a coin and evaluating its condition based on the resulting sound. Today, automatic tap testing devices which analyse the sound signal exist [25]. Still, this method is most sensitive to defects close to the surface of a structure and works best on thin laminates. Further, it will only detect defects such as debonding and delaminations which reduce the effective stiffness of the structure normal to the surface [26].

2.2.3 X-ray

X-rays have high energy and can penetrate most structural components. Polymeric materials, however, have low density and are not ideal to be investigated using X-ray NDT [27]. Moreover, this method is challenging to perform in-service, as many safety precautions are required due to health hazards concerning radiation [27].

2.2.4 X-ray Computed Tomography

X-ray computed tomography (CT) is becoming an increasingly useful non-destructive technique for applications where the three-dimensional nature of the damage is essential or where the evolution of critical features is of interest, which is both the case for composite materials [28]. The heterogeneous nature of composites benefits from 3D assessment, and understanding damage evaluation is critical to the material's structural integrity.

2.2.5 Thermography

Thermography is a method that analyses the heat flow through a laminate. The thermal conductivity of a material may change in the presence of defects, resulting in a change in surface temperature that can be measured using thermal imaging [29]. This method works best for thin laminates. For thick laminates, such as FRP pipes, the heat flows around the defects, making them difficult to detect. As defects are located deeper under the surface of a part, they produce less heat fluctuation making them more difficult to detect [30]. Delamination will influence the thermal flow through the thickness and can be detected if they are close to the surface. Other damage mechanisms such as matrix cracking, fibre failure, and voids cannot be detected.

2.2.6 Shearography

Shearography is a laser optical method that requires loading of the structure. Loading will cause small deformations of the surface, which can be measured with laser optics [31]. The criticality of defects can be deducted by the degree of strain concentration around the defect. Delaminations can be detected; however, characterisation of defect types other than delamination is difficult [30].

2.3 Fundamentals of Digital Image Correlation

Digital Image Correlation (DIC) is an optically based inspection technique that is both non-contact and non-destructive. This section introduces the basic principles of the method as well as some considerations for practical applications. A more in-depth explanation can be found in [32].

2.3.1 Image Correlation Principles

DIC is used to measure full field coordinates of an object subjected to deformation, motion, or load [33]. The object's surface must have a random speckle pattern, and images are taken both before and during loading. By tracking the movement of the speckle pattern from one image to another, quantities such as full field displacements, strains, and strain rates on the surface of the part, can be derived [33].

The fundamental principle of DIC is to match the same physical point in a reference image before an external load is applied and a deformed image taken during or after a load is applied. [34].

Subsets and Region-of-Interest

A user-defined region-of-interest (ROI) is analysed using numerical DIC software. The ROI is divided into smaller squared areas of neighbouring pixels called subsets. Each subset contains a fixed number of pixels and represents one grey level. The subsets are used to track the motion between images by correlating a subset from the reference image to each of the subsequent deformed images.

From speckles to displacements

A matching criterion matches a subset in the reference image to the corresponding area in a deformed image based on the grey-level distribution inside the subset [32]. Moreover, the displacements are estimated from the centre coordinates of the subset in the reference image to the centre coordinates of the subset in the deformed image [35].

An interpolant function is used to approximate the pattern within a subset to obtain subpixel accuracy. This is called grey-level interpolation. A subset shape function is used to account for the distorted shape of the initially squared subset after deformation [32].

Obtaining strain fields

Strain values are obtained by differentiating the displacements along the surface of the test piece. However, the experimentally obtained displacements include errors that are increased through differentiation. The easiest way of reducing the effect of errors is to approximate the displacements using the method of least squares and then to differentiate the approximated functions [32].

Matching bias

The grey-level interpolation is expected to introduce some error as it is a method of approximation [32]. This interpolation bias further directly translates to a bias in displacement and strain measurements. Further, in practical applications, a certain level of noise is inevitable, introduced by imperfect patterns or imaging sensors, as well as Gaussian random noise [32].

2.3.2 Practical Considerations

DIC methods

Digital Image Correlation is typically divided into two-dimensional and three-dimensional methods, called 2D-DIC and stereo-DIC, respectively.

2D-DIC uses a single camera system, with the camera placed perpendicular to the surface of the specimen. With this method, two-dimensional coordinates of the surface can be measured, and in-plane displacements and strain components can be calculated [35].

Stereo-DIC uses two or more cameras simultaneously, observing the part from different angles. This method enables measurements of three-dimensional coordinates, and both out-of-plane and in-plane displacements can be determined. Stereo-DIC can also be used on three-dimensional surfaces [35].

Another image correlation technique that has quite recently been developed is Digital Volume Correlation (DVC). Using DVC, displacements inside a 3D object can be measured from 3D images, typically required from X-ray tomography [36].

Depending on their solution method, DIC methods can also be categorised as either local or global.

In **local DIC**, the coordinate solution at one point is only dependent on a small neighbourhood of surrounding pixels close to the point, called a subset. The solution in one subset is independent of another subset, and the displacement distributions are obtained by repeating the displacement detection throughout the ROI [37].

In **global DIC** the solution at one point of the surface is dependent on the solution in other points, and displacements in all relevant coordinates of the region of interest are determined simultaneously [37]. Global DIC can, for instance, be performed in combination with a finite element mesh.

In the work related to digital image correlation presented in this project, 2D-DIC with a local coordinate solution is used, and unless otherwise specified, the remaining parts of the thesis concern this method.

Measurement setup and calibration

Before starting image acquisition, the DIC system is calibrated using a calibration target with known distances between image features [38], which can be a white image with black dots at fixed distances from each other. The purpose of the calibration is to establish parameters such as lens focal length and image scale and to correct for lens distortion [39]. Once a system is calibrated, the relative distance between the camera and the observed

surface must not be altered. Otherwise, measurement errors will occur.

Configuration of the DIC setup is done before calibration and includes, besides the choice of equipment, setting the focus and aperture, and the lightning and exposure, in the camera and the software simultaneously [40]. A general setup for 2D-DIC is shown in Figure 2.2.

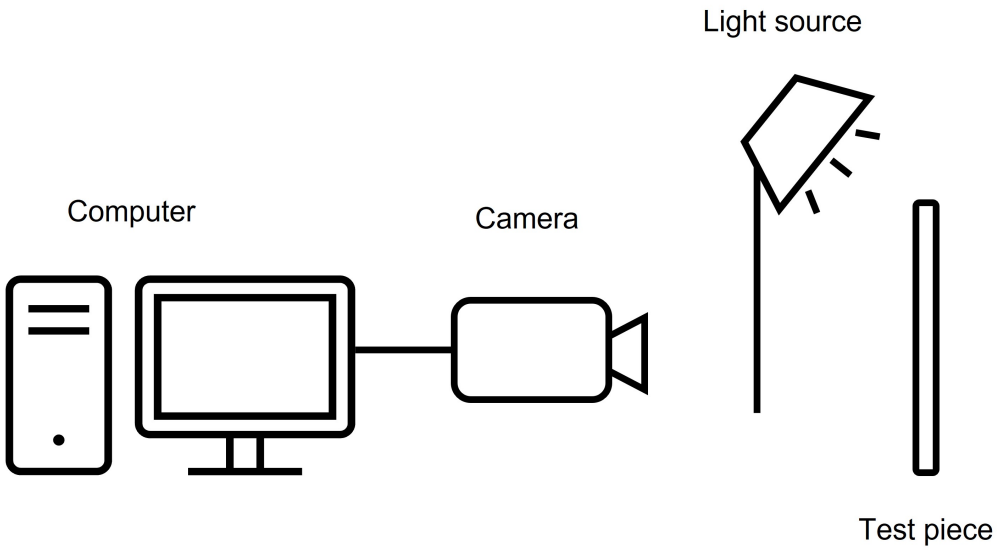

Figure 2.2: General setup 2D-DIC

Patterning methods

A fundamental assumption of DIC is that the motion and deformation of the imaged surface pattern of the specimen follow the deformation of the underlying specimen itself [33]. If the specimens do not have an adequate natural pattern, the pattern must be applied to the surface.

Typically, the applied pattern consists of black circular dots or speckles on a white background or white speckles on a black background. The speckles should be relatively small and uniform, with an optimum speckle size of 3 – 5 pixels [33]. Speckles smaller than this might lead to aliasing [41]. The pattern must be stochastically distributed, non-periodic and non-repetitive so that aperture can be avoided and subsets can be uniquely identified [42]. Further, matte surfaces are preferred to avoid reflection [42].

One of the most common methods for applying a speckle pattern is spray painting with intended overspray, or indirect spray, to obtain a random pattern, as this method easily allows for a fine speckle pattern. A uniform speckle size, however, might be challenging to obtain with this method. Some undersized speckles can be tolerated, but it will lead to increased noise [43]. Other patterning methods include, but are not limited to, stencils, stamps, toner powder, printed stickers with optimised patterns, airbrush, and spray

painting [33]. Examples of applied speckle patterns are shown in Figure 2.3.

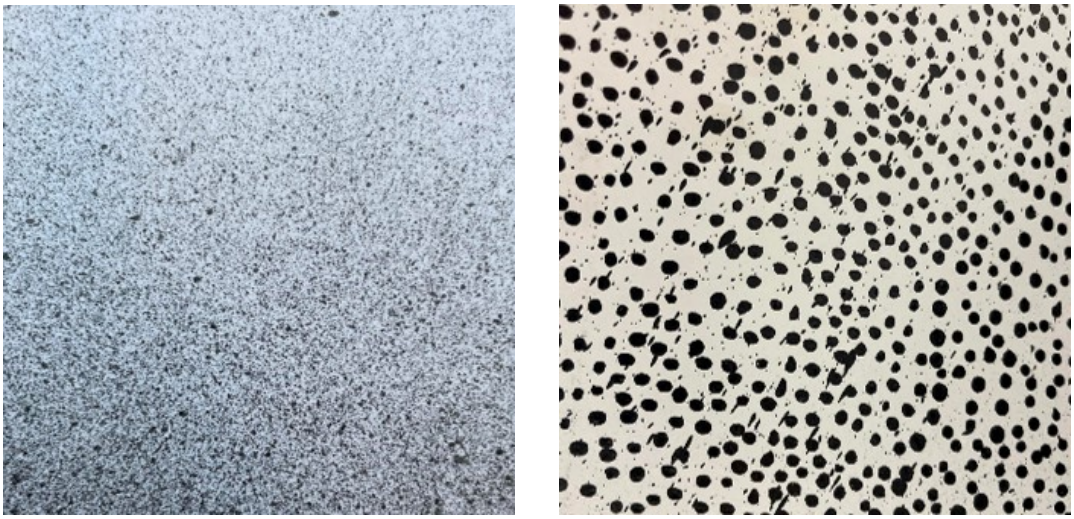

(a) (b)

Figure 2.3: Applied speckle patterns using spray painting with intended overspary (a) and stencil drawing (b).

2.4 Characteristics of Ultrasonic Testing

Ultrasonic testing is the predominant NDT method for composite laminates due to its relatively easy application and its high rate of accuracy. It is used as both production control and for detecting defects during service. The following presents the basic principles of ultrasonic inspection. For a more detailed overview, [44] and [45], can be consulted.

2.4.1 Basic Ultrasonic Principles

The ultrasound refers to the sound generated above the human hearing threshold of about 20 kHz. In ultrasonic testing for industrial purposes, frequencies from 100 kHz to 50 MHz are typically used. Ultrasound has a shorter wavelength than audible sound and can be reflected off small surfaces such as defects inside of materials, which is very useful for non-destructive testing and inspection [46].

The acoustic spectrum can be divided into a sub-sonic-, audible- and ultrasonic range. These are depicted, with the corresponding frequency range, in Figure 2.4.

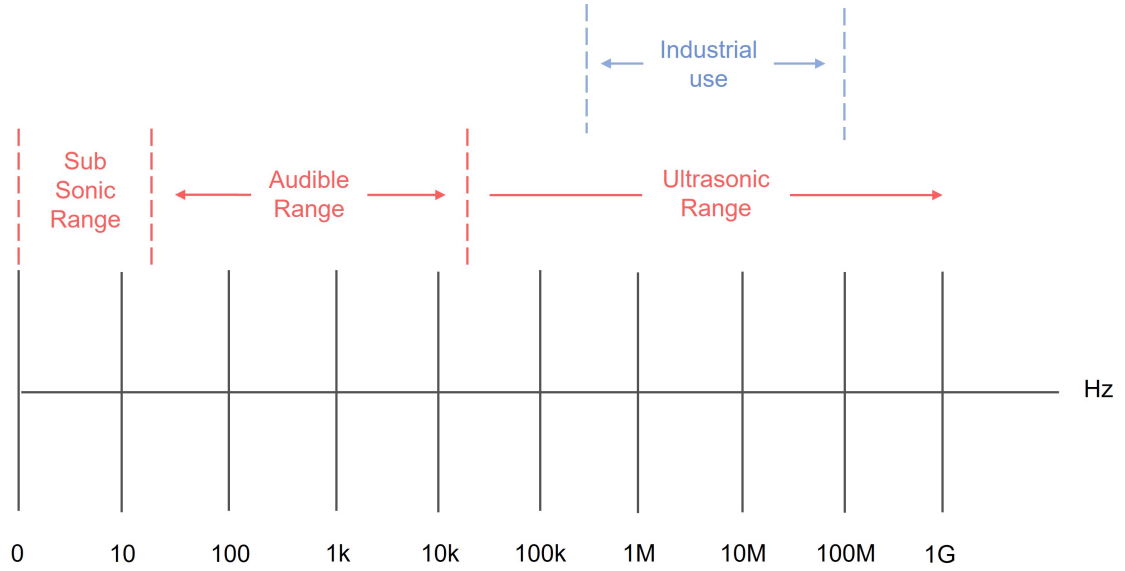

Figure 2.4: The acoustic spectrum

Properties of acoustic waves

The frequency, f, of an ultrasonic wave is the number of cycles N per second, as presented in Eq. (2.1).

$$f = 1/N \tag{2.1}$$

The velocity of ultrasound is constant when in a perfectly elastic material at a given temperature and pressure [46]. The relation between wavelength, material sound velocity and frequency is given in Eq. (2.2).

$$\lambda = c/f \tag{2.2}$$

Where λ is the wave length, c the sound velocity and f the frequency.

Impedance

Transmission and reflection of the ultrasonic waves depend on the acoustic impedance difference between the materials at the material boundary [6].

The acoustic impedance Z is defined as:

$$Z = \rho v \tag{2.3}$$

Where ρ is the material density, and v is the sound velocity of the material.

The amount of the sound pressure of the incident wave reflected at an interface is given by Eq. (2.4), and the amount transmitted is given by Eq. (2.5).

$$R = (Z_2 - Z_1)/(Z_2 + Z_1) \tag{2.4}$$

$$T = 2Z_2/(Z_2 + Z_1) \tag{2.5}$$

Where Z_1 and Z_2 are the acoustic impedance in materials one and two, respectively.

Further, the relation between the reflected and transmitted signal is given by Eq. (2.6).

$$1 + R = T \tag{2.6}$$

The physical principles of ultrasonic waves at material boundaries are further explained in [44].

Wave propagation

Unlike light waves, which can travel in a vacuum, ultrasonic waves requires an elastic medium such as a liquid or a solid. Different types of wave propagation are used for ultrasonic inspection, including longitudinal waves, shear waves, Rayleigh (surface) waves and Lamb (plate) waves. The two types most commonly used in industrial inspections are longitudinal (compression) waves and shear waves [46]. In longitudinal waves, oscillations occur in the direction of the wave propagation, in the form of compression and expansion. Longitudinal waves can propagate in gases, liquids, and solid materials. In shear waves, the particles oscillate at an angle transverse to the direction of the propagation of the wave. Shear waves require a solid material for effective propagation.

2.4.2 Application of Ultrasonic Testing

In ultrasonic non-destructive testing, high frequency acoustic waves are introduced into a material for detection of discontinuities, commonly using one or more piezoelectric transducers [45]. The transducer can act as a transmitter or receiver of the acoustic signal.

Any damage within a material will interrupt the acoustic wave, and possible defects can be detected based on the reflected or the transmitted waves as they propagate across the substrate material. When the waves interact with material boundaries, such as the material back wall or a discontinuity within the material, they will be partly reflected and partly

scattered. If the impedance mismatch between the materials is high, such as between a solid material and air, the reflection of the signal will also be high. The reflected signal or the attenuation of the signal can be used to indicate whether or not a defect is present in the test material [47].

Coupling

Due to the high impedance difference between air and solids, proper coupling between the transducer and the substrate is needed for the acoustic wave to propagate through the test material properly. If not, the signal will simply be reflected at the air-solid interface between the transducer and the test material [6].

Two main methods of ensuring proper coupling between the transducer and the substrate material are contact testing with a coupling agent and immersion testing. In contact testing, a coupling agent such as glycerol, kerosene, or oil is typically used, while in immersion testing, the test piece is typically submerged in water, and water is used as couplant [23].

Different ultrasonic techniques

There are several techniques used in ultrasonic inspection, where pulse-echo (PuE) mode and through-transmission (TT) are two of the most common [6]. In this project, PuE has been used to detect defects in composite materials.

In **pulse-echo** mode one transducer acts as both the emitter and the receiver [48]. Short-duration pulses are sent through the test material. When the acoustic wave meets an interface with an impedance mismatch, such as a discontinuity or the back wall of the object, the wave is reflected to the transducer [49]. The time of flight is used to estimate the thickness from the transducer to the reflector. This way, discontinuities within the material can be located, or the material thickness can be measured when no discontinuities are present. An advantage of this method is that only one side of the object to be tested needs to be accessible.

In **through-transmission** mode, two transducers are used, one on each side of the test material. One transducer act as the emitter and the other as the receiver. In this method, the attenuation of the signal is used to indicate imperfections in the material. Thickness measurement usually is not possible with this technique [47].

Other methods include **pitch-catch** where two transducers are placed closely together on the same side of the material, and **guided waves** where the transducers are placed relatively far away from each other, and the wave is sent at an angle [6].

Figure 2.5 illustrates the four techniques mentioned.

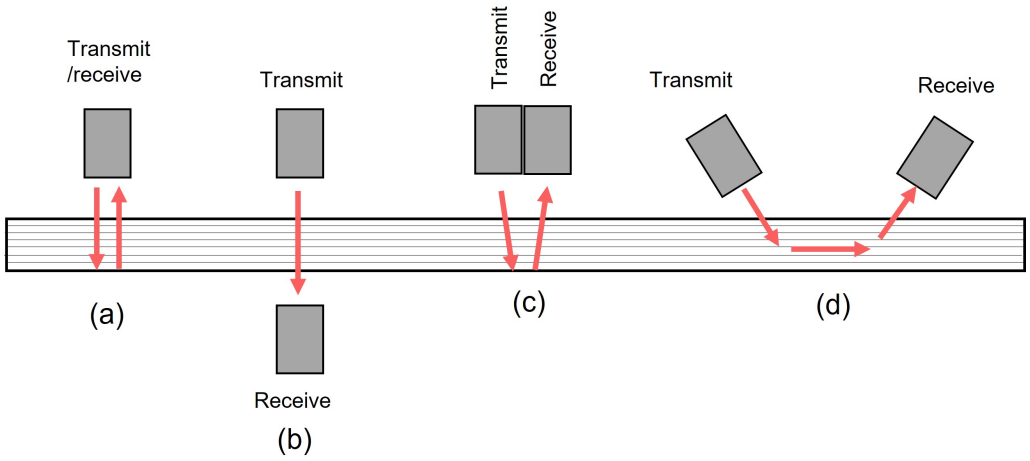

Figure 2.5: Common ultrasonic inspection techniques: (a) Pulse-echo, (b) Through-transmission, (c) Pitch-catch, (d) Guided waves

Time of flight

Using the PuE method, the time of transit of the propagating wave through the test piece, called the time of flight, and the amplitude of the received signal can be measured.

The time of flight is further used to calculate the thickness of the material. For PuE the thickness, T, is given by (2.7), where c is the material sound velocity, and t is the time of flight.

$$T = ct/2 \tag{2.7}$$

The thickness measurements can be used to locate defects. If the acoustic wave interacts with a defect, it will be reflected, and the measured thickness will indicate the position of the defect within the material.

Measurements of the relative change in amplitude can be used to determine the size of the defects or to measure the attenuation of the material. The sizing of defects was covered further in the specialization project leading up to this thesis [8].

Sensitivity and resolution

Sensitivity and resolution refer to an ultrasonic system's ability to locate discontinuities. Sensitivity is the ability to locate small reflectors at a given depth in the material. At the same time, the resolution is the ability of the system to locate and separate reflectors that are close together (range resolution) or located close to the surface (near surface resolution) [46]. Both generally increase with increasing frequency.

Noise

There is always some amount of unwanted noise in a physical system. If no noise had been present, one could amplify all signals to a usable level. However, because of noise, a sensitivity limit will exist, which is reached when the signal falls below the noise floor, as an increase in gain will also increase the noise level [47].

Sound field

A transducer's sound field is divided into two zones; the near field and the far field. The near field is the area directly in front of the transducer. In this area, the echo fluctuates before reaching a last maximum. The distance to the last maximum is called the near field distance and is the natural focus of the transducer. Beyond the near field, distance is the far field, where the echo gradually drops to zero. Therefore, the optimal detection results will be obtained in the area just beyond the near field [46].

The near field distance, N, is given by Eq. (2.8), where D is the diameter of the transducer head, f is its frequency, and c is the sound velocity of the material [46].

$$N = D^2 f / 4c \tag{2.8}$$

Dead zone

For single element transducers used in pulse-echo testing, reflections at short distances from the transducer cannot be detected. Single element transducers act as both transmitters and receivers of the acoustic signal; however, they cannot perform both actions simultaneously, and switching between the two takes up a fraction of the repetition period. If a reflection occurs before the switching is complete, the system cannot detect the echo [47].

The dead zone is the length in millimetres of the material affected by the emission pulse in which it is not possible to detect echoes from reflections due to discontinuities [49]. Thus, the larger the dead zone is, the more challenging it is to accurately locate the first echo of the signal. It can be avoided using immersion testing, where water works as the coupling between the transducer and the test material, and the dead zone will take place in the water and not in the test material.

Test displays

In Ultrasonic Testing, different data presentations are available to locate and identify flaws. In an A-scan, or amplitude mode display, the acoustic echos are displayed as a function of thickness. A B-scan shows a cross-sectional view of the object under testing, while a C-scan presentation provides a plan-type view of the size and location of the test specimen feature. However, an automated data acquisition system is typically needed for C-scan ultrasonic testing [23]. In the work presented in this thesis, A-scan is used.

3 State of the art

This chapter discusses the theoretical capabilities of digital image correlation and ultrasonic inspection as NDT methods for composites, as well as considerations when applying the methods in practice. In addition, some relevant findings from previously conducted research are presented to establish state-of-the-art further.

3.1 Application of Digital Image Correlation for Inspection Purposes

Although not a very established inspection method, advances in camera technology, optical sensors and image processing have made optically based measurement techniques such as digital image correlation appealing for NDT [34].

3.1.1 Areas of Use

Digital Image Correlation is a non-contact technique and does not interfere with the functionality of a part [35]. It can be used in various applications where sizes may vary from small coupons in experimental testing to entire wind turbine blades or sub-assemblies of air crafts [33]. All types of materials can be examined, such as metals, polymers, concrete, geological samples, biological tissues, and composite materials [33]. The principle remains the same regardless of the inspected material, and contrary to ultrasonic inspection, no particular considerations must be taken to inspect composite materials compared to isotropic materials using DIC.

As only a relatively simple optical setup is needed, the requirement for a testing environment is low, enabling, for instance, measurements of submerged objects or testing in environments with elevated temperatures [50], [51], [52].

3.1.2 Defect Detection in Composite Materials

Under load, the deformation of an object without defects is different from the deformation of an imperfect object. If the defect in the object is significant enough, its effect may be visible in a surface strain map. By setting the image acquisition rate to an appropriate order, which could be in the range of milliseconds to days, or even years apart, it is possible to evaluate how the object deformation and surface strain changes during its service life enabling the use of DIC for non-destructive testing. DIC, thus, has the potential to detect failure mechanisms as long as they affect the strain distribution of the component being inspected.

Following the above logic, fibre failure can be expected to be detectable by observing changes in the surface strain as it causes severe changes in the material stiffness of a composite laminate. Moreover, delamination and debonding have an impact on the out-of-plane properties, which may change in-plane strain distributions. Delaminations may also impact in-plane strains if the object is subjected to out-of-plane bending forces. Hence, it is possible that delaminations could be detected using DIC. Matrix cracking reduces the material stiffness but not to the same extent as fibre failure. Still, the presence of matrix cracking can possibly be measured indirectly by changes in the strain field.

Manufacturing defects, such as voids, are a part of the initial state of the inspected object and might therefore be more difficult to detect by comparing in-service measurements to reference values taken before manufacturing unless other types of damage are induced. However, an intact and damaged area will respond differently to an applied load. If strain concentrations appear where a smooth strain field is expected, which is the case for most of the pipeline area, this likely indicates the presence of damage.

3.2 Ultrasonic Inspection for Composite Materials

Ultrasonic testing is one of the most common methods for non-destructive evaluation of composite laminates. It is also a well-known method for inspecting metal structures [14]. Although the principle remains the same, a few different considerations must be taken depending on which material is to be evaluated.

3.2.1 Resolution and Laminate Thickness

The resolution of the method is related to the frequency of the ultrasonic wave. Higher frequency means shorter wavelength and better resolution of the measurements. For this reason, metals are inspected with the highest possible frequency. Composites, however, being non-homogeneous materials, need lower frequency acoustic waves for the signal to go all the way through the laminate and not be reflected at every fibre-matrix interface

causing a loss in signal [53]. The frequency is especially important for glass fibre reinforced composite materials, which have very high reflectivity of the ultrasonic signal [54]. For ultrasonic inspection of composite materials, frequencies below 5MHz and maybe even below 1MHz have to be used, depending on the laminate thickness and the fibre-matrix composition [6].

Typically, the measurement resolution gets lower as the laminate thickness increases, and the defect lies deeper inside the laminate. Meaning that when investigating thin laminates, a higher frequency can be used, giving a better resolution of the measurements, while for thicker laminates, a lower frequency is needed for the signal to carry through the material, resulting in a lower resolution of the measurements. Lower frequency ultrasound, however, poses the risk of missing discontinuities with a diameter smaller than half of the wavelength [53]. The defects must thus be more prominent to be detected in thick laminates, such as in composite pipelines, compared to thin laminates, like the ones used in aerospace structures.

3.2.2 Inspection of Curved Geometries

Complex and curved geometries, such as small diameter pipes, can be challenging to inspect with conventional contact ultrasonic techniques. As the pipe diameter decreases, the contact area between the transducer and the pipe surface decreases accordingly, and maintaining proper transducer positioning can be challenging.

The DNV guideline for non-destructive testing, DNVGL-CG-0051, recommends that the gap between the test surface and the transducer should not exceed 0.5 mm[55], which corresponds to a part radius given in Eq. 3.1.

$$D \geq 15A \tag{3.1}$$

Where D is the diameter of the part, and A is the transducer's length in the inspection's direction.

When the contact area between the inspected part and the probe is too small, there are several strategies for obtaining proper coupling so that components with complex surfaces can also be inspected using ultrasonic testing.

One way of inspecting curved or irregular surfaces is to use **immersion testing**, where the transducer and the inspected test piece are submerged in water, and water is used as the coupling medium [56]. This method enables the inspection of parts with varying geometry as well as rougher surfaces without loss of coupling. It also provides a high level of acoustic performance due to the low attenuation of water and the consistency of the coupling. Immersion testing might be difficult to perform manually as the relative distance

between the transducer and the test piece must remain the same to get a readable signal.

Another method for inspecting curved geometries is to combine a flat transducer with a **contoured wedge** specifically shaped to fit the surface of the part being inspected [57]. Then a fluid couplant is required at both the transducer-wedge interface and the wedge-test piece interface. This technique requires one particular wedge for each surface geometry, which is impractical for applications where the surface profile of the component is inconsistent.

A **conformable wedge** made of a flexible membrane filled with water can also be used [58]. This type of wedge conforms more easily to the shape of the test surface than a contoured one. This method combines the advantages of immersion testing and contact testing with a contoured wedge as it is easy to use for manual inspection while still enabling inspection of parts with varying geometry and having performance similar to water. A drawback of this technique is that the offset of the probe must be carefully selected so that the repeat echoes from the wedge-test piece interface do not interfere with signals from discontinuities within the test piece.

3.2.3 Damage Detection

Delamination is the primary failure that can be detected using ultrasonic testing. Finding the position, depth, and size of a delamination within a laminate is possible. Delamination, as well as debonding, significantly reduce the interlaminar shear strength and through thickness tensile strength. Indirectly these damage mechanisms also reduce the in-plane compressive strength and can propagate, causing catastrophic damage [54].

The acoustic impedance of a typical polymer composite is in the order of 470 000 g/cm^2s, whereas air is only 40 g/cm^2s [6]. In virtue of (2.4) and (2.5), a composite-to-air interface will have a transmission coefficient of 0.0002 and a reflection coefficient of -0.9998, where the negative sign of the reflection coefficient indicates the change of the propagation direction of the reflected signal. This low transmission and high (absolute) reflection explain why delaminations can be detected using ultrasound. For comparison, the acoustic impedance of water is in the range of 150 000 g/cm^2s [59], depending on its temperature.

When it comes to other failure mechanisms, excessive void content will scatter the transmitted signal, causing a reduction in amplitude or complete loss of signal. This way, voids can be detected, and the void content can be estimated. Fibre failure can usually be detected mainly in the presence of nearby delamination, while matrix cracking is difficult to detect using ultrasonic testing [60].

3.3 Summary of Previous Research

Non-destructive testing and evaluation of composites have been developed over many years. However, very little work has been done concerning composite pipelines, other than establishing that the necessity for NDT exists [2], [3], [4], [54].

Most of the NDT work in composites are associated with the aerospace industry, where thin composite laminates are used [61], [62], [63], [64]. Composite pipes, on the other hand, are made of thicker laminates, which reduces the possibilities of NDT methods to some extent. Little attention has been paid to the inspection of thick laminates, but acknowledging the inspection challenges when applying the common testing techniques [65]. An overview of NDT methods is given in section 2.2.

Still, new structural applications of composite materials increase the use of thick laminates. One can find examples of non-destructive evaluations of thicker composite laminates in several areas, such as in relation to composite patch repair of metal structures, as well as inspection of wind turbine blades [66], [67], [68].

3.3.1 Ultrasonic Testing

Amenabar et al. used ultrasonic pulse-echo technique to detect delaminations with a size of 30 mm and thicknesses in the range of 0.055-0.25 mm in 10 mm thick GFRP specimens. They could detect all delaminations using an electronically focused 5 MHz transducer [68]. Still, most attempts at inspections of thicker structures using ultrasonic testing have been performed at frequencies of 1 MHz and lower, with several authors indicating that 0.5 MHz frequency is the best option for GFRP structures up to about 50 mm thickness [69], [70].

The capability of ultrasonic inspection for thick laminates has been further demonstrated by Mouritz et al., who were able to detect delaminations as small as 10 mm more than 100 mm below the surface using pulse-echo ultrasonics [71]. Further, Daniel and Wooh successfully detected Teflon inclusions of 25 µm thickness at a depth of 20.8 mm in a 200-ply-thick composite block [72]. Similarly, Hassen et al. were able to capture fabricated Teflon, and Kapton defects in 14.1 mm thick thermoplastic composite specimens using both pulse-echo mode and through-transmission mode with a 1MHz transducer [73]. They found that though both modes could detect the defects, through-transmission gave a better indication of the shape. Fortunko and Fitting developed a broadband ultrasonic pulse-echo system with an improved Signal-to-noise ratio and successfully inspected through a 50 mm-thick GFRP composite containing two interface layers [69].

Another important aspect to consider when using ultrasonic measurements for evaluating composite pipelines is their curved geometry. Curvature in a composite laminate has the potential to significantly complicate the ultrasound inspection due to the high sensitivity

of wave velocity in the propagation direction. It also gives less contact area between the transducer and the test material. Gresli et al. found that low frequency longitudinal guided waves can be used to detect surface defects with high sensitivity and on relatively large distances in curved parts [74]. Hopkins et al., on the other hand, demonstrate the ability of Surface-Adaptive Ultrasound to mitigate the challenges of complex geometries using linear transducers [75].

3.3.2 Digital Image Correlation

Digital Image Correlation is, contrary to ultrasonic inspection, not yet been established as a conventional non-destructive inspection method, and there are significantly fewer resources on the topic than for more well-known and conventional methods. However, some work on damage detection of composites have been performed [76], [77], [78].

Szebényi and Hliva performed 2D-DIC measurements on 8-layer thick CFRP and GFRP specimens containing different types of artificial through-delaminations while performing tensile and compression tests [79]. The specimens were loaded to 1% strain during the tensile test and 0.4% strain in the compression test. In most cases, the approximate locations of the delaminations could be detected from the strain fields by comparing the strain values in the damaged areas with the strain values in the intact ones.

As for thick composites, Leblanc et al. demonstrated the capabilities of 3D-DIC by inspecting a 9-meter composite wind turbine blade with previously identified damaged areas [80]. The results indicated that the approach could clearly identify failure locations in the blade curvature during load. In addition, a stitching technique was proposed to stitch together several field-of-views allowing simultaneous observation of large structures. While Devivier et al. detected strain singularity, caused by artificial PTFE film delaminations, in the surface strain maps of carbon/epoxy-specimens with 32 layers, subjected to bending [81].

4 | Experimental Method

Two different non-destructive inspection techniques have been tested experimentally, digital image correlation and ultrasonic inspection, to assess their potential for use in polymer composite pipeline inspection. Ultrasonic inspection is tested for both flat composite specimens and thermoplastic pipe samples.

This chapter presents the specimens, equipment, and test setup used for the two inspection techniques in detail.

4.1 Digital Image Correlation

Digital image correlation is used to locate artificial defects, in the form of fabricated delaminations and flat bottom holes (FBH), in 21.5 mm thick composite GFRP specimens under tensile load.

A 28-layer GFRP/epoxy laminate is manufactured using vacuum assisted resin transfer (VART). The defects are positioned at different depths of the test laminate. 2D-DIC is combined with tensile testing to obtain in-plane strain fields of the specimens at different strain levels.

4.1.1 Materials

The specimens investigated are made from glass fibre reinforced polymer (GFRP) laminate with a fibre volume ratio of about 50%. The fibre mats are made of stitched bonded unidirectional glass fibre mats from Devold AMT, while Hexin EpikoteTM RIMR135 epoxy resin mixed with EpikureTM RIMH137 curing agent is used as matrix material. The mixing ratio of the resin and hardener is 100:30 by weight.

The fabricated delaminations are made from PTFE Teflon film brushed with Renlease QV 5110 release wax.

4.1.2 Specimen Preparation and Geometry

Laminate production

A symmetrical and balanced laminate with layup [90/0]14s is produced using VART [82]. The total laminate thickness is 21.5 mm. Hence, the layer thickness is about 0.77 mm.

The laminate is cured under vacuum at room temperature for 48 hours and then 18 hours at 80 C°. After curing, the laminate is cut into 250 mm x 50 mm specimens using a water jet.

Fabricated damage

The composite specimens contain damages in the form of fabricated delaminations and FBHs, machined to have a flat surface at the hole bottom. There are four specimens containing each type of damage, which are located at different depths.

Artificial delaminations are embedded at different positions in the test laminate during the layup process. The delaminations have a thickness of 5 µm and are 20 mm high and 50 mm wide, thus covering the entire width of the specimens. FBHs, with a diameter of 20 mm, are drilled to match the location of the delaminations. Furthermore, the defects are positioned slightly off-centre in the in-plane loading direction, with some specimens having the defect in the upper part and some in the bottom part of the specimen during the mechanical test.

The dimensions of the laminate specimens are illustrated in 4.1, and an overview of the type and approximate position of the introduced damage is presented in Table 4.1.

Application of speckle pattern

A speckle pattern is applied to the specimens using white spray paint for the background and black spray paint with indented overspray to achieve a random speckle pattern with fine speckles. Two layers of white paint are applied to obtain good coverage. Figure 4.2 shows the resulting speckle pattern.

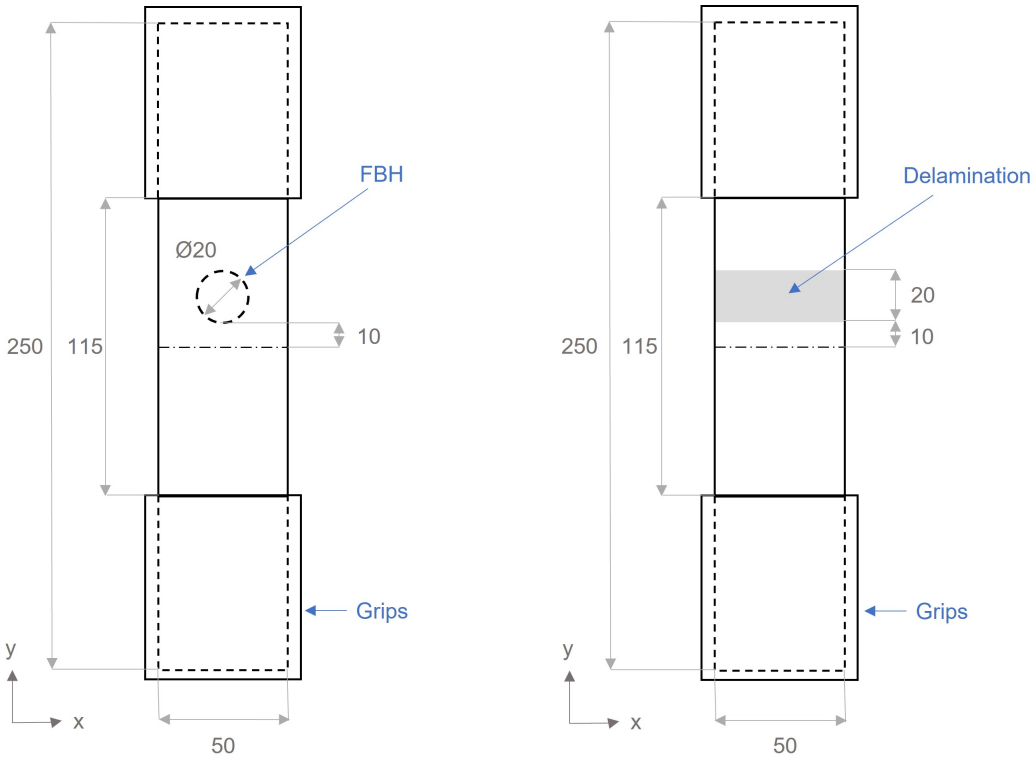

Figure 4.1: Specimen geometry [mm]

Table 4.1: Geometry and position of defects

Specimen	**Type of defect**	**Size**	**In-plane position**	**Depth/ Location**	**Distance test surface**
H1	FBH	Ø20 mm	up	10.8 mm	10.7 mm
H2	FBH	Ø20 mm	down	7.7 mm	13.8 mm
H3	FBH	Ø20 mm	up	4.6 mm	16.9 mm
H4	FBH	Ø20 mm	down	1.6 mm	19.9 mm
D1	Delamination	20 mm	up	Between ply 14 and 15	10.8 mm
D2	Delamination	20 mm	up	Between ply 10 and 11	13.8 mm
D3	Delamination	20 mm	up	Between ply 6 and 7	16.9 mm
D4	Delamination	20 mm	up	Between ply 2 and 3	20.0 mm

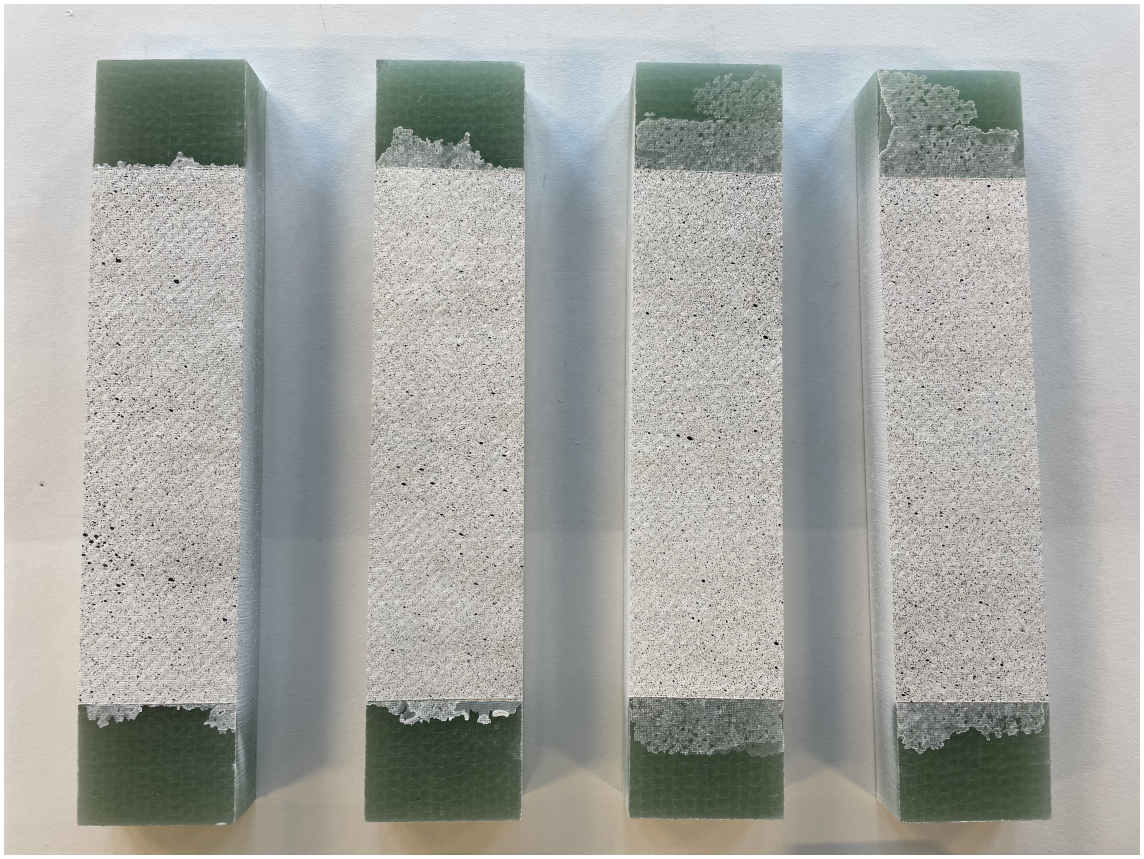

Figure 4.2: Specimens with applied speckle pattern

4.1.3 Equipment and Test Setup

Tensile tests are conducted using an Instron 8854 test machine with a 250 kN loading cell, and 2D-DIC is used to measure the in-plane strain fields of the loaded specimens. A Stingray F-504B camera from Allied Vision, with a resolution of 5 megapixels and a frame rate of 9 frames per second, is utilized in combination with VicSnap image acquisition software from Correlated Solutions to perform the DIC measurements.

The experimental setup is illustrated in Figure 4.3.

The mechanical tests are performed using displacement control, with a 1% strain limit and a displacement rate of 0.5 mm/min. The free length of the specimens is 115 mm. In the VicSnap software, the image acquisition rate is set to 1 Hz, and the exposure time is set to 6.5 ms. Further, the focus and shutter time of the camera is adjusted to obtain optimum resolution.

Before testing, the DIC system is calibrated using a calibration target containing black dots at a known distance from one another on a white background.

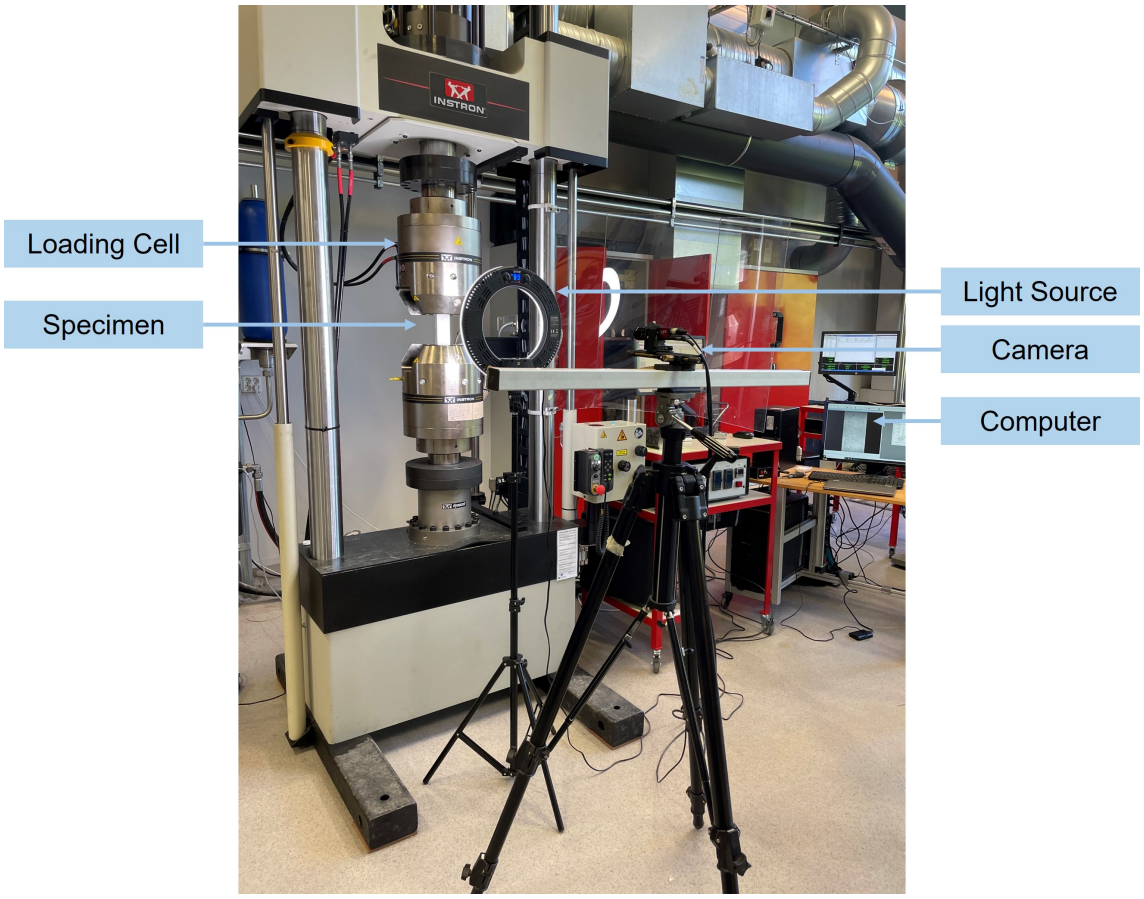

Figure 4.3: Test setup tensile testing with 2D-DIC measurements

4.1.4 Post Processing Procedure

Vic-2D from Correlated Solutions is used as post processing software, providing full-field measurements of in-plain strains of selected ROIs based on images taken before and throughout the test and the calibration. For each evaluated property, a coloured map is displayed. This map can be viewed on a local or global scale. The local scale refers to the unique image, and the global refers to all the images from a test. By choosing a global scale, the main changes throughout the test can be tracked. If an identical global scale is chosen for several tests, different specimens can be compared. The strain fields of the specimens are investigated by comparing areas with known defects with areas without fabricated damages. With images taken continuously throughout the mechanical tensile test, several strain levels can be investigated.

4.2 Ultrasonic Testing of Thick Laminate Specimens

Ultrasonic inspection is performed on 21.5 mm thick composite laminate containing fabricated delaminations and FBH introduced at fixed positions within the test laminate. Three different frequencies of ultrasonic contact testing are used to investigate the damaged areas.

4.2.1 Specimen Preparation and Geometry

Ultrasonic testing was performed on the same samples investigated by DIC. The materials and method used in the preparation of the specimens, as well as their geometry and the position of defects, are further explained in Sections 4.1.1 and 4.1.2.

Note that this inspection is performed after the specimens have been subjected to low-load tensile testing and slight matrix cracking has been introduced. However, matrix cracking at this level cannot be detected by UT, and it was found that there was no difference in the acoustic signal from a reference specimen without matrix cracking to the specimens containing matrix cracks. Therefore, it is deemed that the impact of the matrix cracks on the results from the ultrasonic inspection is negligible. Moreover, this inspection is performed on painted specimens, adding an additional 25 - 75 µm of thickness to the specimens.

4.2.2 Device and Equipment Setup

Ultrasonic Test Machine

Ultrasonic measurements are taken using a 38DL PLUS Ultrasonic thickness gauge from Olympus, shown in Figure 4.4 used for pulse-echo testing. The thickness gauge is used for pulse-echo testing and can measure parameters such as thickness, sound velocity and time of flight and offers an A-scan view. Only inspection mode 1, which measures the time of transit of the first returning echo, is available.

Further, the standard resolution of the thickness measurements is 0.01 mm, and a high penetration software option is available for inspecting attenuating materials such as glass fibre composites.

Figure 4.4: Ultrasonic thickness gauge

Transducers

Three single-element longitudinal wave transducers at different frequencies (5 MHz, 2.25 MHz, and 0.5 MHz) are used to inspect the specimens:

1. Olympus M109-RM 5 MHz Ø13mm
2. Olympus M106-RM 2.25MHz Ø13mm
3. Olympus M2008-SB 0.5Mhz Ø25mm

All three transducers are contact transducers intended for use in direct contact with the test piece. The 0.5 MHz transducer is used with a high penetration software option, while the other two are used with the standard option.

Inspection setup

The specimens are inspected using direct contact between the transducer and the specimen. A glycerin coupling gel is used to ensure an adequate contact area.

4.2.3 Inspection Settings

The specimens are inspected in areas both with and without defects. The thickness and the amplitude of the reflected ultrasonic signal are displayed in an A-scan view. If the measured thickness or amplitude differs from the thickness and amplitude at an intact specimen area, it may indicate the presence of a discontinuity.

In Figure 4.5 an ultrasonic A-scan of a non-defected area is shown. The thickness is measured from the first echo of the back-wall signal, which is the highest peak. The lower peak on the right side of the plot is the second echo from the back wall of the specimen and is equal to twice the thickness. Moreover, the very high amplitude at the beginning of the plot is noise from the transducer-material interface, and the series of smaller peaks that follow are reflections at fibre-matrix interfaces within the material.

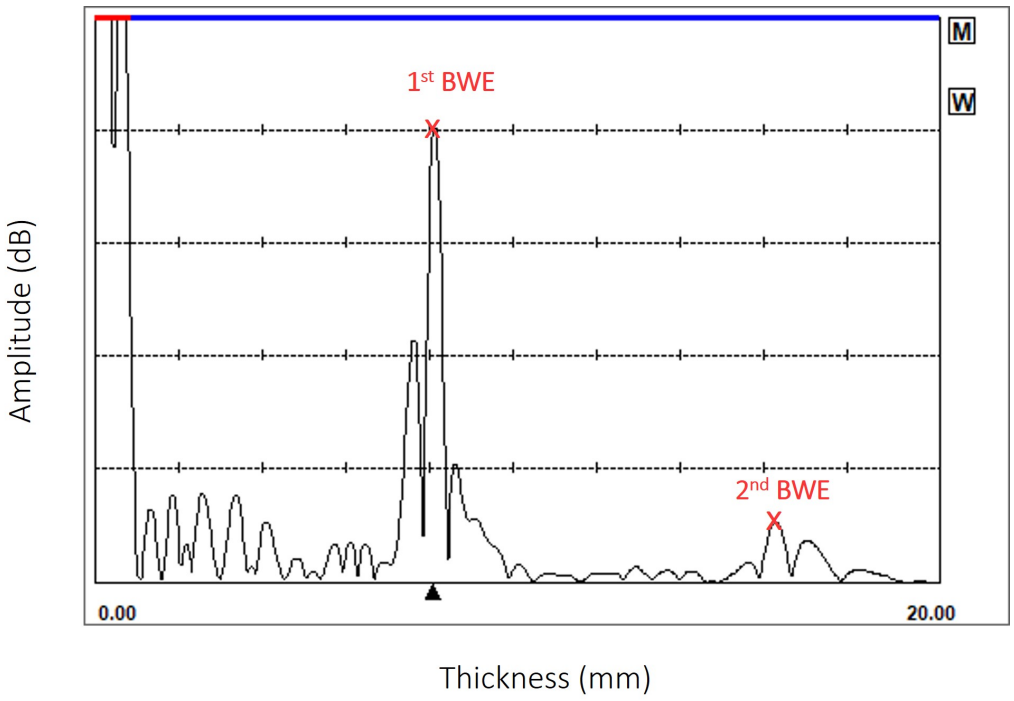

Figure 4.5: A-scan of non-defected area, with 1^{st} and 2^{nd} back wall echo (BWE)

The inspection is performed using a sound velocity of 3.244 µm/s, calibrated using a specimen with known thickness. The receiver gain is set so that the back wall echo (BWE) at a non-defected area is at 80% acfsh.

4.3 Ultrasonic Testing of Pipe Samples

Ultrasonic inspection is also performed on thermoplastic and glass fibre reinforces thermoplastic pipe samples with flat bottom holes (FBH) of various sizes.

FBHs of different diameters are drilled at specific positions and depths to simulate defects in the pipe samples. The samples are inspected using contact and immersion testing with three different frequency transducers. For the transducer with the largest diameter, a contoured epoxy wedge is produced to perform contact testing to obtain a large enough contact area between the transducer and the test piece.

4.3.1 Materials

Two types of pipe samples are investigated: A thermoplastic polymer pipe and a glass fibre reinforced thermoplastic pipe. The polymer pipe is a PE100 polyethylene (PE) pressure pipe from Pipelife Norge AS, while the composite pipe is a glass fibre reinforced PE pipe with a PE liner.

4.3.2 Specimen Preparation and Geometry

The PE pipe has an outer diameter of 140 mm and a measrued thickness of 13.4 mm. The outer diameter of the GFRP pipe sample is 136 mm, and the total thickness is 13.2 mm. The thickness of the glass fibre layer is measured to be 4.5 mm, and the liner is measured to be 8.7 mm.

The pipe samples are cut into four specimens in the axial direction using a band saw. FBH of various diameters and at three different depths are drilled to simulate artificial defects in the pipe material. For the composite pipe, depths of the holes are selected to introduce defects in the fiber reinforced laminate, the liner, and the interface between the two. Moreover, the holes have the same distance from the test surface for the polymer pipe as in the composite specimens. An image of the pipe samples is displayed in 4.6, and an overview of the size and position of the FBH investigated are presented in Table 1.

Table 4.2: Size and position of FBH

Specimen	Hole Diameter	Depth	Location	Distance test surface
PE	4, 6, 15, 20 mm	11.0 mm	-	2.4 mm
PE	4, 6, 15 20 mm	8.7 mm	-	4.7mm
PE	4, 6, 15, 20 mm	3.0 mm	-	10.4 mm
GFRP	4, 6, 15, 20 mm	10.8 mm	PE liner	2.4 mm
GFRP	4, 6, 15, 20 mm	8.5 mm	GFRP/liner interface	4.7 mm
GFRP	4, 6, 15, 20 mm	2.8 mm	GFRP material	10.4 mm

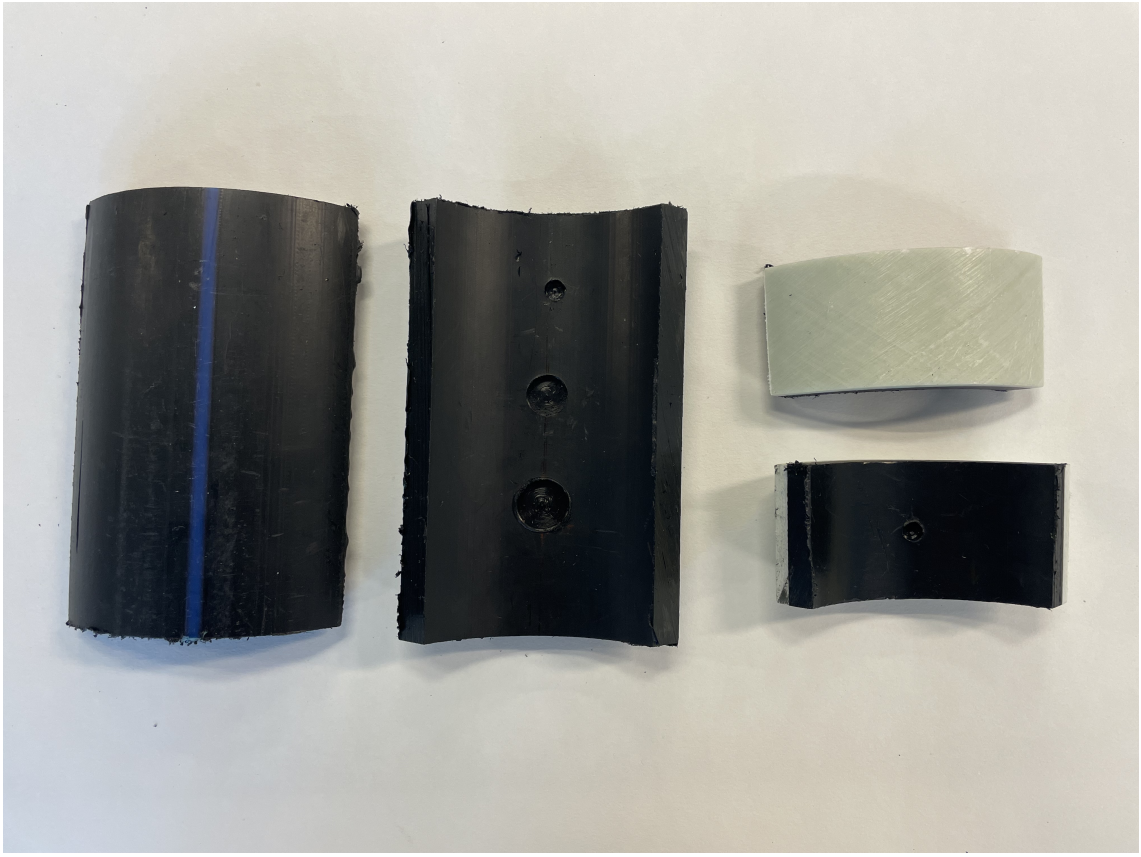

Figure 4.6: PE and GFRP pipe samples

4.3.3 Device and Equipment Setup

A 38DL PLUS Ultrasonic thickness gauge from Olympus is used to perform the ultrasonic measurements, with transducers at frequencies of 5 MHz, 2.25 MHz, and 0.5 MHz. An overview is found in section 4.2.2.

Further, three different inspection setups are used, contact testing with and without the use of a contoured wedge, and immersion testing.

Contact testing

Contact testing with the transducer directly in contact with the test piece is performed using 5 MHz and 2.25 MHz transducer frequencies.

Contact testing with wedge

For the 0.5 MHz transducer, a contoured wedge is used to conduct contact testing due to the diameter of the probe. A wedge is produced for each of the two pipe samples to fit the pipe diameter specifically.

A 3D-printed prototype is used as a positive part to cast a negative silicone mould. The silicone mould is then used to cast a homogeneous epoxy wedge with the exact dimensions as the 3D-printed prototype. The epoxy mould is made of Hexin EpikoteTM RIMR135 epoxy resin mixed with EpikureTM RIMH137 curing agent, with a mixing ratio of 100:30 by weight. The height of the wedge is chosen to be significantly larger than the thickness of the two pipes so that its acoustic reflections do not interfere with the reflected signals from the pipe specimens. Further sketches and models of the wedge is found in Appendix A.

Figure 4.7 (a) shows the setup for contact testing using a contoured wedge between the 0.5 MHz transducer and a PE pipe specimen.

Immersion testing

Immersion testing is performed with the specimen placed in a glass container filled with water. For industry purposes, a waterproof immersion transducer would typically be used for immersion testing; however, single element contact transducers are used for this inspection.

Therefore, a small 3D-printed support structure is used to hold the electric coupling of the transducer above water and hold the transducer still while conducting the inspection. Further illustrations of the 3D-printed support structures can be found in Appendix B

The inspection setup for immersion testing using the 2.25 MHz transducer and a GFRP specimen is displayed in Figure 4.7 (b).

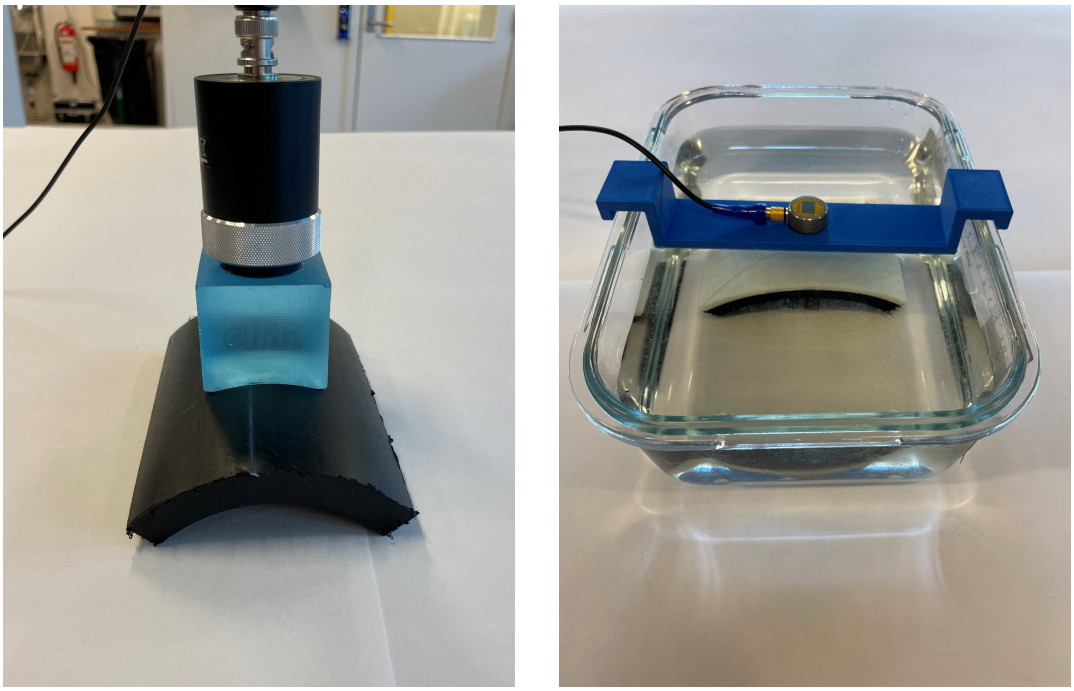

(a) (b)

Figure 4.7: Ultrasonic inspection setup for (a) contact testing with contoured wedge and (b) immersion testing

4.3.4 Transducer Settings and Inspection Interval

Each specimen is investigated in the area of the FBHs as well as a non-defected area, using both contact testing and immersion testing, at inspection mode 1. The sound velocity of the polyethylene material is calibrated to be 2.344 mm/µfrom the PE pipe sample. For the GFRP pipe, the same velocity is assumed, as calibrations for the two separate pipe layers are not possible. The same velocity is used for all transducers.

For contact testing with direct contact between the transducer and the test piece, the through-thickness location of the FBH can be found directly from the measured thickness output of the detected FBH, which is explained in section 4.2.3.

Contact testing with wedge

When a wedge is used between the transducer and the test piece, the reflections from the wedge-test piece interface will also be displayed in the ultrasonic A-scan. To neglect these, the inspected interval is adjusted manually.

Figure 4.8 shows a measurement of a non-defected area using a contoured wedge. The first peak indicated is the wedge-test piece interface, and the second peak is the second echo of the interface. The valid inspection area is the area between these two echoes.

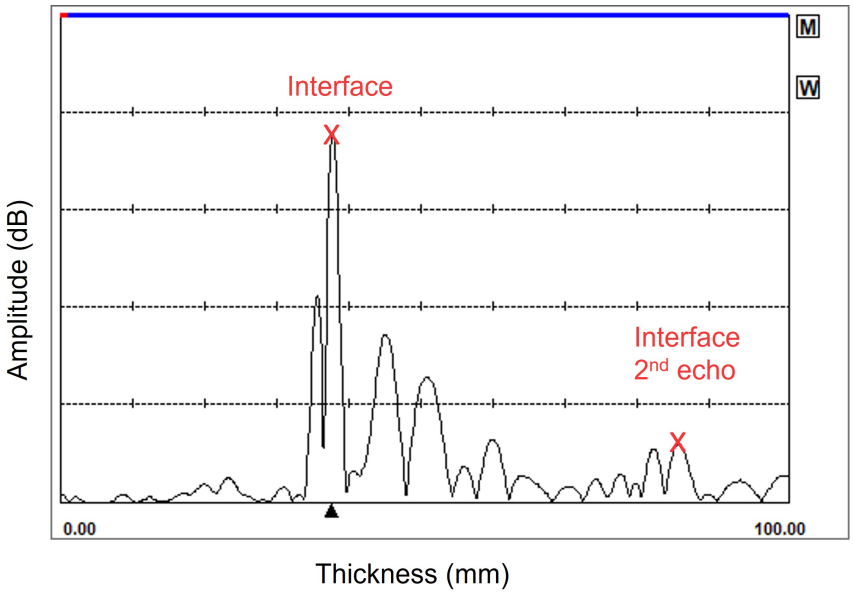

Figure 4.8: A-scan of measurement with wedge

The inspection interval is set by adjusting the parameters main bang blank (MB blank) and echo range. The MB blank is a manually set dead zone intended to protect the receiver from false readings generated by the main bang, while the echo window is the time interval after the main bang during which echoes can be detected. Setting these parameterns so that everything before and including the wedge-test piece interface falls inside the dead zone and the echo window ends before the second echo of the interface, only the echoes from the specimen are considered.

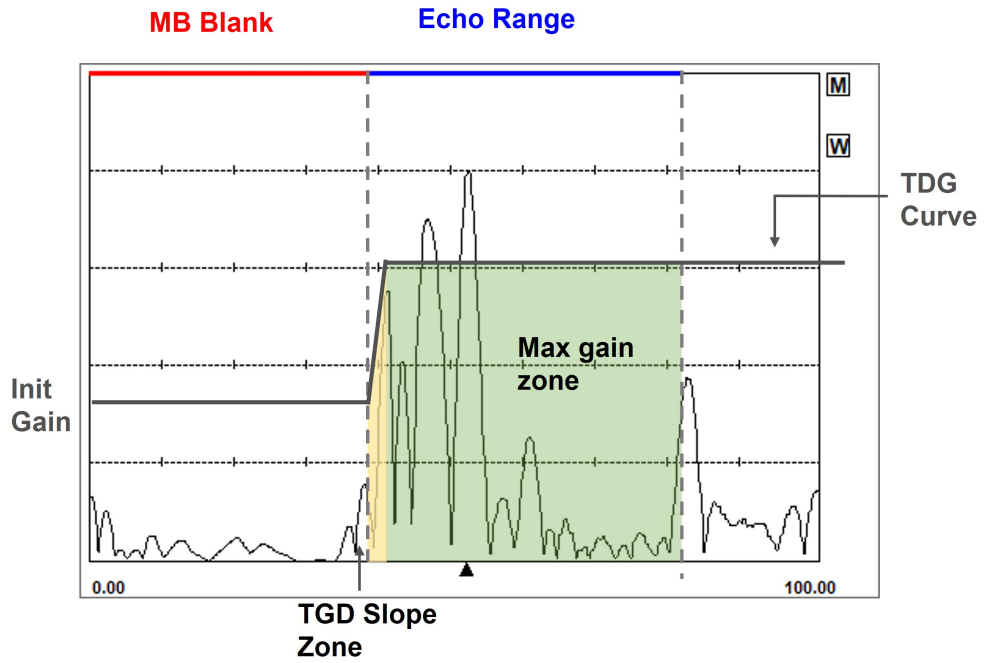

Figure 4.9: Inspection interval and TDG curve for contact testing with wedge

Moreover, the time-dependant gain (TDG) slope, which controls the rate at which the receiver gain increases from initial gain to maximum gain, is increased so that the near surface resolution is optimized. Together, these three parameters create the TDG curve.

Figure 4.9 illustrates the inspection interval and TDG curve set for the measurements taken with the contoured wedge. The interval in which echoes can be detected is underneath the blue line representing the echo range and is also illustrated by the maximum gain zone and the TDG slope zone.

Immersion testing

Similarly to testing using a wedge, the appropriate inspection interval must be set manually, ignoring the reflected signals from the water-test piece interface and the water-container interface.

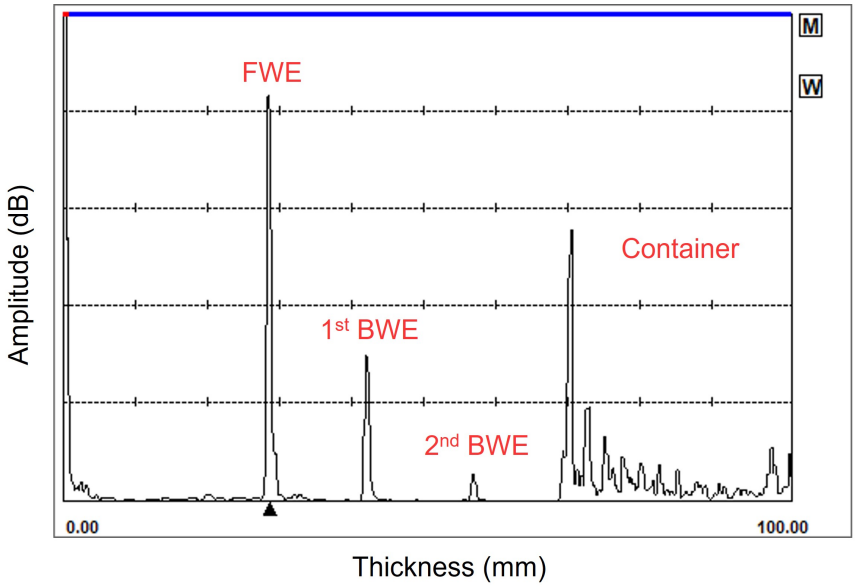

Figure 4.10: A-scan of measurement taken with immersion technique

Figure 4.10 shows an A-scan of a measurement taken with immersion technique of an area without defect. The high peak to the left is the reflected signal from the front wall of the test piece, while the multiple peaks to the right are reflections from the glass container. Between these are the test piece's first and second BWE.

The MB blank is set to include the front wall echo (FWE) and the echo range to stop before the water-container interface so that these echoes are not detected. Further, the TDG slope is increased to obtain high near-surface resolution. In Figure 4.11 the transducer parameters affecting the inspection interval and TDG curve is illustrated.

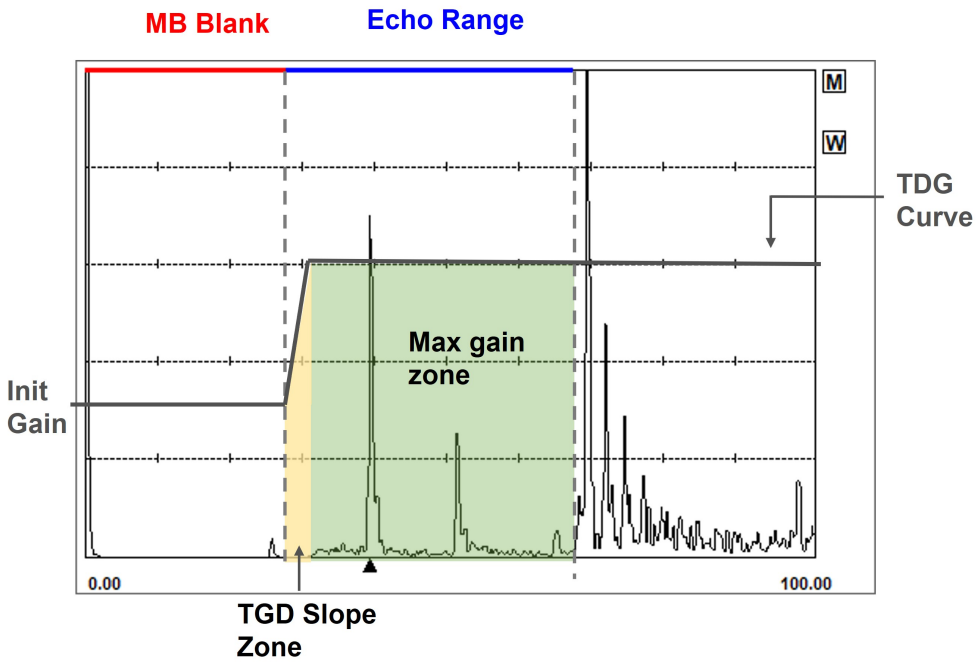

Figure 4.11: Inspection interval and TDG curve for immersion testing

5 | Results

In this chapter, the main findings from the experimental work are presented. Both digital image correlation and ultrasonic testing have been performed to detect fabricated delaminations and flat bottom holes in GFRP specimens, and different ultrasonic testing techniques have been explored to investigate pipe samples with curved geometry. The findings are summarised at the end of each main section.

5.1 Digital Image Correlation

GFRP specimens containing FBHs and fabricated delaminations have been inspected using 2D-DIC. This section presents the main findings, and an overview of which defects could be detected is given in Tables 5.1 and 5.2.

The specimens are investigated at three strain levels: 0.4%, 0.2%, and 0.1% average tensile strain. All in-plane strain components are considered, including tensile-, transverse-, and shear strain. However, only the results for tensile- and transverse strain are presented below, as no damage was detected by investigating the shear strain fields.

In the results presented in this section, two ROI are considered and compared for each specimen. These are a target zone, T, the area containing and surrounding the defect, and a non-defected reference zone, R. The position of the two ROIs is illustrated in Figure 5.1, and the location of the FBHs and delaminations are indicated. The purpose of the reference zone is to compare the strain fields of the damaged target zone with an intact area within the same specimen undergoing the same load. The two ROIs are evaluated at the same global strain interval, and for a completely intact specimen, a similar strain case would be expected in the two ROIs. As some defects are positioned in the bottom half of the specimen, the target zone and the reference zone is sometimes interchanged. A more detailed overview of the position of the defects is given in Table 4.1 in Section 4.1.2.

Damages within the specimens can be detected by observing strain values deviating from the average strain and the strain in the reference zone. It may be noted that in the measured strain fields, outlier strain values and fluctuations do appear from one image to another. Such outliers might appear as defects or even have strain values more extreme than what

is expected from a defect. Therefore, to correctly identify and distinguish a defect from an outlier, there must be some consistency in the deviating strain values between several images.

Nb! Please note that the contrast of the images presented in the following sections may differ in the printed and digital versions of this document.

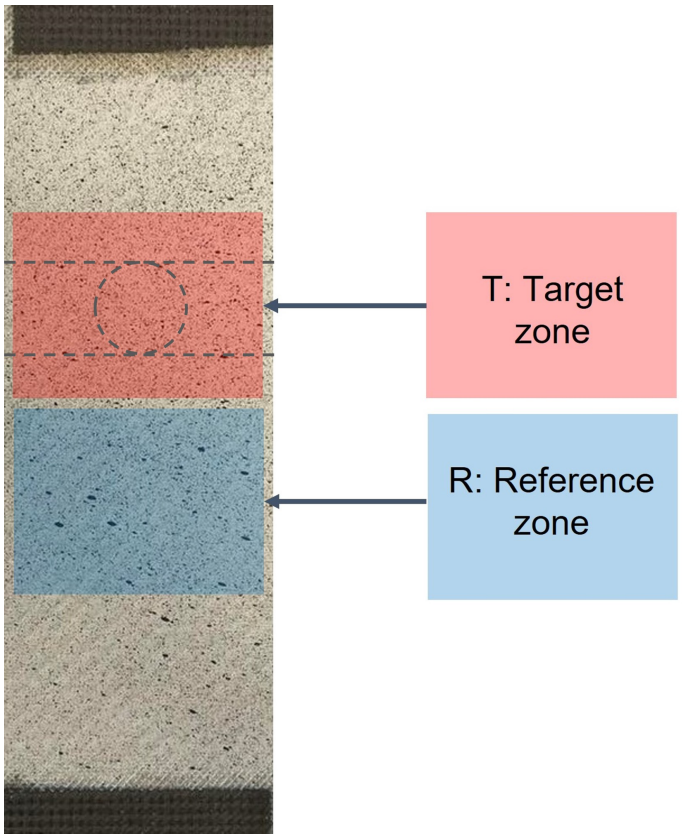

Figure 5.1: Target zone (T) and reference zone (R) of specimen investigated with DIC

5.1.1 Flat Bottom Holes

Average tensile strain $\epsilon_{yy} = 0.4\%$

In Figure 5.2 tensile strain fields, at an average strain level of 0.4%, are shown for the specimens containing FBHs. The strain is scaled at a an interval from $\epsilon_{yy} = 0.002$ to $\epsilon_{yy} = 0.006$. There are clear differences between the strain in the damaged target zone and the reference zone for all four samples. In samples H1 and H2, containing the deepest FBHs, the position of the hole within the target zone can be seen as the area with slightly higher strain between the areas with low strain, and the strain fields exhibit similarities to the ones expected from a through-thickness hole in tension. Also, for specimens H3 and H4

with more shallow FBHs, positioned further away from the inspected surface, it is clear that the strain values in the target zone deviate from the reference zone. The presence of the damage is revealed, although an exact location is not visible.

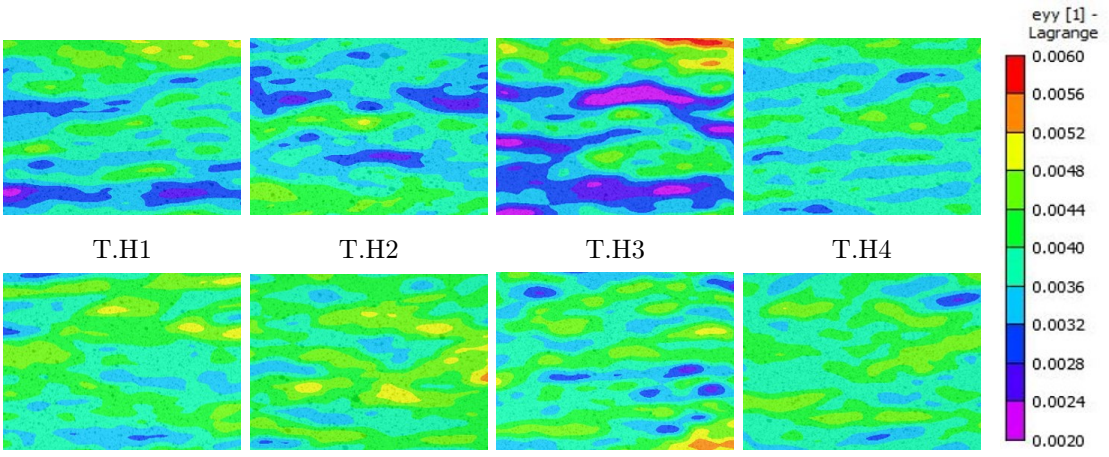

Figure 5.2: Comparison of tensile strain fields for specimens with FBH at $\epsilon_{yy} = 0.4\%$

In Figure 5.3 transverse strain fields for the specimens with FBHs are shown. The strain scale displays strain levels from ϵ_{xx} = -0.0012 to ϵ_{xx} = 0.0003. In specimen H1, with the deepest FBH, an area with low transverse strain is visible, indicating the presence of a FBH. No consistency could be detected in the deviating strains for the rest of the specimens.

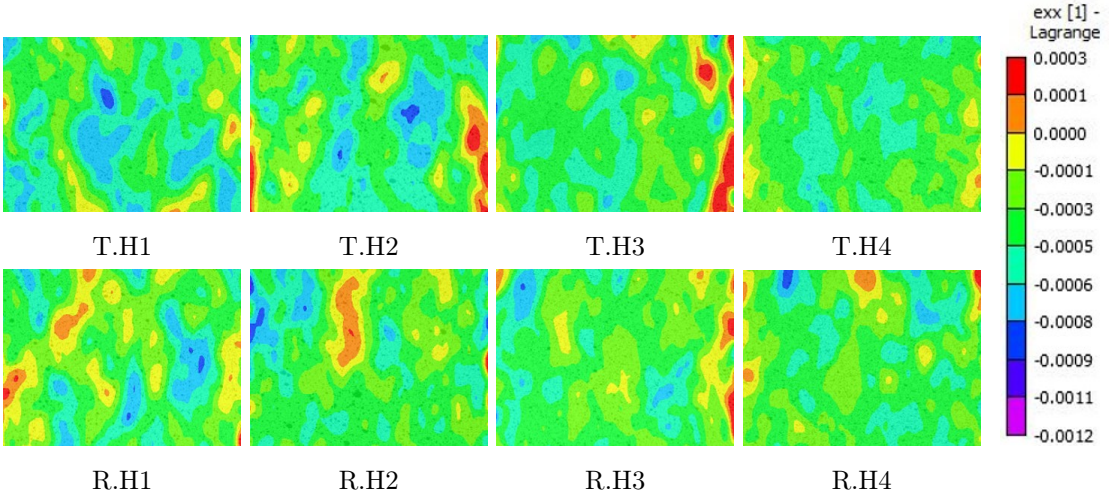

Figure 5.3: Comparison of transverse strain fields for specimens with FBH at $\epsilon_{yy} = 0.4\%$

Average tensile strain $\epsilon_{yy} = 0.2\%$

For all specimens but H4, a low tensile strain can be detected in the areas close to the defects compared to the corresponding reference zone, at an average tensile strain, ϵ_{yy}, of 0.2%. While for specimen H4, no significant difference can be seen between the target zone and the reference zone when investigating the tensile strain field. Figure 5.4 shows the tensile strain fields for the specimens with FBHs at an average tensile strain of 0.2%. The strains maps in the figure are scaled from $\epsilon_{yy} = 0.0005$ to $\epsilon_{yy} = 0.0035$.

In the transverse strain maps, no damage can be detected at this strain level.

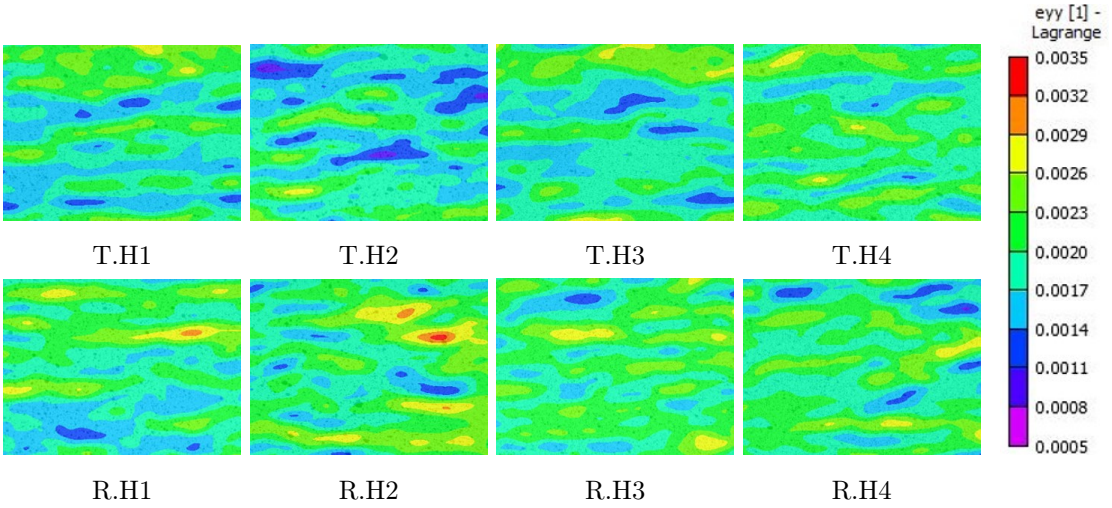

Figure 5.4: Comparison of transverse strain fields for specimens with FBH at $\epsilon_{yy} = 0.2\%$

Average tensile strain $\epsilon_{yy} = 0.1\%$

In Figure 5.4 the tensile strain fields for the specimens with FBHs at an average strain level of 0.1% are displayed, scaled at a strain interval from $\epsilon_{yy} = 0.0000$ to $\epsilon_{yy} = 0.0020$. At this strain level, it is difficult to observe a clear difference between the target zone, T, and the reference zone, R, in any specimens. However, a slight difference can be found for specimen H1.

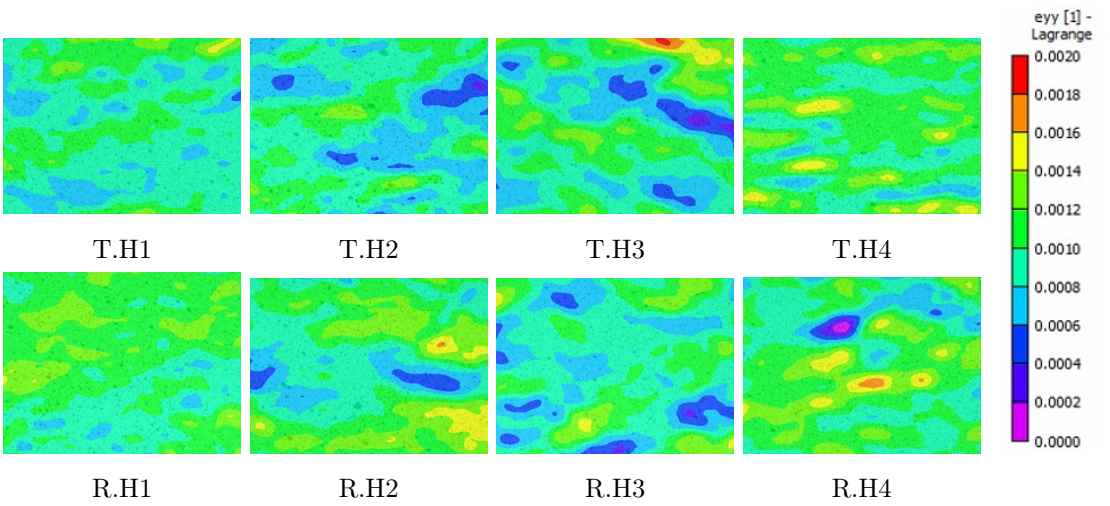

Figure 5.5: Comparison of tensile strain fields for specimens with FBH at $\epsilon_{yy} = 0.1\%$

5.1.2 Fabricated Delaminations

Average tensile strain $\epsilon_{yy} = 0.4\%$

For the specimens containing fabricated delaminations, a clear difference between the target zone and the reference zone can be found in specimens D1 and D2, where the surrounding high strain values can reveal the delaminated area. No significant difference in strain values can be found for samples D3 and D4, with delaminations embedded further away from the observed surface. The full field tensile strain for the specimen at global strain level $\epsilon_{yy} = 0.4\%$ is displayed in Figure 5.6, scaled from $\epsilon_{yy} = 0.0020$ to $\epsilon_{yy} = 0.0055$.

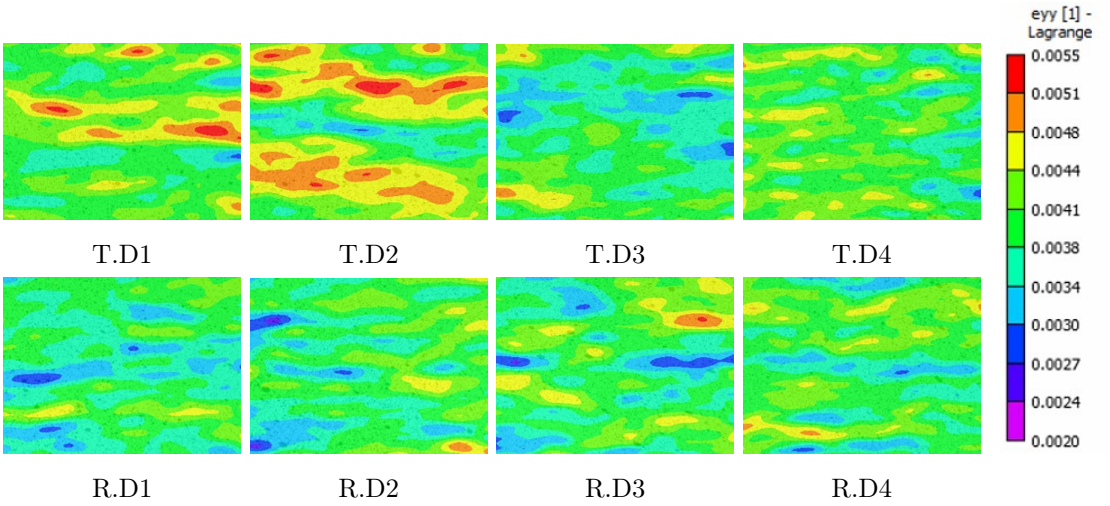

Figure 5.6: Comparison of tensile strain fields for specimens with fabricated delaminations at $\epsilon_{yy} = 0.4\%$

For the specimens containing fabricated delaminations, the transverse strain field demon-

strates no consistent strain values out of the ordinary, indicating detectable damage. Transverse strain fields scaled at an interval of ϵ_{xx} = -0.0012 to ϵ_{xx} = 0.0003 are presented in Figure 5.7.

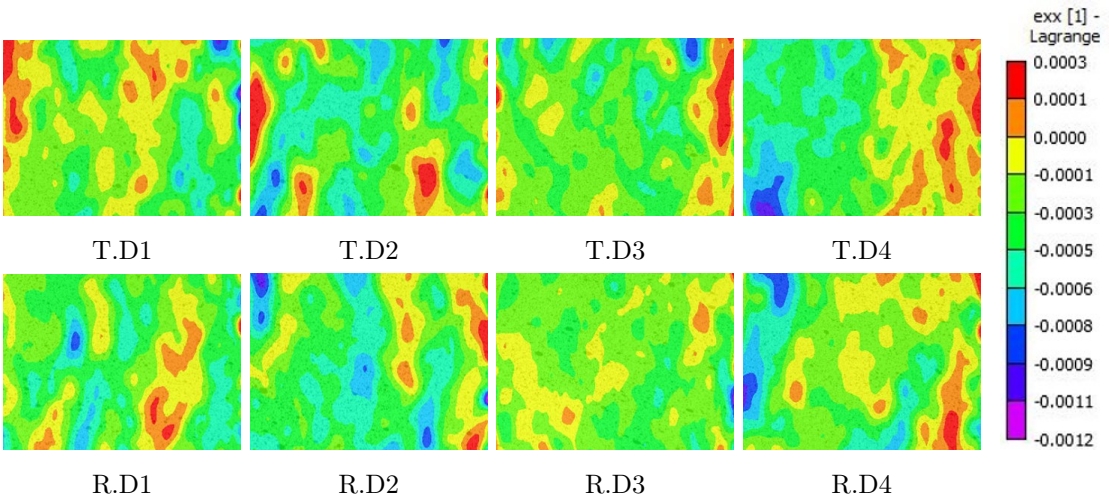

Figure 5.7: Comparison of transverse strain fields for specimens with fabricated delaminations at ϵ_{yy} = 0.4%

Average tensile strain ϵ_{yy} = 0.2%

In Figure 5.8 the tensile strain fields for the specimens with fabricated delaminations at an average strain level of 0.2% is displayed, scaled at a strain interval from ϵ_{yy} = 0.0003 to ϵ_{yy} = 0.0030. At this strain level, a consistent difference between the target zone, T, and the reference zone, R, can be seen for specimens D1 and D2.

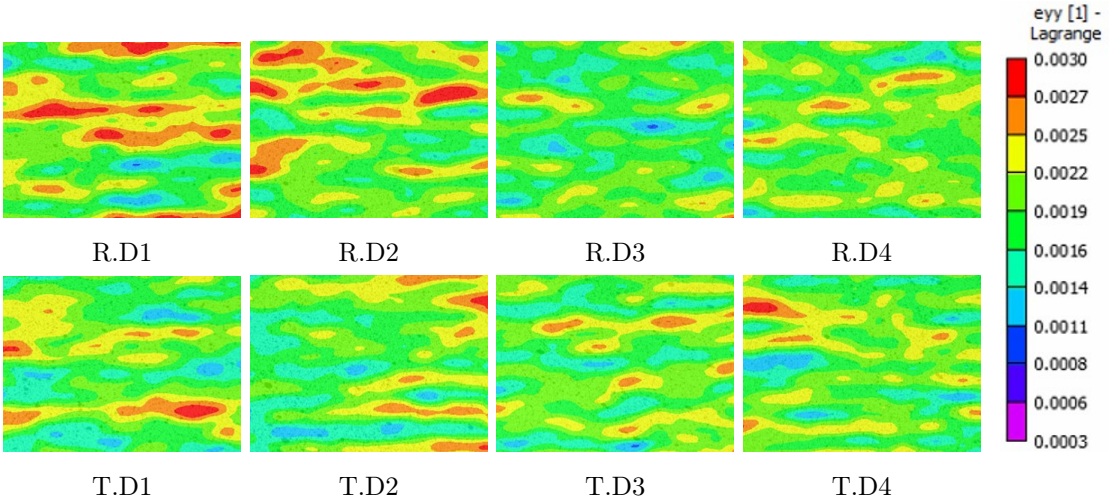

Figure 5.8: Comparison of tensile strain fields for specimens with fabricated delaminations at ϵ_{yy} = 0.2%

Average tensile strain $\epsilon_{yy} = 0.1\%$

At an average strain of $\epsilon_{yy} = 0.1\%$, only specimen D1, with a delamination embedded between the two middle layers of the laminate, display a consistent difference between the target zone and the reference zone, with higher strain in the target zone containing delamination. In Figure 5.9 full field strains, at a strain interval from $\epsilon_{yy} = 0.0$ to $\epsilon_{yy} = 0.0015$ are presented.

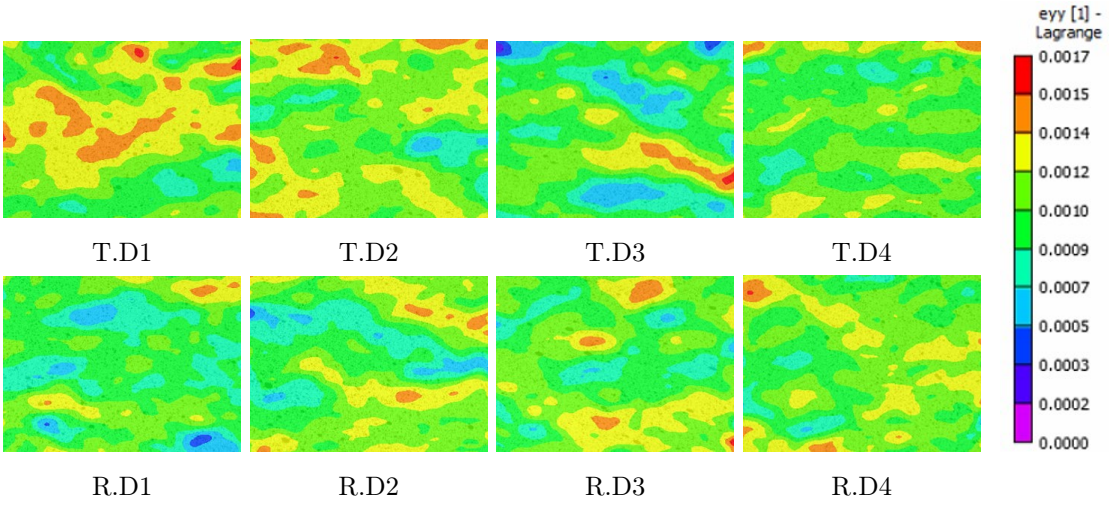

Figure 5.9: Comparison of tensile strain fields for specimens with fabricated delaminations at $\epsilon_{yy} = 0.1\%$

5.1.3 Summary of Results

Table 5.1: Summary of DIC results for FBHs

Avg. tensile strain	Specimen	Distance test surface	Defect is detected [yes/no]	Strain component
0.4%	H1	10.7 mm	yes	ϵ_{yy}, ϵ_{xx}
	H2	13.8 mm	yes	ϵ_{yy}
	H3	16.9 mm	yes	ϵ_{yy}
	H4	19.9 mm	yes	ϵ_{yy}
0.2%	H1	10.7 mm	yes	ϵ_{yy}
	H2	13.8 mm	yes	ϵ_{yy}
	H3	16.9 mm	yes	ϵ_{yy}
	H4	19.9 mm	no	-
0.1%	H1	10.7 mm	yes	ϵ_{yy}
	H2	13.8 mm	no	-
	H3	16.9 mm	no	-
	H4	19.9 mm	no	-

Table 5.2: Summary of DIC results for delaminations

Avg. tensile strain	Specimen	Distance test surface	Defect is detected [yes/no]	Strain component
0.4%	D1	10.7 mm	yes	ϵ_{yy}
	D2	13.8 mm	yes	ϵ_{yy}
	D3	16.9 mm	no	-
	D4	19.9 mm	no	-
0.2%	D1	10.7 mm	yes	ϵ_{yy}
	D2	13.8 mm	no	-
	D3	16.9 mm	no	-
	D4	19.9 mm	no	-
0.1%	D1	10.7 mm	yes	ϵ_{yy}
	D2	13.8 mm	no	-
	D3	16.9 mm	no	-
	D4	19.9 mm	no	-

5.2 Ultrasonic Inspection of Thick Laminate Specimens

Ultrasonic contact testing is performed on GFRP specimens containing flat bottom holes and fabricated delaminations. Three transducer frequencies are considered: 5 MHz, 2.25 MHz, and 0.5 MHz. This section presents the main findings. An overview over the detected defects can be found in Table 5.3 and 5.4.

All three transducers gave accurate thickness measurements of the specimens and stable A-scans in non-defected areas. 5 Mhz and 0.5 Mhz required a higher gain than the 2.25 MHz transducer to obtain an adequate acoustic signal with an amplitude of 80% of full screen height in the A-scan. For inspection with 2.25 MHz transducer frequency, a maximum gain of 60 dB gave sufficient signal for the thickness measurements, while for inspection with 0.5 MHz and 5 MHz, 70 dB and 85 dB maximum gain was necessary, thereby also increasing the surrounding noise.

5.2.1 Flat Bottom Holes

All three transducers could detect all the FBHs, and their depth could be measured. The figures below compare measurements from an intact area to an area with a FBH 16.8 mm from the inspected surface in specimen H3. Figure 5.10 show A-scans taken with 5 MHz frequency, Figure 5.11 with 2.25 MHz and Figure 5.12 with 0.5 MHz frequency, all with a thickness range on the x-axis from 0 to 50 mm

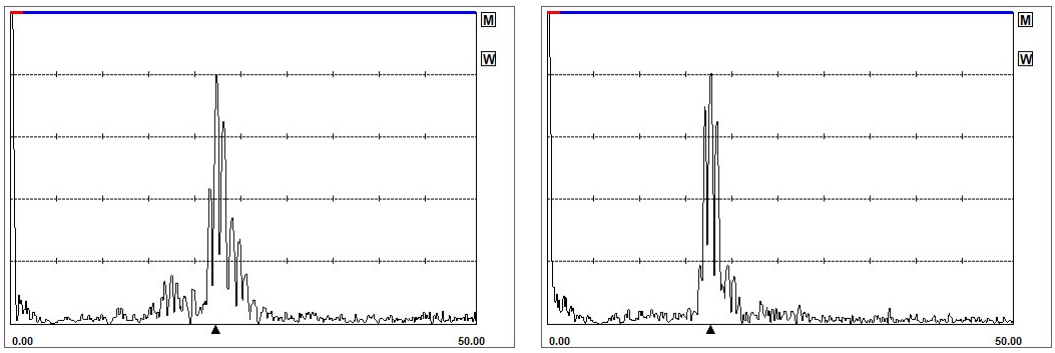

(a) Non-defected area (b) H3: FBH 16.8 mm from surface

Figure 5.10: A-scan of non-defected area (a) and FBH (b) with 5.0 Mhz transducer

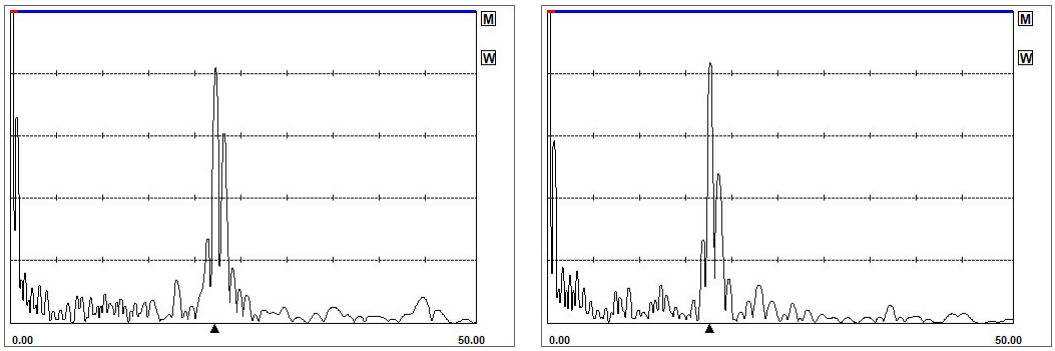

(a) Non-defected area (b) H3: FBH 16.8 mm from surface

Figure 5.11: A-scan of non-defected area (a) and FBH (b) with 2.25 Mhz transducer

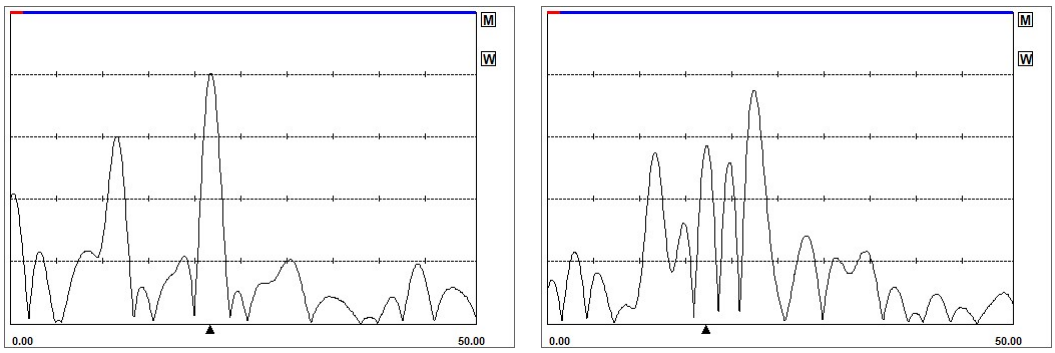

(a) Non-defected area (b) H3: FBH 16.8 mm from surface

Figure 5.12: A-scan of non-defected area (a) and FBH (b) with 0.5 Mhz transducer

5.2.2 Fabricated Delaminations

Similarly to the FBHs, all delaminations could be detected at all the three transducers frequencies. The figures below display measurements of the damaged areas of specimens D1 and D4, with fabricated delaminations, positioned 10.7 mm and 20.0 mm from the inspected surface. Figure 5.13 shows A-scans from measurements taken with the 5.0 MHz transducer, while the A-scans in Figure 5.14 and 5.15 are from measurements with 2.25 MHz and 0.5 MHz frequency, respectively. The thickness range on the x-axis is 0 to 50 mm.

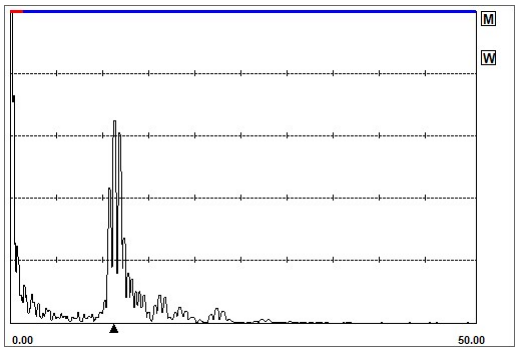

(a) D1: Delamination 10.8 mm from surface

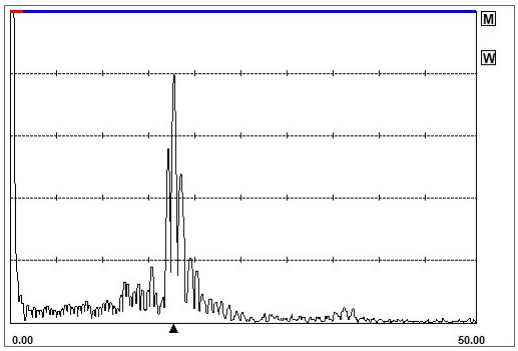

(b) D4: Delamination 20.0 mm from surface

Figure 5.13: A-scan of delaminated area with 5.0 MHz transducer

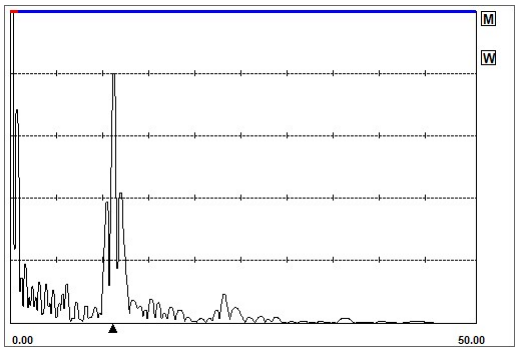

(a) D1: Delamination 10.8 mm from surface

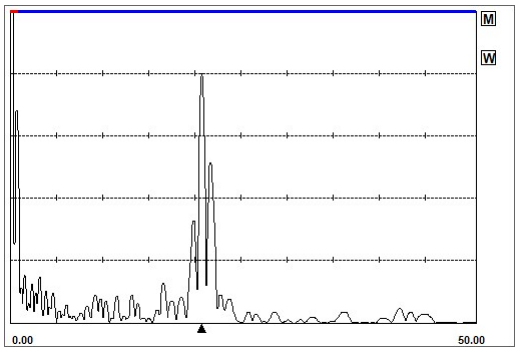

(b) D4: Delamination 20.0 mm from surface

Figure 5.14: A-scan of delaminated area with 2.25 MHz transducer

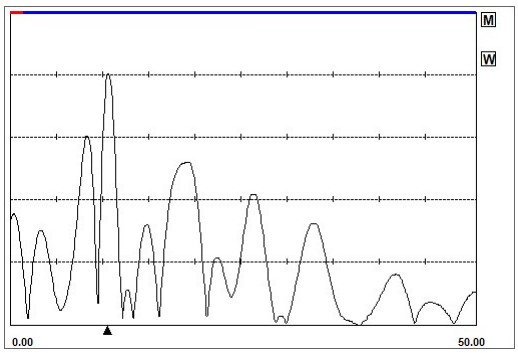

(a) D1: Delamination 10.8 mm from surface

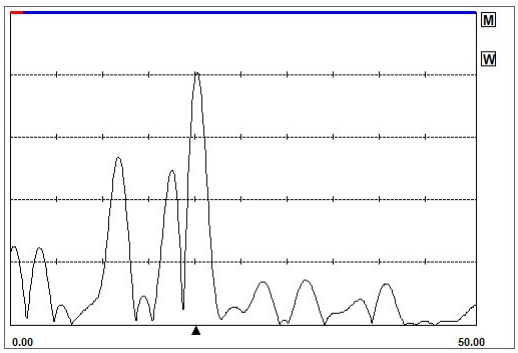

(b) D4: Delamination 20.0 mm from surface

Figure 5.15: A-scan of delaminated area with 0.5 MHz transducer

By comparing measurements taken at the three frequencies, it can be seen that measurements taken at lower frequencies have lower resolution, giving less detailed A-scans, while at higher frequencies, the measurements have a higher scattering of the signal from fibre-matrix interfaces within the laminate, displayed in the A-scan as many small peaks.

5.2.3 Summary of Results

Table 5.3: Summery of FBHs detected with UT

Avg. tensile strain	Specimen	Distance test surface	Defect is detected [yes/no]	Measured depth
5 MHz	H1	10.7 mm	yes	10.60 mm
	H2	13.8 mm	yes	13.95 mm
	H3	16.9 mm	yes	17.00 mm
	H4	19.9 mm	yes	19.93 mm
2.25 MHz	H1	10.7 mm	yes	10.55 mm
	H2	13.8 mm	yes	13.81 mm
	H3	16.9 mm	yes	16.94 mm
	H4	19.9 mm	yes	19.85 mm
0.5 MHz	H1	10.7 mm	yes	9.77 mm
	H2	13.8 mm	yes	13.28 mm
	H3	16.9 mm	yes	16.55 mm
	H4	19.9 mm	yes	20.06 mm

Note: 0.5 mm is subtracted from the measured depth to account for the paint layer on the specimen surface.

Table 5.4: Summary of delaminations detected with UT

Frequency	Specimen	Distance test surface	Defect is detected [yes/no]	Measured depth
5 MHz	D1	10.8 mm	yes	10.65 mm
	D2	13.8 mm	yes	13.87 mm
	D3	16.9 mm	yes	17.02 mm
	D4	20.0 mm	yes	20.12 mm
2.25 MHz	D1	10.8 mm	yes	10.54 mm
	D2	13.8 mm	yes	13.73 mm
	D3	16.9 mm	yes	17.88 mm
	D4	20.0 mm	yes	20.01 mm
0.5 MHz	D1	10.8 mm	yes	9.99 mm
	D2	13.8 mm	yes	13.27 mm
	D3	16.9 mm	yes	16.09 mm
	D4	20.0 mm	yes	19.49 mm

Note: 0.5 mm is subtracted from the measured depth to account for the paint layer on the specimen surface.

5.3 Ultrasonic Inspection of Pipe Samples

In this section, the results from ultrasonic inspection of pipe samples will be presented, along with selected ultrasonic A-scan measurements. As a great number of measurements were carried out, only the main findings are presented, while a summary of which FBHs could be detected using the different inspection methods and transducer frequencies are presented in Table 1 and 5.6 in section 5.3.3.

5.3.1 Contact Testing

Inspection of PE pipe samples

Investigating the PE pipe specimens using direct contact technique, accurate thickness measurement, and stable A-scans with low noise levels were obtained using both 5 MHz- and 2.25 MHz transducer frequency. FBHs of all sizes and positions could be detected.

Figure 5.16 displays ultrasonic A-scans of measurements taken of the PE pipe samples using the 5 MHz transducer. The thickness range of the x-axis is 0 to 50 mm. Figure 5.16a shows an area without defects. The three peaks in the scan represent the 1^{st}, 2^{nd}, and 3^{rd} echo reflected from the back wall of the specimen. The position of the first peak along the x-axis corresponds to the thickness of the specimen, while the 2^{nd} and 3^{rd} echo corresponds to two times and three times the specimen thickness. Figure 5.16b and 5.16c shows an area with a 15 mm and 4 mm wide FBH respectively. In 5.16c the FBH can be seen as the small peaks appearing to the left for the back wall echo of the specimen. By adjusting the initial gain of the acoustic signal, measuring the through-thickness location of the FBH is possible, shown in 5.16d.

A contoured wedge was applied when performing contact testing with the 0.5 MHz transducer. Proper coupling between the transducer and the specimens was obtained using the wedge and thickness measurements of the specimens with a consistent signal as possible. The largest FBHs, at Ø20 mm and Ø15 mm, could be detected with thickness measurement, while for the smaller FBHs, at Ø4 mm and Ø7 mm, no notable changes could be observed in the ultrasonic A-scan.

Figure 5.17a and 5.17b shows the A-scan of an area without defect and with a 20 mm wide FBH, respectively. Note that the thickness output indicated by the triangle below the x-axis of the scan equals the measured thickness of the wedge and the measured thickness of the specimen added together. The thickness range is 0 to 100 mm.

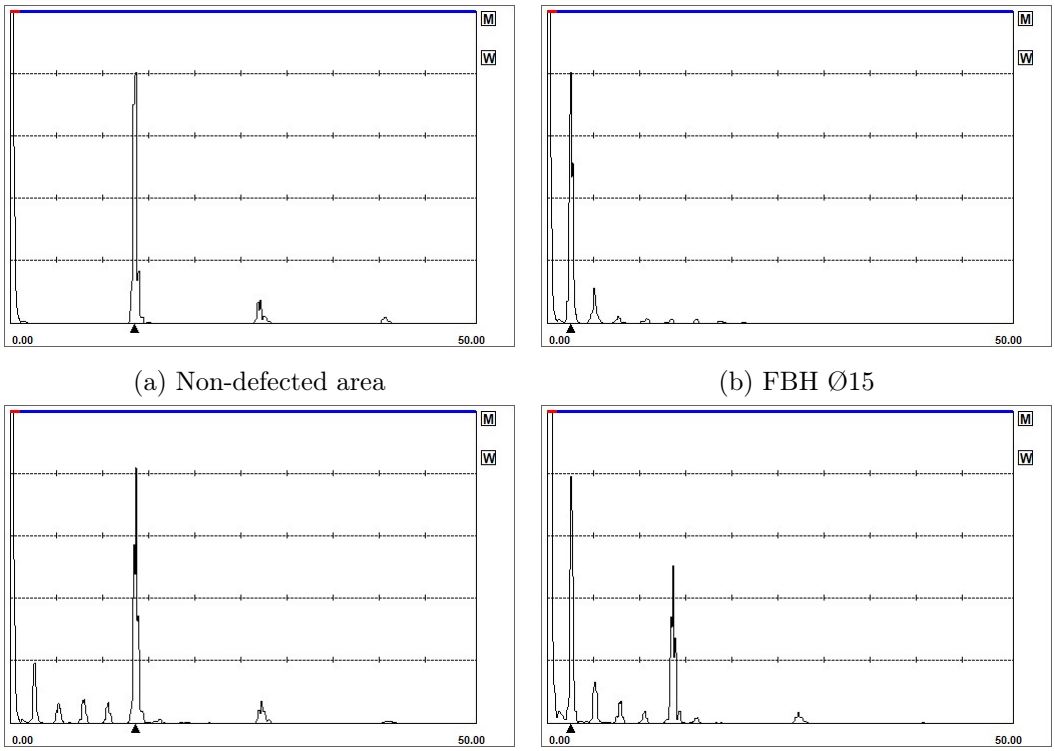

(a) Non-defected area

(b) FBH Ø15

(c) FBH Ø4

(d) FBH Ø4 with increased gain

Figure 5.16: Contact testing of PE specimens with 5 MHz transducer frequency

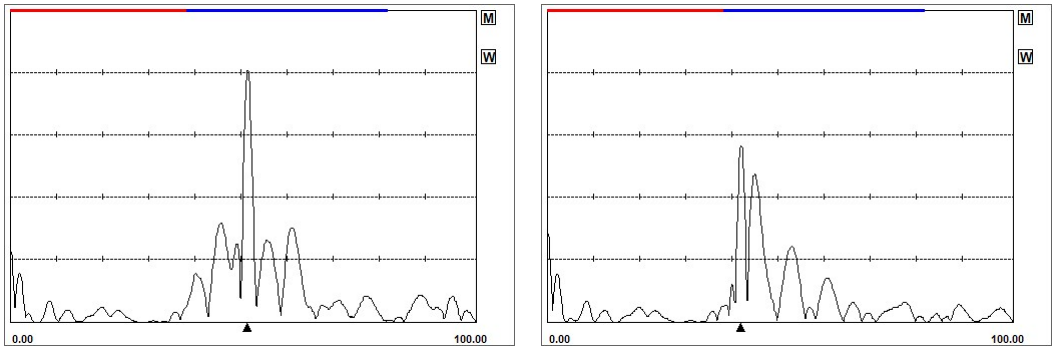

(a) Non-defected area

(b) FBH Ø20

Figure 5.17: Contact testing with contoured of PE specimens with 0.5 MHz transducer frequency

Inspection of GFRP pipe samples

Inspecting the GFRP pipe specimens, all transducer frequencies used could adequately identify the interface between the fibre layer, the liner, and the specimen back wall.

All FBHs in the PE liner could be detected with a measured location output using both the 5 MHz and 2.25 MHz transducer. Inspection with 2.25 MHz could also successfully

locate all defects located in the fibre laminate close to the test surface. While with 5 MHz transducer, although the defects could be detected, the signal was heavily distorted by high noise levels making it difficult to obtain reliable readings. FBHs from Ø15 mm located in the laminate-liner interface could be detected at both 5 MHz and 2.25 MHz by a significant increase in the amplitude of the reflected signal at the interface. FBHs smaller than this could not be detected.

In Figure 5.18 A-scans from measurements taken with 2.25 MHz transducer frequency inspecting GFRP specimens are shown. The range of the x-axis is from 0 to 20 mm. The scan presented in Figure 5.18a is from an intact area without damage. The high peak to the right is the echo from the back wall of the specimen, while the smaller peak to the left is the echo from the laminate-liner interface. In both Figure 5.18b and 5.18d an additional peak can be observed from a 4 mm wide FBH located in the fibre laminate and the liner, respectively. To obtain thickness outputs for the two FBHs, the initial gain has been increased. In Figure 5.18c the presence of the FBH in the laminate-liner interface can be observed indirectly by the loss of amplitude of the BWE and the increased amplitude at the interface.

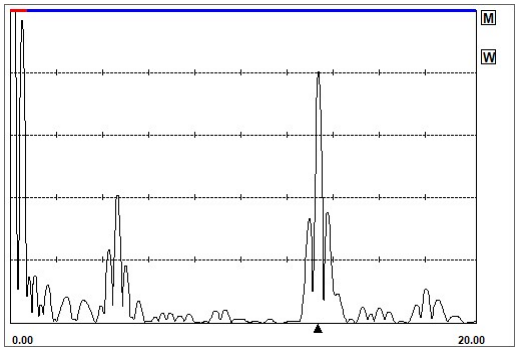

(a) Non-defected area

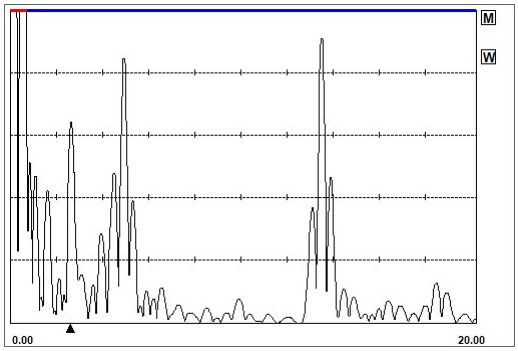

(b) FBH Ø4 in fiber layer

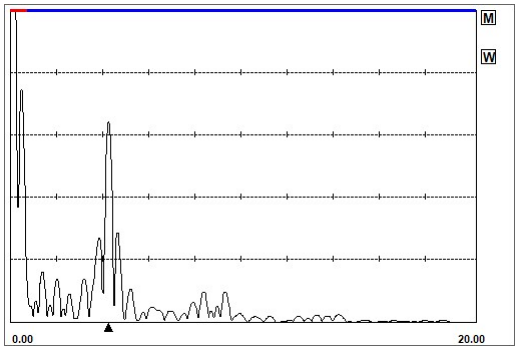

(c) FBH Ø15 in interface

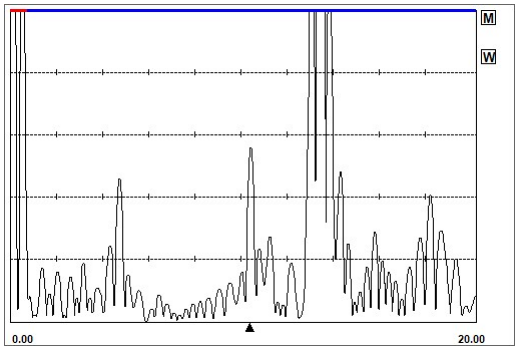

(d) FBH Ø4 in liner

Figure 5.18: Contact testing of GFRP specimens with 2.25 MHz transducer frequency

Inspection at 0.5 MHz with a contoured wedge could identify FBHs from Ø15 mm in the outer fibre laminate of the GFRP specimen. FBHs located in the liner and the laminate-

liner interface could not be detected at this frequency with this inspection method.

In Figure 5.19a and 5.19b measurements taken at an area without defect and with a 20 mm FBH in the fibre laminate of a GFRP specimen can be seen. The x-axis is scaled from 0 to 100 mm in thickness.

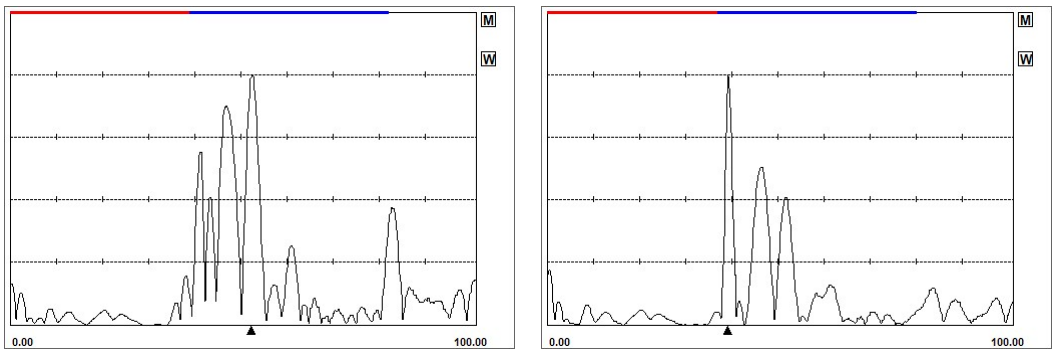

(a) Non-defected area (b) FBH Ø20 in fiber layer

Figure 5.19: Contact testing with contoured wedge of GFRP specimens with 0.5 MHz transducer frequency

5.3.2 Immersion Testing

Inspection of PE pipe samples

The immersion technique could detect all FBHs in the PE pipe specimens at 5 MHz and 2.25 MHz inspection frequencies. At 0.5 MHz, the FBHs with diameters of 15 mm and 20 mm could be detected.

In Figure 5.20 measurements taken of PE specimens using immersion technique at 5 MHz frequency are shown. The whole x-axis ranges from 0 to 100 mm, and the inspection interval is adjusted only to consider the area between the water-specimen interface and the glass container is considered, illustrated in the A-scan as the area under the blue line. Figure 5.20a is from an area without defect, where the two peaks within the inspection interval are the 1^{st} and 2^{nd} echo of the back wall of the specimen, while Figure 5.20b is from an area with a 4 mm FBH.

Similarly, Figure 5.21a and 5.21b are measurements from an area without defect and an area with a 15 mm FBH taken with the 0.5 MHz frequency transducer.

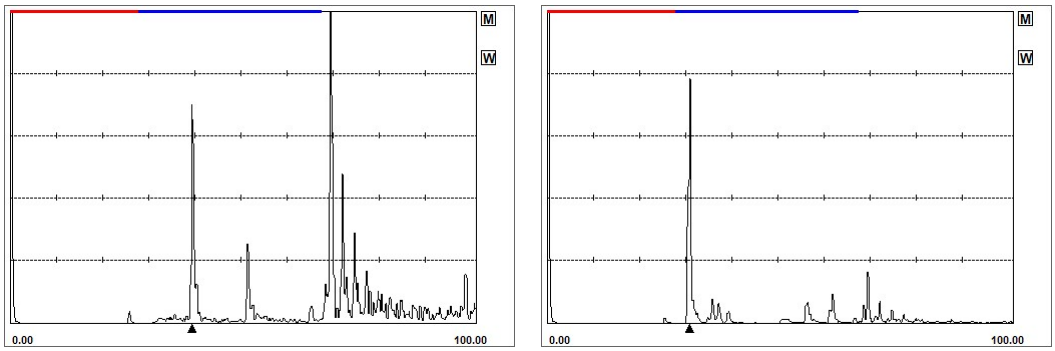

(a) Non-defected area (b) FBH Ø4

Figure 5.20: Immersion testing of PE specimens with 5 MHz transducer frequency

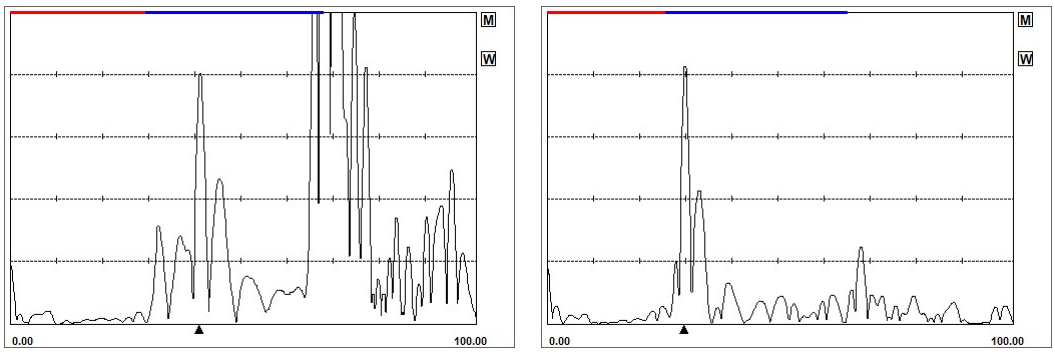

(a) Non-defected area (b) FBH Ø15

Figure 5.21: Immersion testing of PE specimens with 0.5 MHz transducer frequency

Inspection of GFRP pipe samples

Performing immersion testing on the GFRP specimens, all transducers could detect the laminate-liner interface and the specimen back wall. All defects in the liner and fibre laminate of the pipe sample could be detected using the 5.0 MHz and 2.25 MHz transducers, however, the measurements of defects within the fiber laminate taken with the 5 MHz transducer were prone to high levels of noise. FBHs at the interface became apparent due to the increased amplitude of the signal reflected at the interface from a Ø7 mm. While for the 0.5 MHz transducer, FBHs of Ø15 mm could be detected in the fibre laminate and the liner, only the FBH of Ø20 mm could be detected in the interface.

Figure 5.22 shows measurements taken performing immersion testing with 2.25 MHz transducer frequency. Figure 5.22a shows an intact area, while Figures 5.22b, 5.22c, and 5.22d, shows measurements taken at FBHs in the fiber laminte, interface, and liner respectively. Further, Figure 5.23a-5.23d show measurements from the same areas with transducer frequency 0.5 MHz. Both in Figure 5.22 and Figure 5.23 have x-axis ranging from 0 to 100 mm.

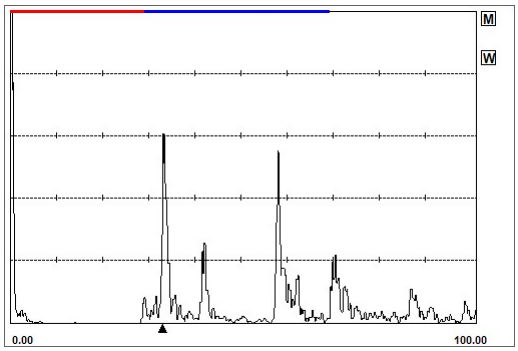

(a) Non-defected area

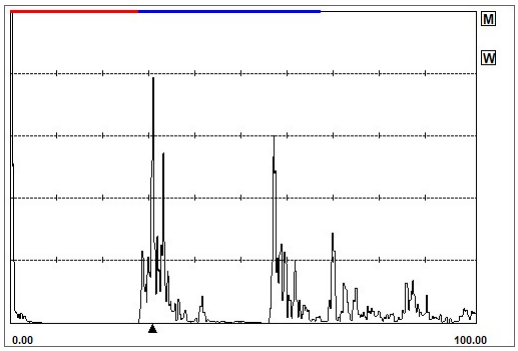

(b) FBH Ø4 in fiber layer

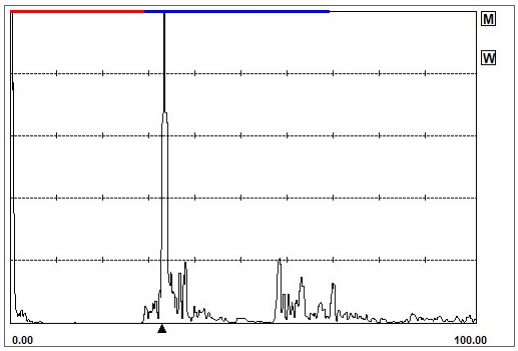

(c) FBH Ø7 in interface

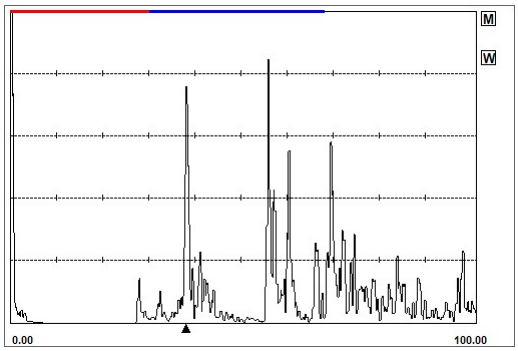

(d) FBH Ø4 in liner

Figure 5.22: Immersion testing of GFRP specimens with 2.25 MHz transducer frequency

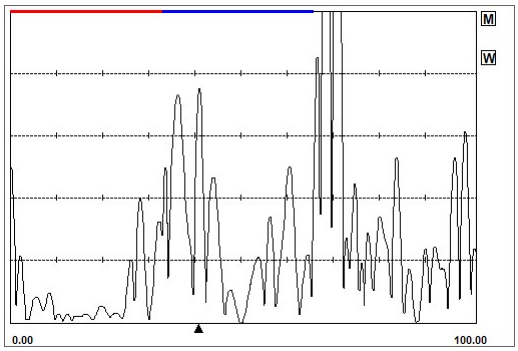

(a) Non-defected area

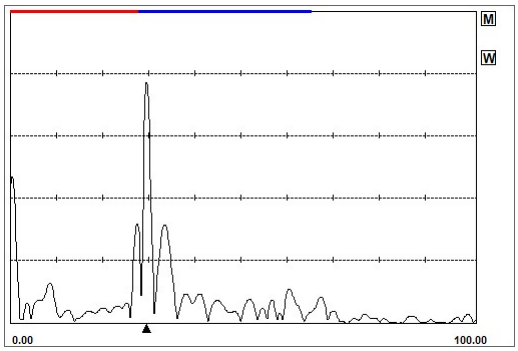

(b) FBH Ø15 in fiber layer

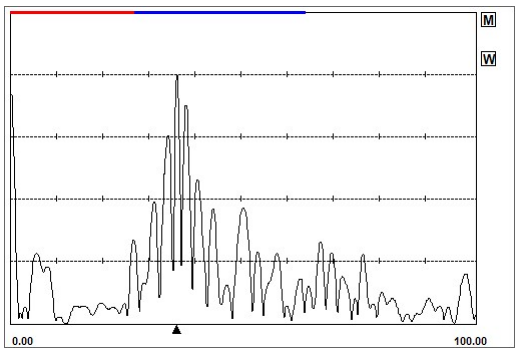

(c) FBH Ø20 in interface

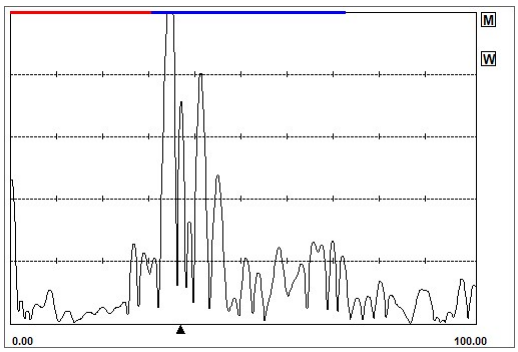

(d) FBH Ø15 in liner

Figure 5.23: Immersion testing of GFRP specimens with 0.5 MHz transducer frequency

5.3.3 Summary of Results

Table 5.5: Summary of results for PE pipe

Frequency	Inspection Method	Size of smallest FBH detected
5 MHz	contact testing	Ø4 mm
	immersion testing	Ø4 mm
2.25 MHz	contact testing	Ø4 mm
	immersion testing	Ø4 mm
0.5 MHz	contact testing w/ wedge	Ø15 mm
	immersion testing	Ø7 mm

Table 5.6: Summary of results for GFRP pipe

Frequency	Inspection Method	Position of FBH	Smallest FBH detected
5 MHz	contact testing	fiber laminate	Ø4 mm*
		liner	Ø15 mm
		interface	Ø4 mm
	immersion testing	fiber laminate	Ø4 mm*
		liner	Ø7 mm
		interface	Ø4 mm
2.25 MHz	contact testing	fiber laminate	Ø4 mm
		liner	Ø15 mm
		interface	Ø4 mm
	immersion testing	fiber laminate	Ø4 mm
		liner	Ø7 mm
		interface	Ø4 mm
0.5 MHz	contact testing	fiber laminate	Ø15 mm
	w/ wedge	liner	-
		interface	-
	immersion testing	fiber laminate	Ø15 mm
		liner	Ø20 mm
		interface	Ø15 mm

* High noise level

6 | Discussion

6.1 Digital Image Correlation

6.1.1 Quality of Results

Specimens containing FBHs and fabricated delaminations were inspected using 2D-DIC while submitted to low tensile load. In-plane train maps were analysed at strain levels of 0.4%, 0.2% and 0.1% average tensile strain.

Observing the strain fields obtained from 2D-DIC measurements, it was found that all FBHs and two out of four fabricated delaminations could be detected at the highest investigated strain level of 0.4% average tensile strain. The most shallow FBH was 1.6 mm deep and 19.9 mm away from the observed test surface, while delaminations could be detected at 10.8 mm and 13.8 mm from the test surface. The delaminations deeper inside the laminate could not be detected at the investigated strain levels. As lower strains were investigated, it limited the possibility of detecting defects deep within the specimens, far from the inspected surface.

Flat bottom holes are expected to be visible on an in-plane strain map. Strain concentrations appear close to the hole when submitted to load. Moreover, the hole essentially breaks the fibres in the laminate, which substantially affects the strength of the laminate in the fibre direction. The decrease in strength affects the laminate's out-of-plane properties and will be visible in the strain field on the surface of the specimen.

At lower loads, the through-thickness impact of the hole is less significant and more challenging to observe in a strain map. Moreover, holes that are more shallow cut through fewer layers of fibre and have less impact on the overall strength of the specimen.

As for delamination, it can also impact the specimens' out-of-plane properties, which may cause changes in in-plane strain distributions. However, not to the same extent as FBHs. Therefore, as expected, delaminations might be more difficult to detect than FBHs. Furthermore, delaminations will typically not be induced during this loading condition. By investigating the specimens during bending, the delaminations might be easier to detect

than in tension.

In the tensile strain fields for the specimens containing FBHs presented in Section 5.1, it can be seen that the strain is lower in the area close to the FBH compared to the non-defected reference area. The low strains might seem slightly in-intuitive, as higher strains are typically expected close to a hole or a notch. Therefore, finite element (FE) analyses were performed, which supports the experimental results. The FE-results show that in the outermost laminate layers, furthest away from the FBH, the strains are lower in front of and close to the hole compared to the rest of the specimen. While layers further back in the laminate, closer to the hole, have high strains close to the hole. Results from the FE-analysis are presented in Appendix C. Therefore, it is expected that for thinner laminate specimens or deeper FBH, the surface strain at the defected area may display high strain values, contrary to what is observed for the specimens investigated.

Moreover, when analysing the images taken during the mechanical test, it was found that there were significant variations between images taken at approximately the same strain level, both between different specimens and with the same specimen. These variations made it difficult to compare one specimen to another, such as to compare a specimen containing a defect to a non-defected reference specimen. Therefore, it was chosen to compare a reference zone and a target zone within the same specimen so that the two ROIs could be taken from the same exact image.

It may also be noted that, in the measured strain fields, many outlier strain values and fluctuations do appear from one image to another of the same specimen. An example is demonstrated in Figure 6.1, where two images taken at subsequent strain levels are displayed. In 6.1a an area of low strain is visible before disappearing in Figure 6.1b.

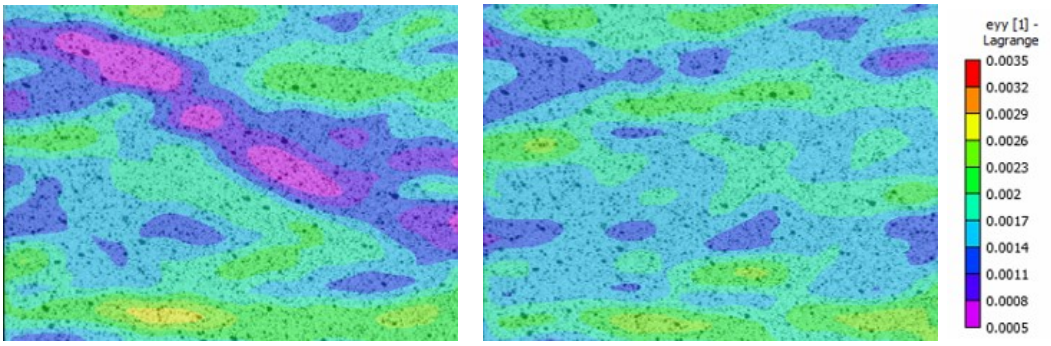

(a) $\epsilon_{yy} = 0.17\%$ (b) $\epsilon_{yy} = 0.18\%$

Figure 6.1: Tensile strain field of specimen with flat bottom hole (H1) illustrating the presence of outlier values at similar strain intervals

These outlier values are easy to mistake as damage in the specimens. The strain values of the outliers may be similar to the ones caused by embedded defects or deviate even

more from the average strain. It is therefore difficult to quantify what strain values are caused by outliers in one single image. In order to properly identify a defect within the specimen and distinguish it from random outlier values and false positive results, a level of consistency is necessary in the strain fields throughout a series of images.

Although only one image is displayed for each strain level in the previous, only considering these might not give a correct image of the damage state. Therefore, several images close to the selected strain level have also been verified to obtain more accurate results.

A consequence of the outlier strain values beyond the risk of being incorrectly identified as a defect is that very high or low strain values might conceal the location of actually damaged areas in the strain maps so that actual damage is not detected.

6.1.2 Sources of Error

There might be several reasons for the fluctuations and outlier values in the measured strain fields. It is possible that unintended defects were introduced during laminate production, such as voids entrapped within the laminate. Areas with high void content may cause high strain values to appear on the surface strain map. The effect of production defects on the strain maps is, however, expected to stay relatively consistent and not fluctuate from image to image.

Moreover, the speckle pattern was applied to the specimens using spray paint. Although providing a non-repetitive speckle pattern, there was quite a substantial variation in the size of the speckles. There is, therefore, both the risk of aliasing caused by large size speckles and increased noise caused by small speckles. The number of speckles might also be too low, having too many white areas in the pattern, which can cause aperture problems.

Another aspect that might have influenced the quality of the results is the out-of-plane motion in the specimens. 2D-DIC can only measure in-plane displacements; therefore, a symmetrical and balanced $[0/90]_{14s}$ layup was chosen to avoid out-of-plane curvature during the tensile test. However, when introducing defects into the laminate, in the form of a FBH or delamination, the assumption of a symmetrical laminate is in reality no longer valid, and in-plane loads can cause out-of-plane displacements and curvature of the laminate that 2D-DIC does not consider. Misalignment of fibre mats during laminate production may also have the same effect.

Finally, when performing the mechanical test, a 1% strain limit was set. From the strain fields calculated by the Vic-2D post processing software, the specimens obtained a maximum average strain in the range of 0.4%, which was used as the highest strain investigated strain level. This considerable deviation might be due to slipping in the grips or movement in the cross piece of the machine.

6.1.3 Application and Significance for Composite Pipelines

Advancements in camera technology and image processing algorithms have made optically based methods such as digital image correlation appealing for non-destructive inspection. There is, however, little experience in using digital image correlation for in-service inspections.

Still, both the results from the experimental work performed in connection with this thesis and previous research presented in Section 3 suggest that image correlation in combination with low external load can be used to detect defects such as delaminations in composite materials. Delaminations at a distance of 13.8 mm from the inspected surface could be detected at an average strain level of 0.4% in the tensile direction. The in-plane position of the defect and, to some degree, the size could be visualised in the coloured strain maps. However, a drawback of the method is that, when observing normal to a surface, it does not give information on the through-thickness location of the defect. It was also found that delaminations far from the surface were difficult to detect.

DIC has a great advantage in that it is both fast to perform and non-contact. Moreover, there are no material limitations. For this project, only in-plane laboratory measurements of relatively small specimens are considered but using stereo-DIC with multiple cameras large three-dimensional objects can be inspected, such as pipelines.

The method has the potential to be used both as quality control at the end of a production line or as automated inspection during service life. However, the results presented in Section 5.1 merely make up a basis for further evaluation and examination.

6.2 Ultrasonic Testing

6.2.1 Quality of Results

Ultrasonic testing of thick laminate samples

Flat GFRP with a thickness of 21.5 mm, containing FBH and fabricated delaminations at different depths, was inspected using ultrasonic PuE testing with direct contact between the transducer and the specimens. Three different transducers were used: 5 MHz, 2.25 MHz and 0.5 Mhz. All three transducers could be used to detect and measure the through-thickness location of all defects, both FBH and delaminations.

However, it was found that a substantially higher amplification of the acoustic signal was needed for the measurements performed a 5 MHz compared to the ones at 2.25 MHz. The heterogeneous nature of the material and attenuating glass fibres is most likely causing high scattering and loss of the acoustic signal throughout the depth of the laminate. By

increasing the gain of the signal. The surrounding noise is also increased. It is therefore expected that as the laminate thickness increases, the quality of the measurements will decrease.

Inspection using the lowest frequency of 0.5 MHz gave a visibly lower level of detail in the ultrasonic A-scans due to the lower resolution of the measurements. The measured depth of the defects also deviated slightly from the actual defects position, compared to the two other transducers. Still, all defects could be located. While using 2.25 MHz gave accurate measurements with both high resolution and low amplification of the receiver signal.

Although all three transducers proved to have an equally high defect detection rate in the investigated samples, the best resolution to noise balance was obtained at 2.25 MHz.

Ultrasonic testing of pipe samples

Techniques for investigating pipe samples with curved geometry have been explored, including contact testing with and without a contoured wedge and immersion testing. Thermoplastic PE pipe samples and GFRP PE samples containing FBH of different dimensions and locations were inspected.

It was chosen to use contact testing with direct contact for the two smallest transducers, 5 MHz and 2.25 Mhz which has a transducer diameter of 13 mm, while for the larger 0.5 MHz transducer with a diameter of 25 mm, a contoured wedge was produced to ensure adequate contact between the wedge and the pipe samples.

Even the smaller transducer slightly exceeded the recommended gap of 0.5 mm between the pipe surface and transducer edge, in virtue of Eq. (3.1). However, it was found that a good signal was still obtained using direct contact with these two transducers. Both the 5 MHz and the 2.25 MHz transducer could locate all FBHs in the PE pipe, with stable A-scans and low noise levels. PE is a homogeneous material and not prone to high attenuation and signal scattering compared to composites, and high inspection frequencies can, therefore, be used.

For the GFRP pipe samples, it was found that all defects in the PE liner could be located, while close to the surface in the fibre laminate, the acoustic signal was sensitive to noise, especially when using the 5 MHz transducer. Moreover, the already reflected echo of the laminate-liner interface can conceal minor defects loacted in the interface.

A contoured epoxy wedge enabled good contact between the 0.5 MHz transducer and the pipe samples. The BWE of the pipe could be detected, and FBHs from Ø15 mm could be detected in the PE pipe. For the GFRP pipe, only defects in the PE liner could be detected. The lower detection rate in the GFRP might be due to the slightly rough surface of the outer fibre laminate of the GFRP pipe providing a poorer coupling between the

wedge and the pipe, scattering the signal at the surface. Another reason is the difficulties separating the echoes from the interface and back wall of the specimen from defects due to the low range resolution of the transducer.

Immersion testing proved an excellent method for obtaining consistent coupling between the transducers and the pipe samples. Stable measurements were provided for all three transducers, both investigating the PE pipe samples and the composite pipe samples. The 0.5 MHz transducer could not locate the smallest FBH, which is as expected due to the large diameter of the pipe. The low attenuation of water might also have contributed to the high level of acoustic performance.

Moreover, immersion testing might be difficult to perform manually as the relative distance between the transducer and the test piece must remain the same to get a readable signal. A small support structure was modelled to hold the transducer at a fixed position above the specimen when performing the inspection to achieve this. As this structure was mounted on the glass container, only inspections in the longitudinal direction of the pipe were possible. Inspections in the circumferential direction would constantly change the relative distance between the transducer and the pipe and not provide stable measurement. Contact testing with and without a wedge can, on the other hand, be performed in both longitudinal and circumferential directions.

Both the 2.25 MHz and 5 MHz transducers demonstrated good options for inspection of both the PE pipe and the composite pipe. As expected, the 0.5 MHz transducer had a lower resolution and could not detect the smallest FBHs. For the PE pipe, both the 5 MHz and the 2.25 MHz demonstrated the same detection rate. However, the 5 MHz transducer provided the most detailed measurements. By contrast, the 2.25 MHz transducer demonstrated the best near-surface resolution for the composite pipe, both in contact testing and immersion testing. For the PE pipe, both contact testing and immersion testing provided the same quality results. While, for the composite pipe with a slightly rough and uneven surface, the best coupling was obtained with the immersion technique, both when using the contoured wedge and direct contact.

6.2.2 Sources of Error

Ultrasonic inspection is a highly manual method, and the results might depend on the inspector and the transducer settings. When performing inspections of specimens with fabricated defects, the position of the defects is already known before testing, which might increase the chances of detection.

For the experimental work presented in this thesis PuE testing with mode one is used. Mode 1 is meant to measure the thickness from the transducer to the first reflected echo, and only one sound velocity can be calibrated. Therefore, when the acoustic wave penetrates

multiple materials of different sound velocities, as is the case for inspection of the GFRP pipe with the PE liner, specimens with coating, inspection using a wedge and immersion testing, there will be thickness measurement errors.

Usually, mode 2 or 3 will be used, enabling several sound velocities to be calibrated. However, this was not available with the ultrasonic thickness gauge used.

For the flat GFRP specimens, the thickness of the applied paint was estimated to be 50 µm, which was therefore subtracted from the measurements when estimating the the through-thickness location of the defects. However, the thickness of the applied paint in reality be slightly uneven. Moreover, the actual position of the defects might also deviate from the reported value as the layer thickness of the laminate can have small variations and some error should be assumed for the depth of the FBHs, in the range of ±50.

6.2.3 Application and Significance for Composite Pipelines

Two of the main challenges of inspecting polymer and polymer composite pipelines considered in this project are inspecting thick composite laminates and curved geometries.

Fabricated delaminations in the size of 20x50 mm were successfully detected at depths up to 20.0 mm away from the inspected surface, and the through-thickness location could be measured. Single element transducers at three different frequencies were used, 5 MHz, 2.25 MHz and 0.5 MHz. Although all transducers exhibited the same detection rate, it was found that the 2.25 MHz transducer gave the best resolution to nose balance for the evaluated thickness range of 10.8-20.0 mm.

These results demonstrate the capability of ultrasonic testing to be used as NDT method for thick composite laminates. As the thickness of the laminate increases, it is expected that the attenuation of the reflected signal will also increase and that lower frequencies are necessary. However, as 5 MHz could be used to detect defects at 20 mm depth, it is expected that 2.25 MHz could be used at laminates with substantially higher thickness than what has been investigated in this thesis. Moreover, since the 0.5 MHz transducer could successfully detect delaminations at a thickness of about 5 µm, it shows that the resolution, although lower than the other two transducers, is high enough to detect delaminations and can be used in cases where the attenuation is too high using 2.25 MHz.

Furthermore, several methods were explored to inspect curved surface geometries, inspecting both thermoplastic polyethylene pipe samples and GFRP pipe samples. Proper coupling and stable ultrasonic readings were obtained using both contact testing with and without a contoured wedge and immersion testing. For the GFRP pipe, with a slightly uneven surface, it was found that immersion testing provided the best coupling between the transducer and the specimen, while for the PE pipe with a smooth surface, both contact testing and immersion testing gave equally reliable results.

Finally, it can be mentioned that ultrasonic inspection does not require a complicated inspection setup and is easy to perform both for in-service inspection and quality control.

6.3 Comparison of Inspection Methods

The necessity of integrity management for composite pipelines, including non-destructive testing techniques, is brought up in literature, but little tangible research has been done on the topic so far. Still, ultrasonic testing is one of the more well-known inspection methods for composites. It can detect delaminations and has a high level of accuracy. The exact position of a defect can be found, both in-plane and through-thickness.

Digital image correlation, on the other hand, is not yet an established method for non-destructive testing. However, it shows good potential based on the experimental work presented in this thesis and previous research presented in Section 3, although the detection rate for delaminations embedded far from the inspected surface appears to be lower than for ultrasonic testing.

DIC still has a significant advantage in that it is non-contact, whereas ultrasonic testing requires coupling between the transducer and the inspected component. Moreover, DIC provides full-field strain maps of the surface being inspected and can easily be used to inspect large components. However, as small strain intervals are considered, the possibility of outlier strain values being incorrectly identified as defects exist. Such outliers can also make it more difficult to identify damaged areas.

Good use of digital image correlation might be as a first inspection method that can rapidly inspect large surface areas, thereby revealing suspicious areas to be further examined by more accurate methods, such as ultrasonic testing.

7 | Conclusions

This master thesis has covered common failure mechanisms in polymer composite materials as well as non-destructive inspection methods, focusing on thick laminates used in composite pipelines. Delamination is the primary failure mechanism evaluated, and ultrasonic testing and digital image correlation have proven useful for the detection of delamination in composite materials.

Although little research has been related directly to non-destructive testing of composite pipelines, thick laminates have been investigated and associated with other sectors, introducing the potential of low-frequency ultrasonic testing and digital image correlation as inspection methods.

Digital image correlation in combination with low tensile load was performed on glass fibre reinforced epoxy specimens with a total thickness of 21.5 mm. The specimens contained defects in the form of flat bottom holes and fabricated delaminations made of PTFE Teflon inserts at different depths within the laminate ranging from 10.7 mm to 20.0 mm from the inspected surface. It was found that all flat bottom holes could be detected at the highest investigated strain level of 0.4% average tensile strain, while two of the four delaminations could be detected. The delaminations embedded furthest away from the surface could not be detected.

Ultrasonic pulse-echo testing was performed on the same composite specimens as inspected by digital image correlation at three different frequencies, 5 MHz, 2.25 MHz, and 0.5 MHz. Using ultrasonic testing, all defects, both flat bottom holes and delaminations, could be detected with all three transducer frequencies. Still, using 2.25 MHz frequency enabled measurements at the lowest gain of the three transducers.

Moreover, ultrasonic test setups for inspecting curved pipe samples have been explored. Two types of pipes were examined, a thermoplastic polyethylene (PE) pipe and glass fibre reinforced PE pipe with PE liner. Flat bottom holes with sizes from 4 mm to 20 mm in diameter were drilled at different depths. The samples were investigated using contact testing with and without a contoured wedge and immersion testing. Contact testing was performed with direct contact for the smallest transducers of 5 MHz and 2.25 MHz and with a wedge for a larger transducer of 0.5 MHz. All methods enabled thickness

measurements and defect detection. However, it was found that immersion testing provided better coupling for the composite pipe with a slightly uneven surface than contact testing.

Moreover, higher frequency transducers of 5 MHz and 2.25 MHz could detect most defects from 4 mm in diameter and larger, while the 0.5 MHz transducer could only detect holes of 15 mm in diameter or larger. For the GFRP pipe samples, the 2.25 MHz transducer exhibited the best near surface resolution, and for all transducers, defects positioned in the laminate-liner interface had to be larger to be detectable than defects positioned within the fibre laminate or the within the liner.

8 | Further Work

This master thesis is an introduction to non-destructive evaluation of composite pipelines. Suggestions to further work on this topic include:

- Evaluate other failure mechanisms
- Evaluate alternative NDT methods
- Further evaluation of digital image correlation, such as in combination with flexural load
- Further determination of thickness limitations at different frequencies using ultrasonic testing

Bibliography

[1] M. Roseman, R. Martin and G. Morgan, '10 - composites in offshore oil and gas applications,' in *Marine Applications of Advanced Fibre-Reinforced Composites*, ser. Woodhead Publishing Series in Composites Science and Engineering, J. Graham-Jones and J. Summerscales, Eds., Woodhead Publishing, 2016, pp. 233–257.

[2] K. Yu, E. V. Morozov, M. A. Ashraf and K. Shankar, 'A review of the design and analysis of reinforced thermoplastic pipes for offshore applications,' *Journal of Reinforced Plastics and Composites*, vol. 36, no. 20, pp. 1514–1530, 2017.

[3] O. O. Ochoa and M. M. Salama, 'Offshore composites: Transition barriers to an enabling technology,' English, *Composites Science and Technology*, vol. 65, no. 15-16, pp. 2588–2596, 2005.

[4] J. Cao, W.-f. Ma, X.-f. Meng *et al.*, 'Integrity management of non-metallic pipeline,' in *Proceedings of the International Petroleum and Petrochemical Technology Conference 2020*, J. Lin, Ed., Singapore: Springer Singapore, 2021, pp. 664–673.

[5] T. Jollivet, C. Peyrac and F. Lefebvre, 'Damage of composite materials,' *Procedia Engineering*, vol. 66, Dec. 2013.

[6] R. Bossi and V. Giurgiutiu, '15 - nondestructive testing of damage in aerospace composites,' in *Polymer Composites in the Aerospace Industry*, P. Irving and C. Soutis, Eds., Woodhead Publishing, 2015, pp. 413–448.

[7] V. V. Vasilev and E. V. Morozov, *Advanced mechanics of composite materials and structural elements, third edition*, eng, 3rd ed. Waltham, MA: Elsevier, 2013, ISBN: 008098231X.

[8] T. Bakken, *Non-destructive evaluation of polymer composites using ultrasonic testing*, Norway, 2022.

[9] U. K. Vaidya and K. K. Chawla, 'Processing of fibre reinforced thermoplastic composites,' eng, *International materials reviews*, vol. 53, no. 4, pp. 185–218, 2008.

[10] R. Heslehurst, *Defects and Damage in Composite Materials and Structures*. Apr. 2014, ISBN: 9781466580480.

[11] W. Cantwell and J. Morton, 'The impact resistance of composite materials — a review,' *Composites*, vol. 22, no. 5, pp. 347–362, 1991, ISSN: 0010-4361.

[12] J. Nairn, 'Matrix microcracking in composites,' *Polymer Matrix Composites*, vol. 2, Jun. 2000.

[13] R. Talreja and C. V. Singh, 'Damage in composite materials,' in *Damage and Failure of Composite Materials*. Cambridge University Press, 2012, pp. 36–56.

[14] R. Adams and P. Cawley, 'A review of defect types and nondestructive testing techniques for composites and bonded joints,' *NDT International*, vol. 21, no. 4, pp. 208–222, 1988, ISSN: 0308-9126.

[15] J. Prichard and P. Hogg, 'The role of impact damage in post-impact compression testing,' *Composites*, vol. 21, no. 6, pp. 503–511, 1990, ISSN: 0010-4361.

[16] W. Chung, B. Jang, T. Chang, L. Hwang and R. Wilcox, 'Fracture behavior in stitched multidirectional composites,' *Materials Science and Engineering: A*, vol. 112, pp. 157–173, 1989, ISSN: 0921-5093.

[17] U. Polimeno and M. Meo, 'Detecting barely visible impact damage detection on aircraft composites structures,' *Composite Structures*, vol. 91, no. 4, pp. 398–402, 2009, Sixth International Conference on Composite Science and Technology, ISSN: 0263-8223.

[18] P. Kumar and B. Rai, 'Delaminations of barely visible impact damage in cfrp laminates,' *Composite Structures*, vol. 23, no. 4, pp. 313–318, 1993, ISSN: 0263-8223.

[19] M. Mehdikhani, L. Gorbatikh, I. Verpoest and S. V. Lomov, 'Voids in fiber-reinforced polymer composites: A review on their formation, characteristics, and effects on mechanical performance,' *Journal of Composite Materials*, vol. 53, no. 12, pp. 1579–1669, 2019.

[20] W. Cantwell and J. Morton, 'The significance of damage and defects and their detection in composite materials: A review,' *The Journal of Strain Analysis for Engineering Design*, vol. 27, no. 1, pp. 29–42, 1992.

[21] C. Soutis and P. W. Beaumont, *Multi-scale modelling of composite material systems: The art of predictive damage modelling*. Elsevier, 2005.

[22] M. V. Brook, *Ultrasonic inspection technology development and search units design : Examples of practical applications*, eng, Hoboken, New Jersey, 2012.

[23] C. J. Hellier, *Handbook of nondestructive evaluation*, eng, New York, 2001.

[24] M. Khattak, A. Mukhtar, I. Shahid and S. M. Sufian, 'A review on application of non destructive techniques on composites,' pp. 12–21, Jan. 2016.

[25] J. Gryzagoridis and D. Findeis, 'Tap testing vs. thermography,' *e-Journal of Nondestructive testing (NDT*, 2017, ISSN: 1435-4934.

[26] 'The mechanics of the coin-tap method of non-destructive testing,' *Journal of Sound and Vibration*, vol. 122, no. 2, pp. 299–316, 1988, ISSN: 0022-460X.

[27] M. Ibrahim, '7 - nondestructive testing and structural health monitoring of marine composite structures,' in *Marine Applications of Advanced Fibre-Reinforced Composites*, ser. Woodhead Publishing Series in Composites Science and Engineering, J. Graham-Jones and J. Summerscales, Eds., Woodhead Publishing, 2016, pp. 147–183.

[28] S. Garcea, Y. Wang and P. Withers, 'X-ray computed tomography of polymer composites,' *Composites Science and Technology*, vol. 156, pp. 305–319, 2018, ISSN: 0266-3538.

[29] Y. Hung, N. Ng, R. Ng, S. M. Shepard, Y. Hou and J. R. Lhota, 'Review and comparison of shearography and pulsed thermography for adhesive bond evaluation,' *Optical Engineering*, vol. 46, no. 5, pp. 1–16, 2007.

[30] S. Gholizadeh, 'A review of non-destructive testing methods of composite materials,' *Procedia Structural Integrity*, vol. 1, pp. 50–57, 2016, XV Portugese Conference on Fracture, PCF 2016, 10-12 February 2016, Paco de Arcos, Portugal, ISSN: 2452-3216.

[31] Y. Hung, Y. Chen, S. Ng *et al.*, 'Review and comparison of shearography and active thermography for nondestructive evaluation,' *Materials Science and Engineering: R: Reports*, vol. 64, no. 5, pp. 73–112, 2009, ISSN: 0927-796X.

[32] H. Schreier, J.-J. Orteu and M. A. Sutton, *Image Correlation for Shape, Motion and Deformation Measurements: Basic Concepts,Theory and Applications*, eng, 1. Aufl. New York, NY: Springer-Verlag, 2009, pp. 1–321, ISBN: 9780387787466.

[33] E. Jones and M. Iadicola, *A good practices guide for digital image correlation*, 2018.

[34] C. Niezrecki, J. Baqersad and A. Sabato, 'Digital image correlation techniques for nde and shm,' in *Handbook of Advanced Nondestructive Evaluation*, N. Ida and N. Meyendorf, Eds. Springer International Publishing, 2019, pp. 1545–1590.

[35] M. Merzkirch, 'Introduction and theoretical background,' in *Mechanical Characterization Using Digital Image Correlation: Advanced Fibrous Composite Laminates*. Cham: Springer International Publishing, 2022, pp. 1–45.

[36] B. K. Bay, T. S. Smith, D. P. Fyhrie and M. Saad, 'Digital volume correlation: Three-dimensional strain mapping using x-ray tomography,' English (US), *Experimental Mechanics*, vol. 39, no. 3, pp. 217–226, Sep. 1999, ISSN: 0014-4851.

[37] F. Hild and S. Roux, 'Comparison of local and global approaches to digital image correlation,' *Experimental Mechanics*, vol. 52, Nov. 2012.

[38] P. Reu, 'Calibration: Care and feeding of a stereo-rig,' *Experimental Techniques*, vol. 38, no. 3, pp. 1–2, 2014.

[39] ——, 'Calibration: 2d calibration,' *Experimental Techniques*, vol. 37, no. 5, pp. 1–2, 2013.

[40] ——, 'Calibration: Pre-calibration routines,' *Experimental Techniques*, vol. 37, no. 4, pp. 1–2, 2013.

[41] ——, 'All about speckles: Aliasing,' *Experimental Techniques*, vol. 38, no. 5, pp. 1–3, 2014.

[42] ——, 'All about speckles: Edge sharpness,' *Experimental Techniques*, vol. 39, no. 2, pp. 1–2, 2015.

[43] ——, 'Calibration: Sanity checks,' *Experimental Techniques*, vol. 38, no. 2, pp. 1–2, 2014.

[44] J. Krautkrämer, *Ultrasonic testing of materials*, eng, Berlin, 1990.

[45] D. Ensminger and L. J. Bond, *Ultrasonics : Fundamentals, technology, and applications*, eng, 2011.

[46] O. S. S. A. Corp. and O. N. C. Inc., *Ultrasonic transducers - wedges, cables, test blocks*, Olympus, Walthham, MA, USA, 2016.

[47] *Ultrasonic Nondestructive Evaluation Systems : Industrial Application Issues*, eng, 1st ed. 2015. Cham: Springer International Publishing : Imprint: Springer, 2015, ISBN: 3-319-10566-3.

[48] G. E. Clarckson, 'Baseline values for non-destructive structural evaluation of glass reinforced plastic,' Oct. 2014.

[49] I. Papa, V. Lopresto and A. Langella, 'Ultrasonic inspection of composites materials: Application to detect impact damage,' eng, *International Journal of Lightweight Materials and Manufacture*, vol. 4, no. 1, pp. 37–42, 2021, ISSN: 2588-8404.

[50] B. Chen and B. Pan, 'Calibration-free single camera stereo-digital image correlation for small-scale underwater deformation measurement,' *Optics Express*, vol. 27, pp. 10 509–10 523, Apr. 2019.

[51] B. Pan, D. Wu, Z. Wang and Y. Xia, 'High-temperature digital image correlation method for full-field deformation measurement at 1200 °c,' *Measurement Science and Technology*, vol. 22, p. 015 701, Nov. 2010.

[52] J. Lyons, J. Liu and M. Sutton, 'High-temperature deformation measurements using digital-image correlation,' *Experimental Mechanics*, vol. 36, pp. 64–70, Mar. 1996.

[53] Q. Baltzersen, J. Bang, B. Moursund and B. Melve, 'Ultrasonic inspection of adhesive bonded coupler joints in grp piping systems,' *Journal of Reinforced Plastics and Composites*, vol. 14, no. 4, pp. 362–377, 1995.

[54] A. A. Hassen, U. Vaidya and F. Britt, 'Structural integrity of fiber reinforced plastic piping,' *Materials Evaluation*, vol. 73, pp. 918–929, Jul. 2015.

[55] 'Non-destructive testing,' DNV, Class Guidline, 2015.

[56] B. Yılmaz, A. Asokkumar, E. Jasiuniene and R. Kazys, 'Air-coupled, contact, and immersion ultrasonic non-destructive testing: Comparison for bonding quality evaluation,' *Applied Sciences*, vol. 2020, p. 6757, Sep. 2020.

[57] B. W. Drinkwater and A. I. Bowler, 'Ultrasonic array inspection of the clifton suspension bridge chain-links,' eng, vol. 51, no. 9, pp. 491–498, 2009, ISSN: 1354-2575.

[58] J. Russell, R. Long, D. Duxbury and P. Cawley, 'Development and implementation of a membrane-coupled conformable array transducer for use in the nuclear industry,' eng, *Insight (Northampton)*, vol. 54, no. 7, pp. 386–393, 2012, ISSN: 1354-2575.

[59] R. Rogers, 'Chapter two - deep ocean sediment–hydrate relationships,' in *Offshore Gas Hydrates*, R. Rogers, Ed., Boston: Gulf Professional Publishing, 2015, pp. 21–63.

[60] A. Fahr, 'Ultrasonic c-scan inspection of composite materials,' *Engineering Journal of Qatar University*, vol. 5, Jan. 1992.

[61] *Non-Destructive Inspection and Relationships to Aircraft Design and Materials*, eng. 1978.

[62] P. Lloyd, 'Ultrasonic system for imaging delaminations in composite materials,' *Ultrasonics*, vol. 27, no. 1, pp. 8–18, 1989, ISSN: 0041-624X.

[63] C. Boller, 'Fundamentals on damage monitoring,' in Oct. 1996, pp. 1–4.

[64] C. Boller and W. Staszewski, 'Aircraft structural health and usage monitoring,' in Feb. 2003, pp. 29–73, ISBN: 9780470092866.

[65] M. Ibrahim, 'Nondestructive evaluation of thick-section composites and sandwich structures: A review,' *Composites Part A: Applied Science and Manufacturing*, vol. 64, pp. 36–48, 2014, ISSN: 1359-835X.

[66] L. Pieczonka, W. Staszewski, T. Uhl, S. Pavlopoulou and C. Soutis, 'Nondestructive testing of composite patch repairs,' Oct. 2014.

[67] F. Liu, Z. Zhou, S. Liu, Y. Yang and L. Zhang, 'Evaluation of carbon fiber composite repairs using asymmetric-frequency ultrasound waves,' *Composites Part B: Engineering*, vol. 181, p. 107 534, 2020, ISSN: 1359-8368.

[68] I. Amenabar, A. Mendikute, A. López-Arraiza, M. Lizaranzu and J. Aurrekoetxea, 'Comparison and analysis of non-destructive testing techniques suitable for delamination inspection in wind turbine blades,' *Composites Part B: Engineering*, vol. 42, no. 5, pp. 1298–1305, 2011, ISSN: 1359-8368.

[69] C. Fortunko and D. Fitting, 'Apropriate ultrasoni system components for nde of thick polymer-composites,' in *Review of Progress in Quantitative Nondestructive Evaluation*. Springer, 1991.

[70] K. Borum, 'Evaluation of the quality of thick fibre composites using immersion and air-coupled ultrasonic techniques,' English, in *roceedings (CD-ROM)*, 9. European conference on non-destructive testing ; Conference date: 01-01-2006, German Society for Non-Destructive Testing, 2006.

[71] A. Mouritz, C. Townsend and M. Shah Khan, 'Non-destructive detection of fatigue damage in thick composites by pulse-echo ultrasonics,' *Composites Science and Technology*, vol. 60, no. 1, pp. 23–32, 2000, ISSN: 0266-3538.

[72] I. M. Daniel and S. C. Wooh, 'Ultrasonic techniques for characterization of manufacturing defects in thick composites,' in *Review of Progress in Quantitative Nondestructive Evaluation: Volume 8, Part A and B*, D. O. Thompson and D. E. Chimenti, Eds. Boston, MA: Springer US, 1989, pp. 1605–1612.

[73] A. A. Hassen, H. Taheri and U. K. Vaidya, 'Non-destructive investigation of thermoplastic reinforced composites,' *Composites Part B: Engineering*, vol. 97, pp. 244–254, 2016, ISSN: 1359-8368.

[74] M. Gresil, A. Poohsai and N. Chandarana, 'Guided wave propagation and damage detection in composite pipes using piezoelectric sensors,' *Procedia Engineering*, vol. 188, pp. 148–155, 2017, Structural Health Monitoring - From Sensing to Diagnosis and Prognosis, ISSN: 1877-7058.

[75] D. Hopkins, M. Brassard, G. Neau, J.-N. Noiret, W. V. Johnson and L. le Ber, 'Surface-adaptive ultrasound (saul) for phased-array inspection of composite specimens with curved edges and complex geometry,' 2013.

[76] F. Laurin, J.-S. Charrier, D. Lévêque, J.-F. Maire, A. Mavel and P. Nuñez, 'Determination of the properties of composite materials thanks to digital image correlation measurements,' *Procedia IUTAM*, vol. 4, pp. 106–115, 2012, IUTAM Symposium on Full-field Measurements and Identification in Solid Mechanics.

[77] M. Caminero, S. Pavlopoulou, M. López-Pedrosa, B. Nicolaisson, C. Pinna and C. Soutis, 'Using digital image correlation techniques for damage detection on adhesively bonded composite repairs,' *Advanced Composites Letters*, vol. 21, no. 2, p. 096 369 351 202 100 203, 2012.

[78] Bataxi, X. Chen, Z. Yu, H. Wang and C. Bil, 'Strain monitoring on damaged composite laminates using digital image correlation,' *Procedia Engineering*, vol. 99, pp. 353–360, 2015.

[79] G. Szebényi and V. Hliva, 'Detection of delamination in polymer composites by digital image correlation—experimental test,' *Polymers*, vol. 11, no. 3, 2019.

[80] B. LeBlanc, C. Niezrecki, P. Avitabile, J. Chen and J. Sherwood, 'Damage detection and full surface characterization of a wind turbine blade using three-dimensional digital image correlation,' *Structural Health Monitoring*, vol. 12, no. 5-6, pp. 430–439, 2013.

[81] C. Devivier, D. Thompson, F. Pierron and M. Wisnom, 'Correlation between full-field measurements and numerical simulation results for multiple delamination composite specimens in bending,' in *Advances in Experimental Mechanics VII*, ser. Applied Mechanics and Materials, vol. 24, Trans Tech Publications Ltd, Aug. 2010, pp. 109–114.

[82] *Manufacturing techniques for polymer matrix composites (pmcs)*, eng, Philadelphia, Pa, 2012.

Appendix

A Epoxy Wedge Model

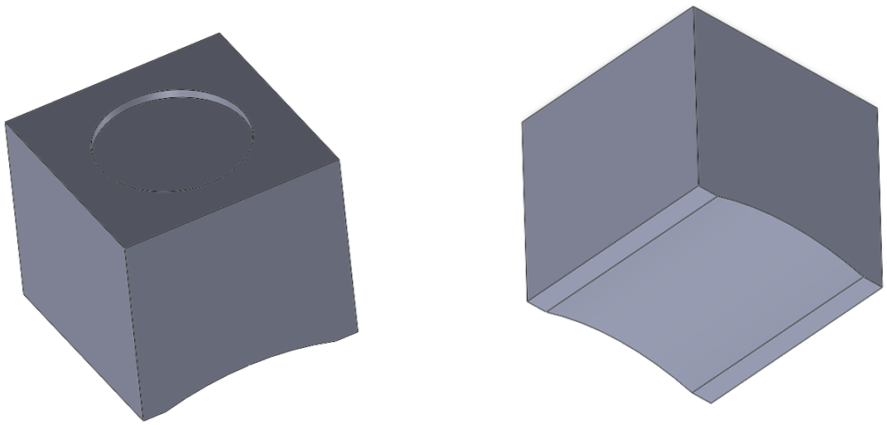

Figure 1: CAD model of wedge used for PE pipe

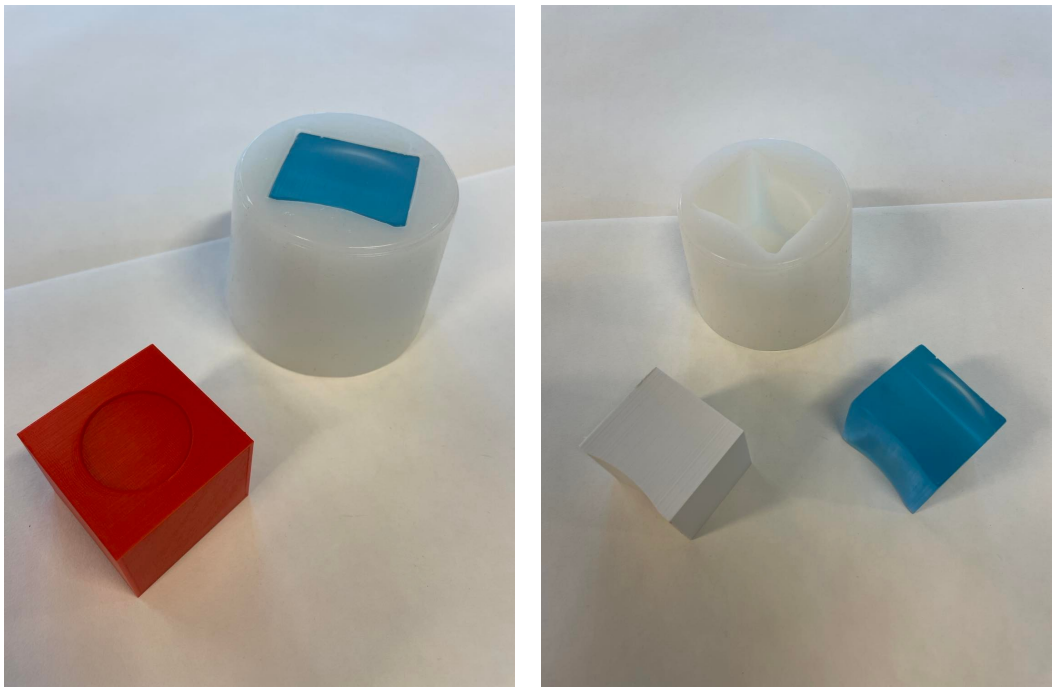

(a) (b)

Figure 2: 3D-printed wedge with silicone mould and cast epoxy wedge for a) PE pipe sample and b) GFRP pipe sample

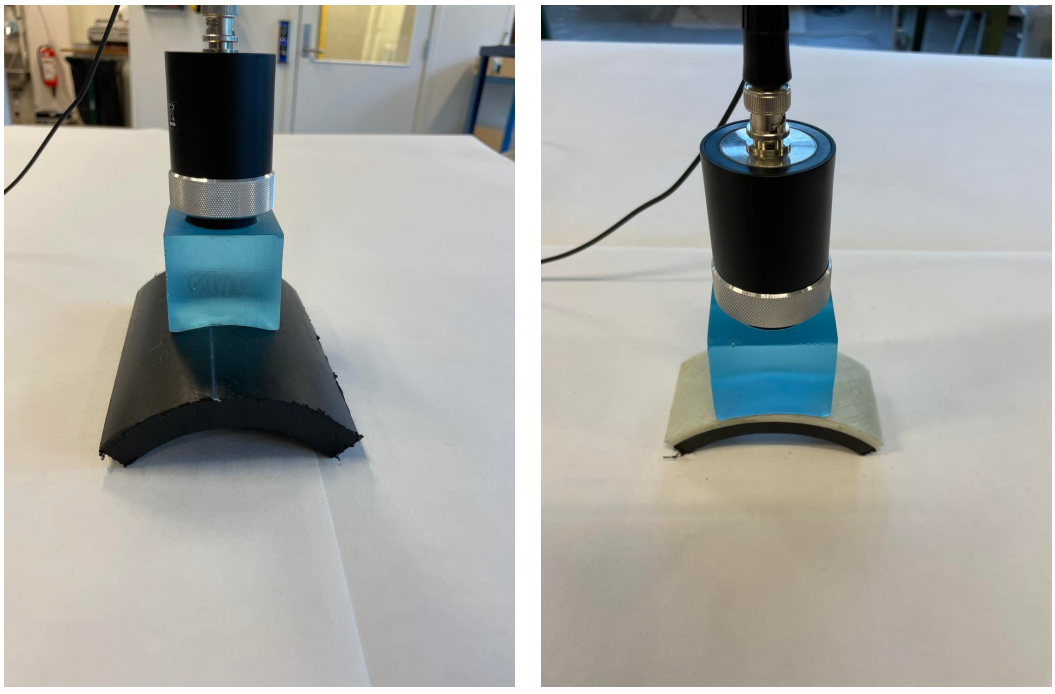

(a) (b)

Figure 3: Test setup for inspection using contoured wedge for (a) PE pipe sample and b) GFRP sample

B Transducer Support Structure Model

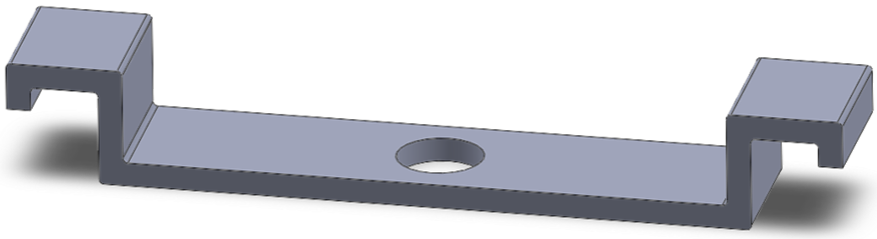

Figure 4: CAD model of transducer support structure for 5 MHz and 2.25 MHz transducers

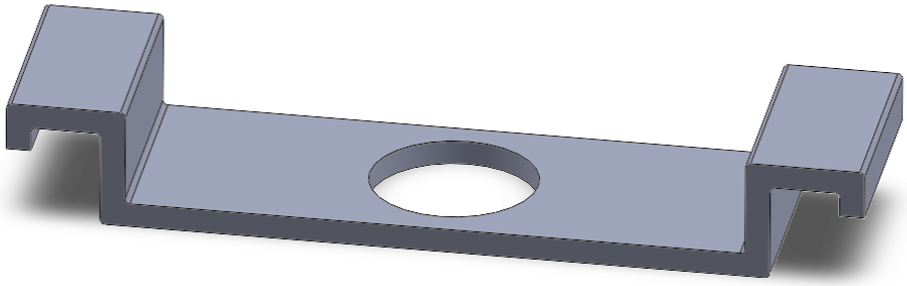

Figure 5: CAD model of transducer support structure for 0.5 MHz transducer

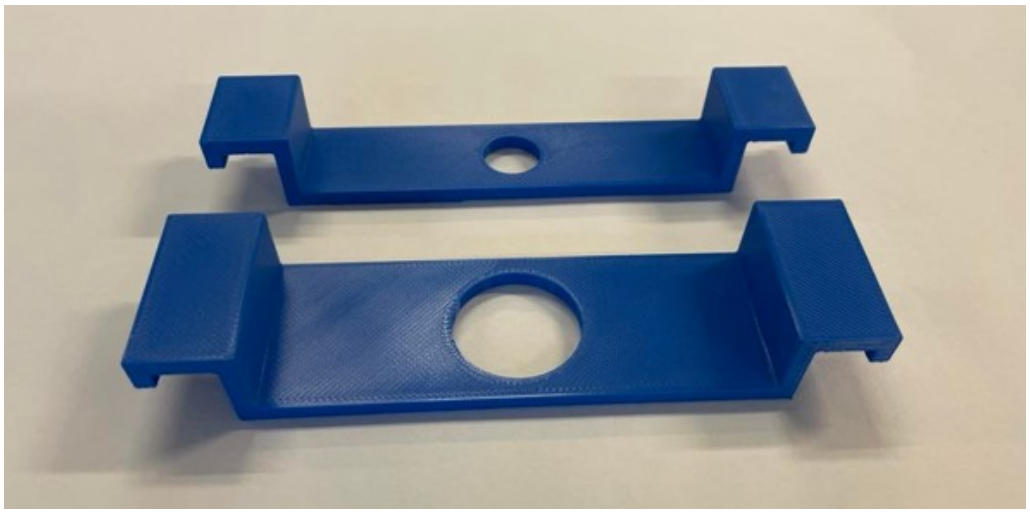

Figure 6: 3D printed support structures

Figure 7: Test setup for immersion testing of PE pipe sample with 2.25 MHz transducer

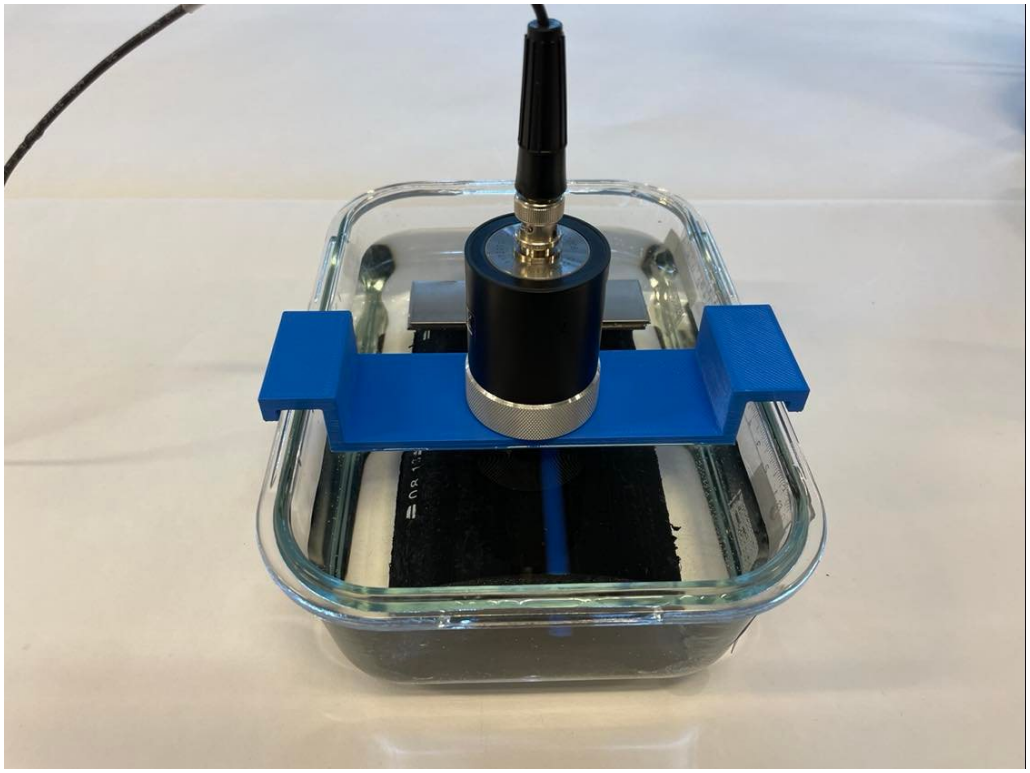

Figure 8: Test setup for immersion testing of PE pipe sample with 0.5 MHz transducer

C Finite Element Analysis in Abaqus CAE

C.1 Analysis Setup

Table 1: Material properties for typical unidirectional E-glass/Epoxy laminate

E1	E2	Nu12	G12	G13	G23
40000 MPa	10000 MPa	0.3	3800 MPa	3800 Mpa	3400 MPa

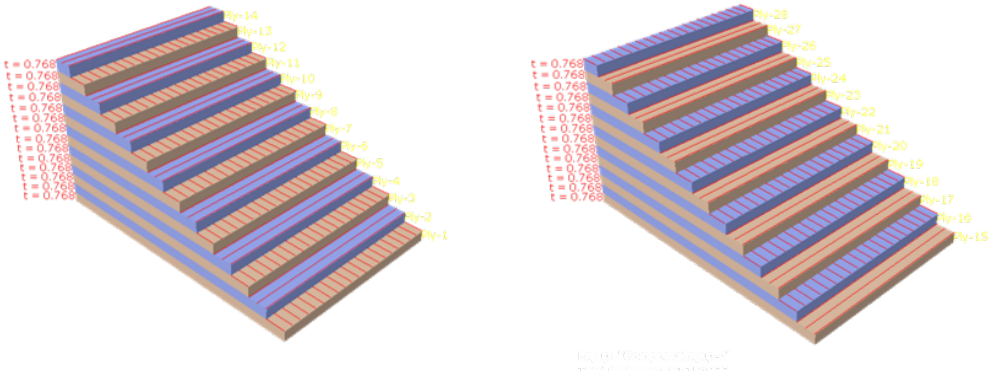

(a) ply 1-14 (b) ply 15-28

Figure 9: Composite layup

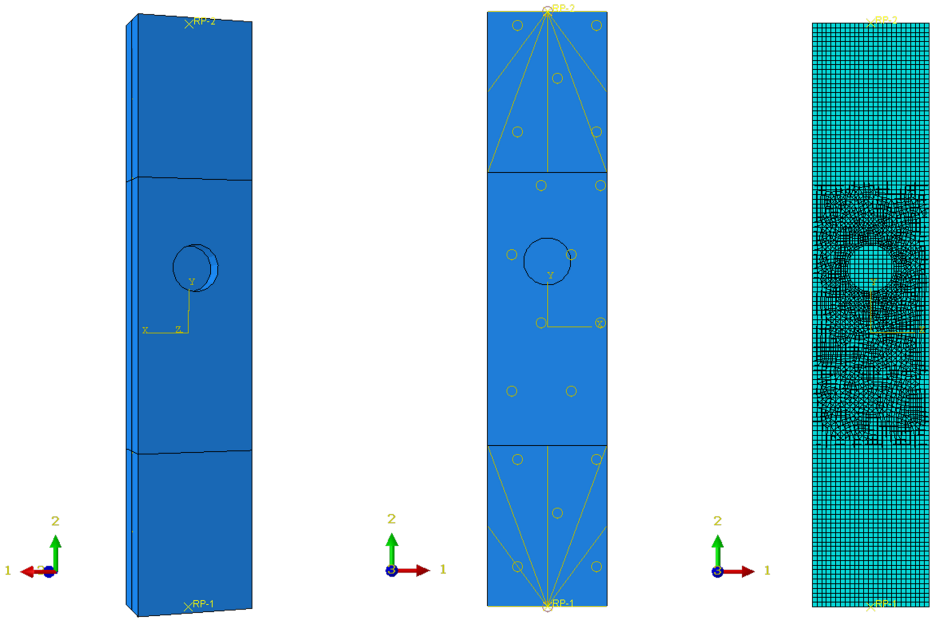

(a) Specimen with rendered thickness

(b) Middle surface

(c) Mesh with S4R element type

Figure 10: The specimens with FBH are made of two shell parts connected with tie constrain

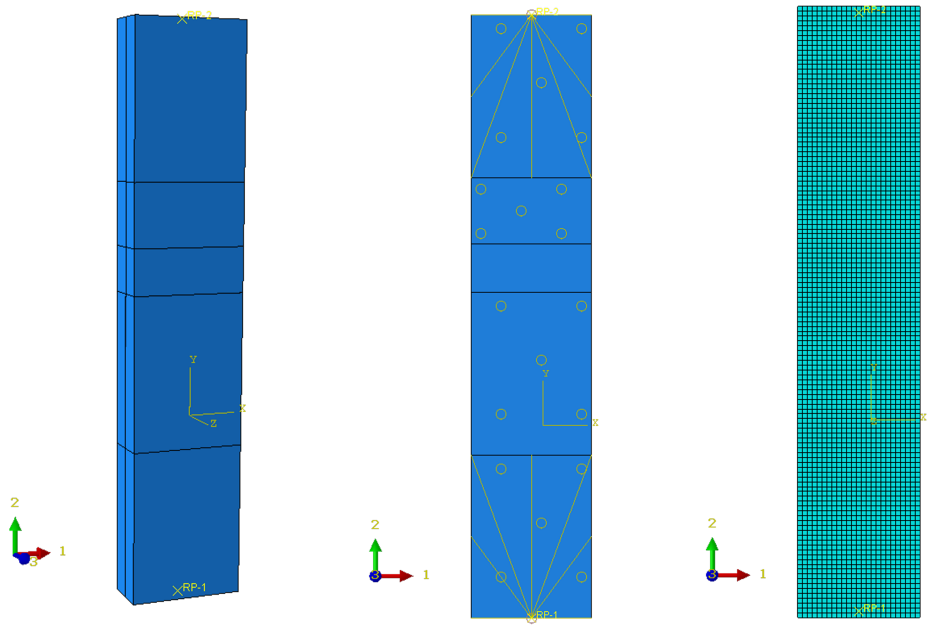

(a) Specimen with rendered thickness

(b) Middle surface

(c) Mesh with S4R element type

Figure 11: The specimens with delaminations are made of two shell parts connected with tie constraint expect at delaminated area.

C.2 Results

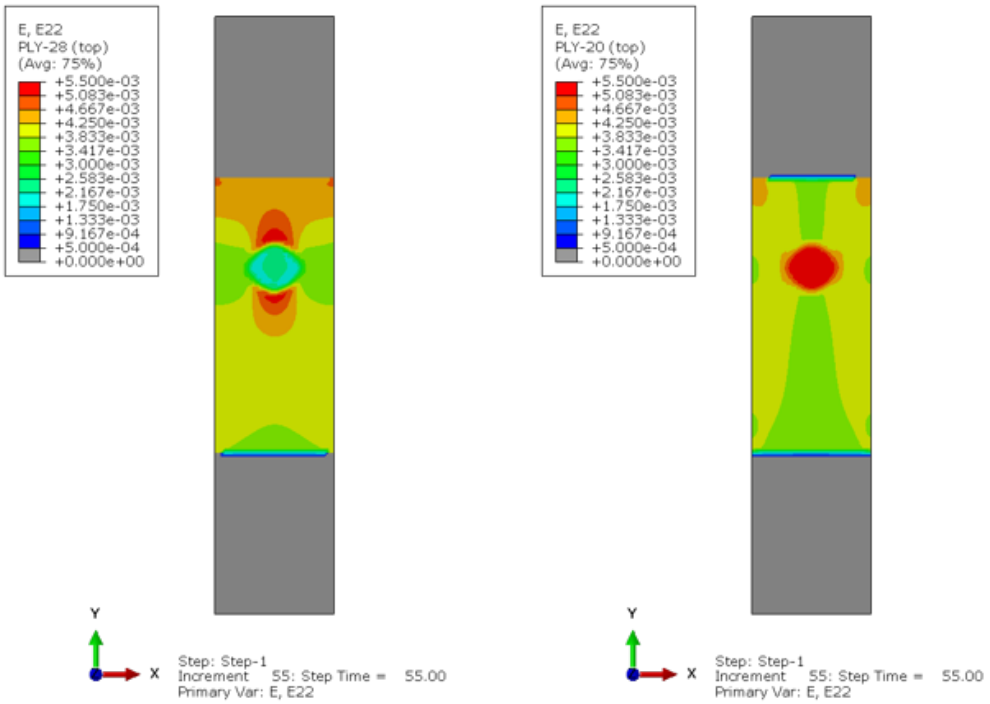

(a) ply 28 (b) ply 20

Figure 12: Computed tensile strain fields for individual plies in specimen with FBH (H1) with a global strain of 0.4%

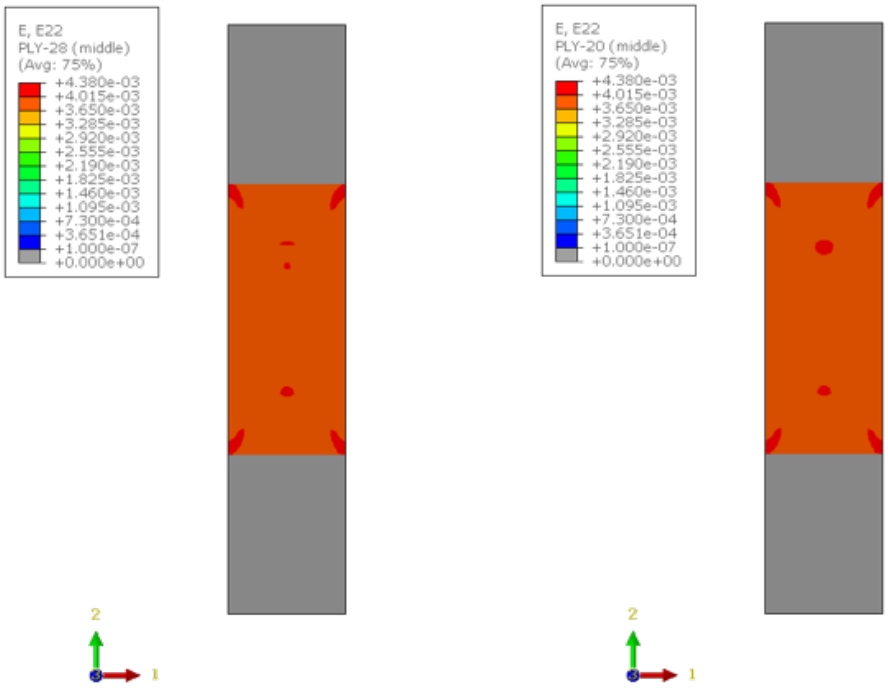

(a) ply 28 (b) ply 20

Figure 13: Computed tensile strain fields for individual plies in specimen with fabricated delaminations (D1) with a global strain of 0.4%

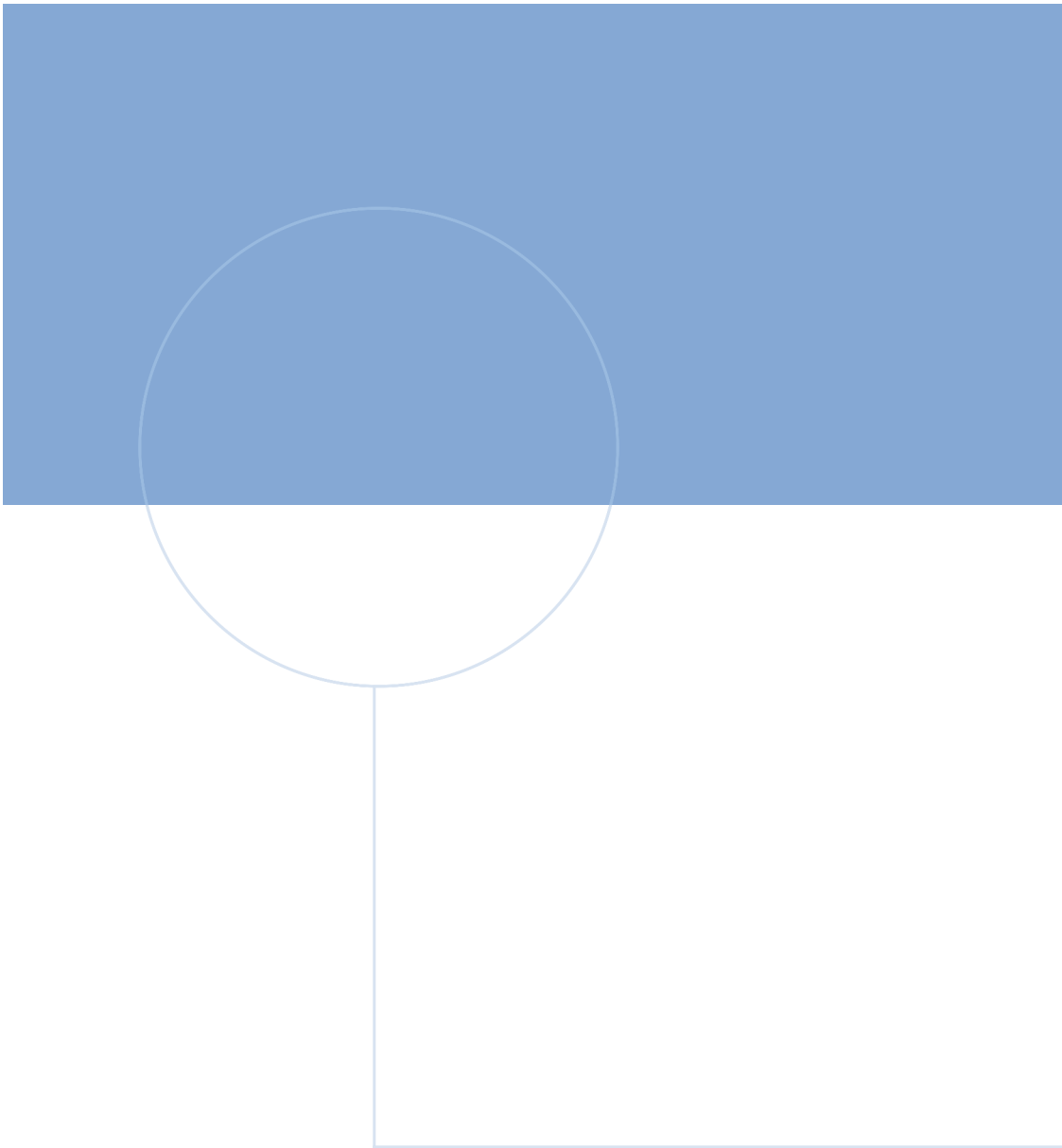

NTNU

Norwegian University of
Science and Technology